Design, Construction, and Application of Synthetic Microbial Consortia

by

Alissa R. Kerner

A dissertation submitted in partial fulfillment
of the requirements for the degree of
Doctor of Philosophy
(Biomedical Engineering)
in the University of Michigan
2013

Doctoral Committee:

Assistant Professor Xiaoxia Nina Lin, Chair
Professor Erdogan Gulari
Professor Jennifer J. Linderman
Professor Shuichi Takayama

Table of Contents

List of Figures

List of Tables

Abstract

Mixtures of interacting microbes, or microbial consortia, may be a key part of the solution to overcoming current environmental and technological challenges, such as a dearth of renewable fuel sources. Microbial consortia have various advantages over single species, or "superbugs", such as efficiency, robustness, and modularity. The goal of this dissertation is to develop tools for making use of microbial consortia and to demonstrate their utility through practical applications. Specifically, our efforts in technology development and application include: a tunable, programmable cross-feeding circuit; production of isobutanol (a next-generation biofuel); and sensing/screening of metabolite secretion.

First, we designed and constructed a programmable genetic circuit based on engineered symbiosis between two *E. coli* auxotrophs. By regulating and tuning the export or production of the cross-fed metabolites we were able to tune the exchanges and achieve a wide range of growth rates and strain ratios. In addition, we created two-dimensional design space plots by inverting the relationship of growth/ratio vs. inducer concentrations. Using the plots, we could "program" the co-culture for pre-specified outcomes. This proof-of-concept circuit can be applied to more complex systems where precise tuning of the consortium would facilitate the optimization of specific objectives.

Next, we engineered a consortium of *E. coli* specialist strains fermenting either hexose or pentose sugars into isobutanol, and demonstrated that this co-culture exhibits improved isobutanol production over a diauxic monoculture under several growth conditions. Notably, the co-culture outperformed the monoculture on an enzymatically-hydrolyzed lignocellulosic biomass, producing up to almost 3 g/L isobutanol without detoxification or supplementation.

Lastly, we demonstrated the utility of a microbial consortium for detecting highly-secreting L-valine (and subsequently isobutanol) production strains. We designed a secretor/sensor pair that can be used to detect increased L-valine secretion by the "secretor" via the changes in growth of the "sensor", a fluorescently-tagged L-valine auxotroph. This will be part of a larger effort to develop a new method for high-throughout screening of microbial over-production strains.

This dissertation presents the design, construction, and/or application of three synthetic microbial consortia. Through tool development and biofuel applications, our work demonstrates the potential, utility, and benefits of microbial consortia in synthetic biology.

Chapter 1 Background and Motivation

1.1 Microbial Consortia

Microbial consortia are groups of interacting microbial populations that can be found in many diverse environmental niches. Often these heterogeneous communities are used for the completion of complex processes such as bioremediation, wastewater treatment (*1*), or assisting mammals in food digestion (*2*). For example, the populations of microbes living in the human gastrointestinal tract (known as the gut microbiota) perform many important functions for their human hosts. These include harvesting important nutrients, synthesizing vitamins, detoxifying foreign substances, supporting the immune system and participating in renewal of the gut epithelium (*2*). Bacterial (or archaeal) consortia used in wastewater treatment plants provide another example that is relevant to humans. These microbial communities can naturally perform many of the tasks needed for wastewater treatment such as nitrogen or phosphorus removal (*1*). They are transported to an artificial environment but still perform the same jobs as they would in their native habitat. However, these individual species cannot act alone, they rely on each other to provide intermediates in the overall toxin degradation pathway since each species can usually perform only one key reaction. In fact, the exact composition of microbial mixtures used for nitrogen removal is unknown -- we are only recently beginning to understand the complexity of the organisms involved (*1*).

Microbial consortia can be grouped into two types: natural or synthetic, with a distinction sometimes made between engineered communities of recombinant organisms or engineered communities of natural organisms. Besides their use in wastewater treatment, undefined microbial mixtures, or "natural/engineered consortia", have been harvested directly from the environment with a goal towards lignocellulosic biomass degradation and fuel production, as recently reviewed by Zuroff and Curtis (*3*). For example, natural microbial mixtures were harvested in soil samples from various

locations throughout China, then the mixtures were further enriched for degradation of filter paper and raw corn stover powder (RCSP) and through this enrichment up to 81% of the filter paper and 51% of the RCSP was broken down (*4*). Several uncultured bacterial species were identified in the culture, though it was unclear what functions each of the species played in the overall process. Although these natural mixtures may initially be better at breaking down plant cell walls, including lignin components, their utility is limited by a lack of genetic tools for further engineering desirable product formation and a lack of general knowledge about the consortia members (*5*). For this reason, we will focus on the use of synthetic microbial consortia for the remainder of this section. Following is a brief review of the state of the art with regard to synthetic consortia, with a focus on the application of such consortia to lignocellulosic biofuel production.

Synthetic microbial consortia may have various advantages over monocultures, or what is commonly referred to as a "superbug". One of the advantages of consortia is the ability to complete tasks that would be too difficult for one organism, such as the co-fermentation of glucose and xylose from lignocellulosic biomass. Eiteman and colleagues engineered two *Escherichia coli* strains to be either glucose- or xylose-specific fermentors, and then grew them together in co-culture (*6*). This system was more robust than a single strain process; since the strains did not compete with each other for nutrients they were able to adapt to fluctuations in the feed composition. This led to a more efficient and faster process when compared to a single-strain fermenting both of the sugars.

The previous example also highlights a second advantage of synthetic consortia over monocultures: the ability to compartmentalize pathways in different strains so that they can be individually optimized without perturbing as many interactions between other important cellular components (*7*). Other advantages include the ability to simplify the optimization process by the division of labor – it is easier to optimize one pathway in each of several different organisms than multiple pathways in one organism (see discussion of work by Tsai *et al*. (*8*), in Section 1.2 below) – and the possibility that the system can be tightly controlled by external signals. Finally, members of microbial communities are thought to be more robust and resistant to environmental changes than

non-communal members, because they can rely on specialized members when faced with environmental stress and nutrient limitations (*7*).

When designing synthetic consortia, there are different types of relationships that might be beneficial to engineer amongst the consortium members, such as sequential utilization, co-utilization of substrate, substrate transformation, and product transformation, and the choice of interaction will often depend on the desired substrate and products (Figure 1.1) (*3*). However, beyond the primary interaction, other control systems may need to be put in place to ensure the stability of a multi-member consortium, such as a tunable control circuit. This is much easier to control with recombinant organisms rather than with natural organisms in an engineered setting due to the lack of tools available to modify these lesser-known organisms, as mentioned above. Therefore, consortia consisting of mostly recombinant organisms are likely to be the most promising option going forward.

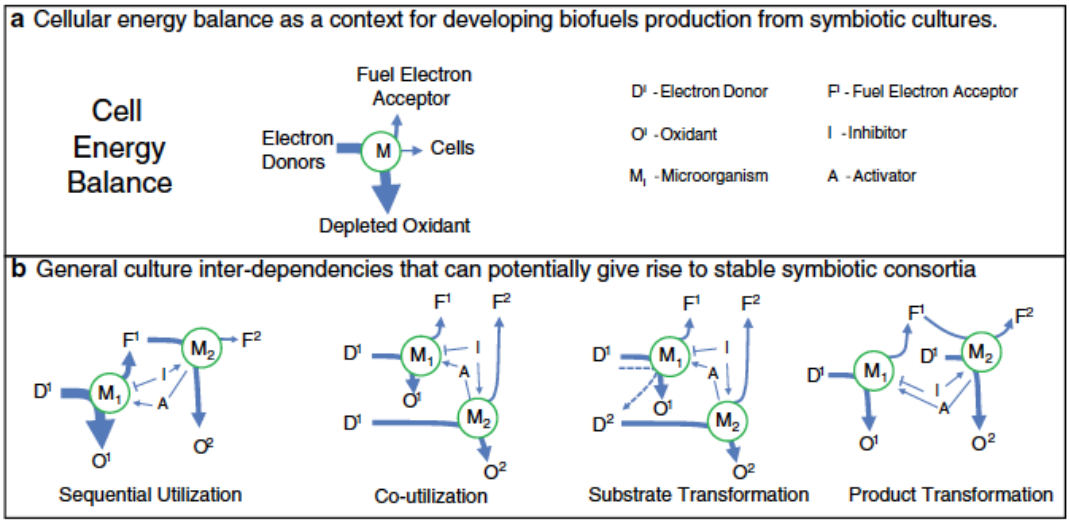

Figure 1.1. Model microbial symbiotic interactions based on consideration of cellular energy balances, adapted from (*3*).

Many interesting and recent advances in the design of synthetic consortia with recombinant organisms have allowed them to move beyond mimicking natural systems (such as a predator-prey network, (*9*)) to also perform specific functions, such a multicellular computational network (*10*), a synthetic mammalian clock (*11*), and

controlling biofilm formation and dispersal (*12*). Additionally, they have been utilized in various formats, ranging from microfluidic devices (*9, 12-14*) to inkjet printers (*15*).

For example, Regot *et al.* (*10*) were able to engineer various Boolean logic gates and outputs from only a few inputs through the use of combinations of different engineered yeast cells (Figure 1.2). The cells can either respond to an external signal and/or a "wire" output from another yeast cell (e.g. a yeast pheromone, α factor) and then release either another wire or the final output, in this case green fluorescent protein (GFP). The various combinations could give rise to Boolean operators such as AND, N-IMPLIES, IDENTITY, and NOT gates, and the overall computation was determined by the number of cells involved and the types of each engineered cell. An example of a three-cell combination giving rise to an OR gate is shown in Figure 1.2. By adding NaCl and galactose, Cell type 1 and Cell type 5 produce α factor which activates Cell type 6 to produce GFP. Once constructed, the cell types can be combined in various ways to make many types of computational outputs in a simple fashion from a small library of cells. They predict that with only three inputs and three cell types, more than 100 functions can be obtained with this library (*10*). This work highlights the modularity of consortia and their ability to perform complex functions through the combination of only a few simple parts.

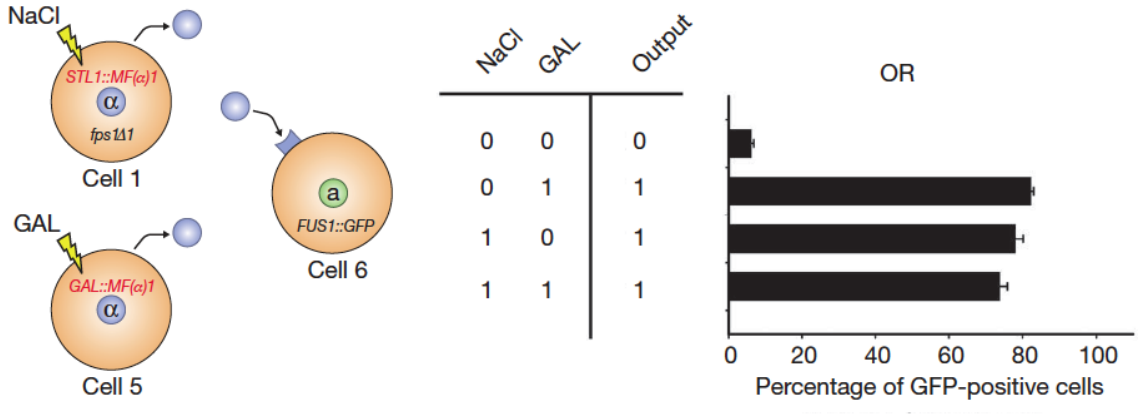

Figure 1.2 An example of an engineered multicellular OR gate using three yeast cells and two extracellular inputs, adapted from (*10*). 0.4 M NaCl and 2% galactose are added to the culture as shown in the table, and the resulting output GFP expression is plotted on the right.

In another interesting application of microbial consortia, biofilm formation and dispersal were controlled via quorum-sensing (QS) and engineered dispersal proteins Hha and BdcA expressed in two *E. coli* cells (a "colonizer" and a "disperser") (*12*). First the colonizer, tagged with RFP, was seeded onto a microfluidic device. This colonizer contained the engineered dispersal protein BdcA under control of the QS promoter P_{lasI}, and also constitutively-expressed the activator LasR. Next the dispersal cells were added to the device, which constitutively-expressed the 3oC12HSL (an acyl homoserine lactone, AHL, signal molecule) synthesis protein LasI. This molecule then bound to LasR in the colonizers, and activated expression of BdcA, causing removal of the colonizer biofilm. The GFP-tagged dispersers then remained until addition of IPTG, which induced expression of another dispersal protein, Hha, under control of the promoter $P_{T5\text{-}lac}$. When grown on the device, the dispersal cells were able to replace 80% of the colonizer cells at 44 hours, and after addition of IPTG, 92% of the disperser cells were then removed by 93 hours (*12*). This work demonstrates an effective way to remove engineered biofilms, which are often difficult to disperse, and may have significance in clinical applications (*12*). In the next section and in Section 3.2.3, synthetic consortia are discussed with an application to lignocellulosic biofuel production.

1.2 Consolidated bioprocessing for biofuel production

A field where microbial consortia are beginning to play a larger role is in the production of next-generation biofuels from lignocellulosic biomass. (Further discussion of feedstock choices, pre-treatment options, and production strains follows in Chapter 3. Here we discuss the role of microbial consortia in the biofuel production process). Consolidated bioprocessing is a process in which cellulase and hemicellulase production, saccharification, and fermentation or conversion of sugars to biofuels occurs in one reactor and has recently been touted as promising solution to current energy issues (*16, 17*). Since enzyme production contributes significantly to the overall cost of ethanol or other biofuel production (Figure 1.3) (*16*), combining this with the rest of the process may greatly reduce costs. Other advantages of CBP may include less cost due to reduced reactor volume, utilities, capital, substrate, and other raw materials. There is also a

possibility of higher hydrolysis rates due to synergy between the microbes and enzymes during production (*16*).

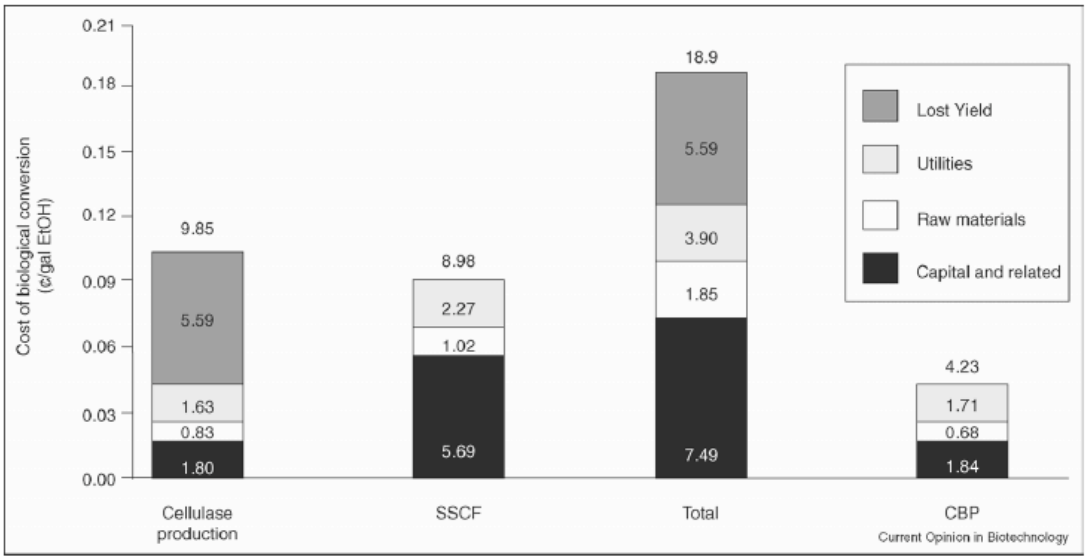

Figure 1.3 Cost of ethanol production for CBP vs. separate cellulase production and simultaneous saccharification and co-fermentation (SSCF) (adapted from (*16*)).

So far, however, no natural organism has been found that can accomplish all of these tasks efficiently and in industrially relevant production levels (*5*). Using a single- or multi-species, engineered or synthetic consortia, may be one way to achieve this goal. To illustrate the idea of enzyme-microbe synergy and modularity of synthetic consortia, a consortium of four yeast strains was engineered by Tsai *et al*. to produce three different cellulases as well as a scaffold protein, creating a synthetic surface-associated cellulosome for fermentation of ethanol from phosphoric acid-swollen cellulose (PASC) (Figure 1.4, (*8*)). In monoculture, only very low yields of ethanol had been obtained with a similar enzyme system, possibly due to the metabolic burden placed on the cells, but with this consortium approach the researchers were able to achieve yields of up to 0.475 g ethanol/g sugar consumed (93% of theoretical yield) by leveraging the modularity of the system (*8*). Since the consortium consists of four separate strains, the ratio between them could be tuned to optimize the release of sugars from cellulose, and subsequently the production of ethanol. While this is a great example of the utility of microbial consortia, the feedstock used here (PASC) is often prepared in such a way as to make it not cost-effective for industrial-scale production (*18*).

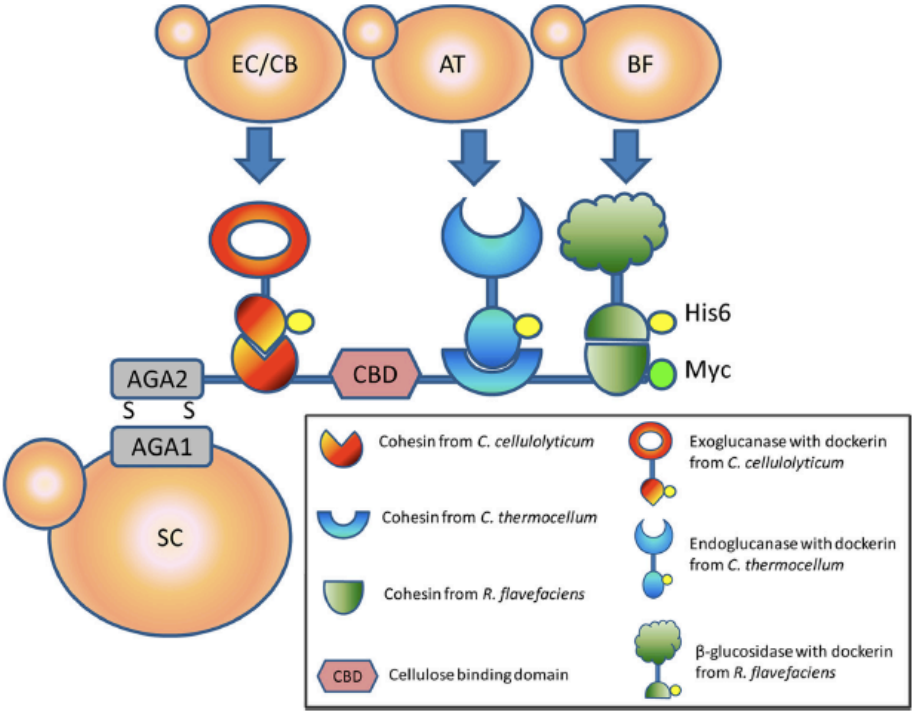

Figure 1.4 A synthetic yeast consortium for assembly of a synthetic cellulosome complex, adapted from (*8*). SC cells display scaffold proteins and the EC/CB, AT, and BF cells secrete cellulases.

Another recent example of a microbial consortium used in consolidated bioprocessing is that of work by Bokinsky *et al*., who engineered two *E. coli* strains to produce either cellulases or xylanases to break down ionic liquid (IL)-treated switchgrass and then convert the feedstock into biofuels or fuel precursors such as butanol, pinene, and fatty acid ethyl esters (FAEE) (*18*). By engineering the *E. coli* to secrete heterologous cellulases and xylanases from species such as *Clostridium stercorarium*, *Bacillus* sp. D04, and *Cellvibrio japonicus*, and also adding in heterologous pathways for product formation, they were able to achieve titers of up to 71 mg/L FAEE, 28 mg/L butanol, and 1.7 mg/L pinene without any external enzyme supplementation (*18*). However, this is only a "proof-of-concept" system at the moment, as the yields are much too low to be used in a commercial process, though it illustrates the promise of co-cultures in CBP systems for converting lignocellulosics directly into various biofuels.

1.3 Dissertation Overview

Our work involves engineering synthetic groups of microbial communities, or consortia, rather then a single microbe, or "superbug", for use in various applications.

Consortia may have numerous advantages over a singular species, such as adaptability, modularity, and robustness. The goal of this dissertation is to demonstrate the utility and benefits of synthetic microbial consortia with a specific application to lignocellulosic biofuel production. We hope to illustrate such advantages through specific tools and applications: a tunable, programmable circuit; production of isobutanol (a next-generation biofuel); and sensing/screening of metabolite secretion.

This project will make various contributions to the current state-of-the-art, including:

1. Demonstration of a method for controlling microbial consortia in a tunable manner, and for making such circuits programmable
2. A more efficient method of producing isobutanol from lignocellulosic biomass (corn stover) by a two-member *E. coli* consortium
3. A process for developing highly-secreting valine and isobutanol production strains and detection of such secretion via the use of cross-feeding auxotrophs

We also discuss our major results and contributions to the field and provide future directions for any ongoing work.

Chapter 2 Design and construction of a programmable, synthetic *E. coli* consortium via tunable symbiosis

2.1 Summary

Synthetic microbial consortia that can mimic natural systems have the potential to become a powerful biotechnology for various applications. One highly desirable feature of these consortia is that they can be precisely regulated. In this work we designed a programmable, symbiotic circuit that enables continuous tuning of the growth rate and composition of a synthetic consortium. We developed a basic model to capture the dynamics of a two-member consortium based on cross-feeding, and demonstrated that the growth rate and composition of such a consortium could be controlled via manipulating the export rate of the essential metabolites. We implemented our general design through the exchange of tryptophan and tyrosine by two *E. coli* auxotrophs. By regulating the expression of genes related to the export of tyrosine or production of tryptophan via inducible promoters, we were able to tune the metabolite exchanges and achieve a wide range of growth rates and strain ratios. In addition, by inverting the relationship of growth/ratio vs. inducer concentrations to create two-dimensional design space plots, we were able to "program" the co-culture for pre-specified attributes with the proper addition of inducers indicated by the plots. This programmable proof-of-concept circuit or its variants can be applied to more complex systems where precise tuning of the consortium would facilitate the optimization of specific objectives, such as increasing the overall efficiency of microbial production of biofuels or pharmaceuticals.

The majority of the work presented in the chapter has been published in PLoS ONE as follows: Kerner A, Park J, Williams A, Lin X. (2012) "A Programmable Escherichia coli Consortium via Tunable Symbiosis". *PloS ONE* 7(3): e34032. (*19*)

2.2 Introduction

Genetic circuits have been used in synthetic microbial consortia to construct programmable patterns (*20*), to render various relationships among consortium members (*9, 21, 22*), and to engineer artificial biofilms (*23, 24*). These systems were created mainly to mimic and investigate the dynamics or other properties of natural consortia and are very well suited for this task. On the other hand, there have been few efforts on developing genetic circuits to enable precise tuning of microbial consortia. The capability of precise regulation could be a crucial property for synthetic microbial consortia in various applications. For example, when two hexose- and pentose-specialists are used for optimal utilization of hexose and pentose sugars derived from lignocellulosic biomass, different ratios of the two strains might be desired depending on the composition of the feedstock.

In this work we have constructed a tunable, synthetic consortium of two *E. coli* auxotrophs which cross-feed and support each other when grown in co-culture. The ability to fine-tune this forced symbiosis is made possible via regulating the exchange of two amino acids (tryptophan and tyrosine) in a continuous manner. Depending on the amount of inducers added to the medium, we are able to obtain a wide range of growth rates and co-culture composition. This system is a proof-of-concept circuit that demonstrates the possibility of programming and tuning a synthetic microbial consortium. Additionally, there is evidence that mutualism may be a desirable symbiotic relationship for industrial processes because it may be more stable than other type of exchange interactions (*3*), and an engineered symbiosis such as the one presented here could help control consortium composition and ensure the prolonged existence of all members, as opposed to one member outcompeting slower-growing members.

2.2.1 General scheme and basic model for two cross-feeding auxotrophs

A general schematic of two cross-feeding, inter-dependent microbes is shown in Figure 2.1. In a minimal medium lacking key metabolites, these two microbes do not grow unless they exchange the required nutrients in an efficient manner. Previous work has suggested that such pair of microbes, when grown together in a batch co-culture and given suitable time for growth, reaches a pseudo steady state characterized by steady

concentrations of cross-fed metabolites and constant consortium composition (Reppas, Lin, *et al*., manuscript in preparation). Serial passaging experiments with auxotroph pairs indicated that this was indeed the case (data not shown). An ODE system was formulated to describe the growth dynamics of a general pair of cross-feeding auxotrophs, as shown in Figure 2.1A. Using Monod kinetics for cell growth on a limiting nutrient, the governing equations are as follows:

$$\frac{dn_1}{dt} = \mu_1 \cdot n_1 \qquad \frac{dn_2}{dt} = \mu_2 \cdot n_2$$

$$\frac{dc_1}{dt} = \alpha_2 \cdot n_2 - \beta_1 \cdot \frac{dn_1}{dt} \qquad \frac{dc_2}{dt} = \alpha_1 \cdot n_1 - \beta_{21} \cdot \frac{dn_2}{dt}$$

$$\mu_1 = \frac{k_1 \cdot c_1}{K_1 + c_1} \qquad \mu_2 = \frac{k_2 \cdot c_2}{K_2 + c_2}$$

where n_1 and n_2 are the cell densities of the two auxotrophs (gDM/L), c_1 and c_2 are the concentrations of the cross-fed metabolites (mM), α_1 and α_2 are the export rates of the metabolites from strain 1 and strain 2 (μmol/gDM-hr), and β_1 and β_2 are the cellular requirement of strain 1 and strain 2 for the essential metabolites (μmol/gDM), respectively. K_1 and K_2 are K_m values -- the concentrations (in mM) of Trp/Tyr when the growth rate of the W or Y strain is half of its maximal value. To model a batch co-culture in the minimal medium without supplementation of the cross-fed metabolites, c_1 and c_2 are set to zeros as the initial condition. Computer simulation showed that given sufficient time, the co-culture would reach a "pseudo steady state" with two characteristics: i) the ratio of the two auxotrophs remains constant, which indicates that they grow at the same rate; and ii) concentrations of the two cross-fed metabolites remain constant. By making use of these conditions we can readily derive the following analytical formulae [1], [2] to describe the system's growth rate, μ, and composition/ratio, r, at this pseudo steady state, as functions of the auxotrophs' properties.

$$\mu = \sqrt{\frac{\alpha_1 \cdot \alpha_2}{\beta_1 \cdot \beta_2}} \qquad [1]$$

$$r = \frac{n_2}{n_1} = \sqrt{\frac{\alpha_1 \cdot \beta_1}{\alpha_2 \cdot \beta_2}} \quad [2]$$

It therefore follows that at this pseudo steady state the growth rate of the co-culture, μ, which is the same as that of each auxotroph ($\mu = \mu_1 = \mu_2$) and the ratio of the two auxotrophs, r, are determined solely by the α and β parameters. At this pseudo steady state the two consortium members would have the same growth rate, and in addition, this growth rate of the co-culture and the ratio of the two microbes would be determined solely by each auxotroph's export rate of its partner's required metabolite and the auxotroph's growth requirement for the metabolite it lacks.

Based on this theoretical prediction, it should therefore be possible to control the co-culture growth rate and the ratio of the two microbes by manipulating either the auxotrophs' export of the two cross-fed metabolites (i.e. α_1 and α_2) or their cellular requirement for the metabolites (i.e. β_1 and β_2). The former strategy appeared more straightforward so we decided to explore the usage of chemical inducers to regulate the synthesis and transport pathways related to the export of the two cross-fed metabolites. We implemented the basic scheme described above with a specific pair of tryptophan and tyrosine *E. coli* auxotrophs, W3 and Y3 (Figure 2.1B). To tune the α experimentally, genes related to Trp and Tyr export were cloned behind inducible promoters that can produce a continuous range of expression levels. The Tyr auxotroph was then tagged with a fluorescent protein (YFP) to allow for determination of consortium composition (see Methods, Section 2.3.3 for details on the composition calibration). Following is a brief background on the choice of targets for increased synthesis and/or export of these two amino acids, as well as the specific implementation of the Basic Model with the Trp/Tyr pair. A complete strain list is given in the Methods, Section 2.3.2, Table 2.1.

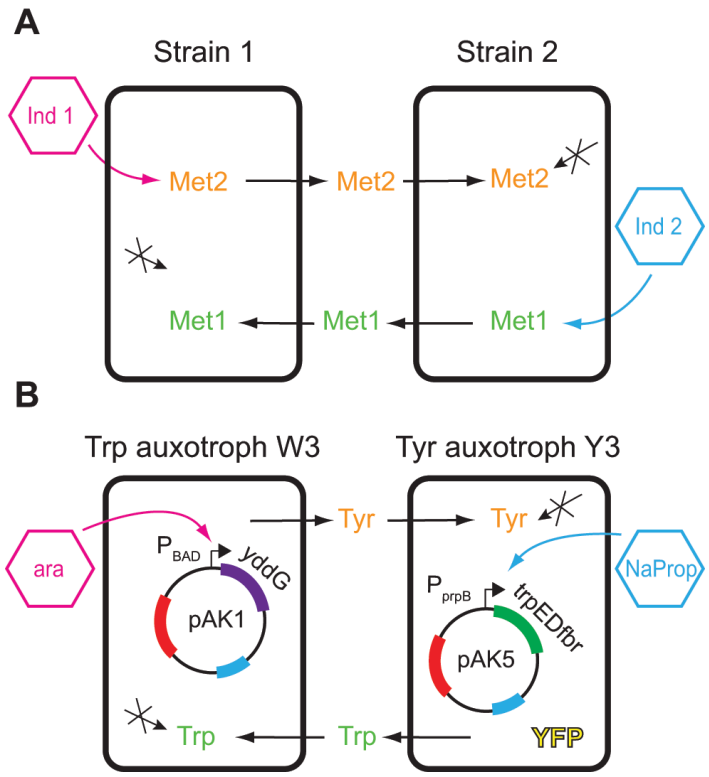

Figure 2.1 Basic schematic of the tunable cross-feeding circuit. (A) In this general design, inducer 1 and inducer 2 control the export of metabolites 1 and 2, respectively. The two auxotrophs must cross-feed in order to survive in the minimal medium. (B) In our specific implementation, two *E. coli* auxotrophic strains exchange tryptophan (Trp) and tyrosine (Tyr). The forced symbiosis is controlled by plasmids pAK1 (in the Trp auxotroph, W3) and pAK5 (in the Tyr auxotroph, Y3). Plasmid pAK1 contains gene *yddG* behind the tunable promoter P_{BAD}, and pAK5 contains *trpEDfbr* behind P_{prpB} (Methods). Strain Y3 is tagged with yellow fluorescent protein (YFP).

2.2.2 Tryptophan and tyrosine over-production

In order to tune the export rate (α) of either amino acid, one could manipulate the actual export of the molecule or attempt to overproduce the molecule, assuming that the extra Trp or Tyr would be exported and passed on to the partner strain. It would also be best to pick exporters and synthesis proteins that have a high specificity for the target amino acid. So far only one aromatic amino acid exporter has been identified, the inner membrane protein YddG which, when over-expressed in *E. coli*, has been shown to increase the export of all three aromatic amino acids from corresponding, engineered Phe-, Tyr-, or Trp-producers, although this may not be its primary function (*25*). Since this protein increases the amount of Tyr in the medium more than Trp (3-fold increase versus 1.5-fold), it was chosen for regulating the export of Tyr in strain W3. When studying the effect of YddG over-expression, Doroshenko *et al.* (2007) also knocked out

the function of the TyrR protein in their aromatic amino acid over-producers. TyrR is a transcriptional regulator with a regulon comprising at least eight transcription units, all having some relation to the central aromatic biosynthesis pathway or aromatic transport (*26*). Genes in the pathway that are regulated by TyrR include: *aroF*, *aroG*, and *aroL* (see pathway in Figure 2.2 below, genes boxed). When *tyrR* is knocked out, the activity of the *aroF* and *aroG* promoters were strongly upregulated indicating increased production of these enzymes (*26*). Due to this effect, the *tyrR* gene has also been knocked out in W3, since this may increase the carbon flux through the tyrosine pathway by up-regulating genes upstream of *tyrAB* and possibly increase the chance that manipulating YddG production will have an effect (in our preliminary studies with YddG manipulation there was an insignificant effect until *tyrR* was knocked out).

On the other side of the circuit, we could have tuned protein YddG in the Tyr auxotroph (strain Y3) as well, but the nonspecific export of Tyr and Trp is not the most desirable control target. There may be some complex response resulting from the export of both molecules from an auxotroph that still needs one of them supplied from the medium. Since the over-production of Trp has been very well studied and several mechanisms to render pathway enzymes feedback-resistant have also been elucidated (*27-29*), we chose to control the biosynthesis of Trp and therefore its export to the W3 strain, as no Trp-specific export protein has yet been identified. One method of Trp over-production is to mutate the *trpE* gene, which encodes subunit I of the first enzyme complex in the Trp biosynthetic pathway, anthranilate synthase-phosphoribosyl transferase (AS-PT) (see Figure 2.2, genes highlighted in blue). The AS-PT complex is a heterotetramer, composed of two molecules of TrpE protein and two molecules of TrpD, which is allosterically feedback-inhibited by Trp binding to the TrpE subunit (*30*). Trp binding to TrpE is sequential and cooperative with a hill coefficient of ~1.2, but one Trp molecule can inhibit the entire structure due to a conformational change that occurs when Trp binds (*31, 32*). Over-expressing a mutant *TrpE* protein that is unable to bind Trp, therefore, should confer resistance to Trp or to analogues such as 5-methyltryptophan (5-MT). Over-expressing these feedback-resistant genes has in fact been the most popular method of Trp over-production, either alone or with the entire Trp operon (*27, 28, 33, 34*).

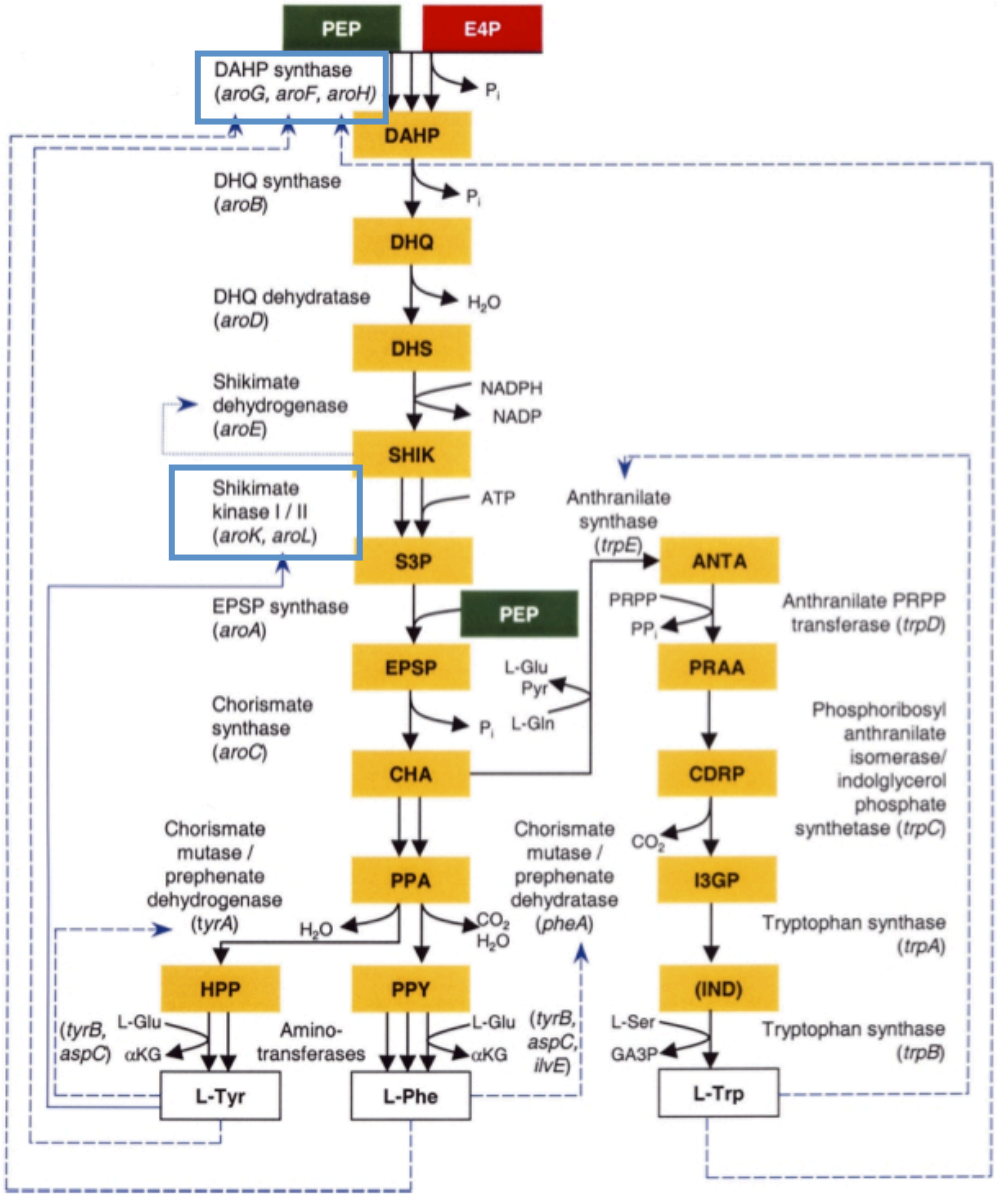

Figure 2.2 Aromatic amino acid biosynthetic pathway. Figure adapted from (*29*). Key abbreviations: PEP: phosphoenolpyruvate; E4P: erythrose 4-phosphate; DAHP: 3-deoxy-D-arobinoheptulosonate 7-phophate; SHIK: shikimate; S3P: shikimate 3-phosphate; CHA: chorisimate; ANTA: anthranilate; PRAA: phosphoribosyl anthranilate. Dotted and dashed lines indicate feedback inhibition.

Based on this previous knowledge, a feedback-resistant mutant of anthranilate synthase (*trpE*) was chosen for over-expression and regulation. The gene construct *trpEDfbr* was commercially synthesized with the mutation S40F inserted into the *trpE* gene. The mutation S40F is an amino acid change from serine to phenylalanine at position 40. Caligiuri and Bauerle (1991) previously mutated plasmids carrying only the

S. typhimurium trpE gene to screen for feedback-resistant mutants when expressed in *E. coli* (*35*). Four mutations were found that conferred a complete loss of inhibition, one of which was the S40F mutation. This site was also one of five sites identified for Trp binding in the *S. marcescens* TrpE subunit; the sequence of this region is conserved among *E. coli*, *S. marcescens*, and *S. typhimurium* (*32*). Both the *trpE* and *trpD* genes were included on the synthesized vector because they encode two subunits of one enzyme complex and we hypothesized it would be best to make sure they are at the same expression level in the cell by placing them both under control of an inducible promoter. Some studies on Trp over-production have amplified and over-expressed the entire Trp operon, however we did not think this was necessary since several studies over-expressing only up to *trpD* or *trpC* have been effective (*35*). The mutated *trpE* and *trpD* genes are expressed together on the plasmid, while the natural Trp promoter will control the *trpC-A* genes on the chromosome (Figure 2.3). The Trp operon suffers from transcriptional attenuation by the binding of two Trp molecules to TrpR, which then binds to the *trpL* leader region, as depicted in Figure 2.3 (*31, 36*). If there is enough intracellular Trp in the Y3 strain to bind to TrpR and inhibit expression from the Trp promoter, *trpC, trpB* and *trpA* can still be transcribed from the internal promoter located in the *trpD* gene (*36*). This promoter, called *trp-p2*, was found to function at 1/6 the level of the principal *trp* promoter in a galactokinase assay, but still at 1/3 the level of the *galP* promoter (used as standard and considered to be a high-level promoter) (*37*). A map of this plasmid is shown in Figure 2.1.

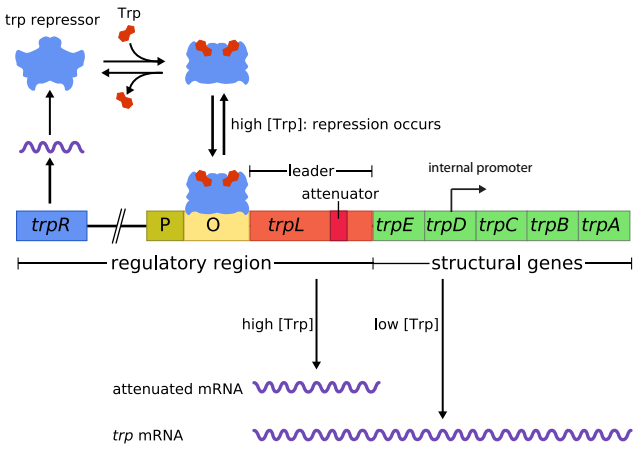

Figure 2.3 Trp operon and regulatory region, modified from (*38*). Two molecules of Trp bind to the Trp operon repressor, TrpR, which then represses the Trp operon by binding to the trpL leader region (*31, 36*).

2.2.3 Choosing suitable inducible promoters

To induce and tune the above genes chosen for regulation of Trp/Tyr export, it would be best to choose two inducible promoters that function simultaneously and do not exhibit crosstalk. There are a number of inducible promoters available for use in *E. coli* but not all of them are tunable or able to produce a large expression gradient (*39*). After comprehensive review of related literature, two compatible promoters were chosen: the arabinose-inducible promoter P_{BAD} and a recently created propionate-inducible promoter, P_{prpB}. Unfortunately, these two promoters do suffer from catabolite repression, meaning that they are repressed by the glucose used as a carbon source in our minimal medium. However, we were still able to obtain a large gradient of expression with each promoter in minimal M9 medium (Figure 2.4) and did not see crosstalk when the promoters were used together (*40, 41*) (Figure 2.4).

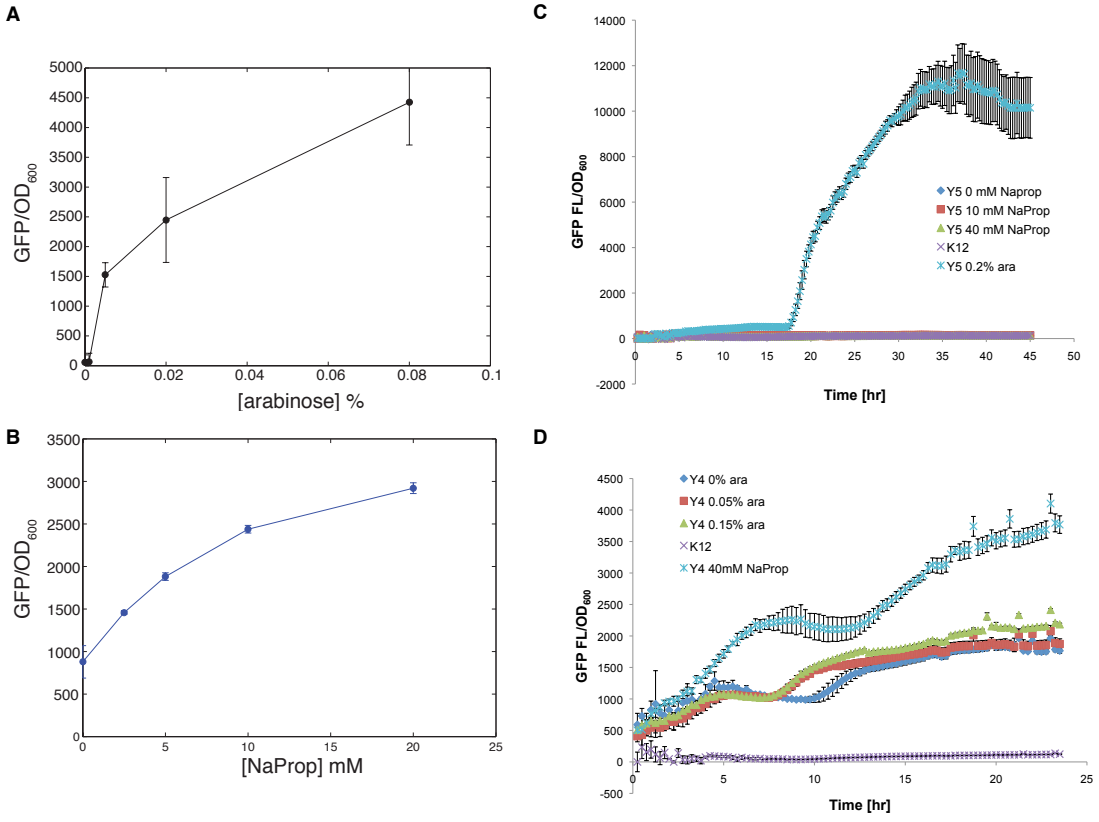

Figure 2.4 Relationship between gene expression level, measured by GFP/OD_{600}, and inducer concentration for the P_{BAD} (A) and P_{prpB} (B) promoters. Inducers were added to cultures of single strains expressing GFP

behind either the arabinose- or propionate-inducible promoters. (A) Strain W5 and (B) strain Y4. Growth and fluorescence data were taken from the end of exponential growth phase when the expression level was constant. P_{BAD} (C) and P_{prpB} (D) do not suffer from cross talk between the promoter and the other's inducer so they can be used together in co-culture. P_{prpB} seems to be leakier than P_{BAD}. The strains used were all tyrosine auxotrophs since only the effect of each inducer on GFP expression from the opposing promoter was being investigated (in this particular experiment). Strain list given in Table 2.1.

2.2.4 Basic model implementation with *E. coli* strains W3 and Y3

To adapt the basic, general model to our cross-feeding Trp and Tyr auxotrophs, we needed to derive an equation to capture the tuning of the export parameter, α, which is controlled by the two chosen inducers, arabinose and propionate. To do this we used a Hill function to model the effect of the inducer-activator complex binding to its respective promoter and inducing gene expression. The general form of this equation is given below [3]. From expression assays with GFP as the reporter protein (Figure 2.4), the best Hill coefficient for P_{BAD} was n = 1.5 and for P_{prpB} was n = 1. The values for the α_0 and α_1 varied according to the strain and the baseline GFP expression of the promoter. Here the α_1 does not refer to the export from strain 1, but is a scaling factor that is dependent on the level of fluorescence.

$$\alpha = \alpha_0 + \alpha_1 \cdot \left(\frac{[ind]^n}{K+[ind]^n}\right) \quad [3]$$

The pseudo steady state total growth rate (μ) and Y3:W3 ratio (r) were plotted over a grid of inducer concentrations. The basic model predicts that as the inducers increase, the growth rate would also increase (Figure 2.5A). This is expected since increasing the inducer concentration increases the cross-feeding. The model also predicts that the highest Y3:W3 ratios will occur at high [inducer 1] and low [inducer 2], and vice versa (Figure 2.5B). This is also an expected result: there will be more of the Y3 strain when W3 is producing the most Tyr and Y3 is producing the least Trp. (Note: graph (A) has the origin (0,0) in front for ease of viewing, whereas graph (B) has the point (5,5) in front). Here we have just used generic inducers, so the units are not shown.

Based on these simulation results, we then tested the circuit experimentally and saw unexpected growth dynamics, discussed in the Results section below. We further refined the model to attempt to capture these dynamics, which is discussed in Section 2.4.3.

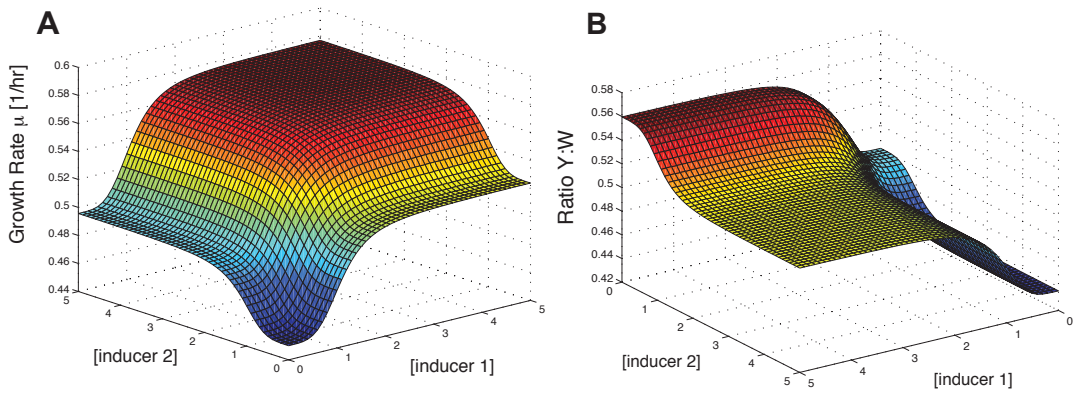

Figure 2.5 Basic model simulation results. Growth rate (A) and Y:W ratio (B) surface plots generated by varying inducer 1 and inducer 2 from 0 to 5 units.

2.3 Methods

2.3.1 Auxotroph construction and YFP addition

A Trp auxotroph, strain W1, was constructed via P1 transduction (*42*) of the *trpE* gene replaced with a KanR cassette from Keio collection strain JW1469-1 (*43*) into wild-type *E. coli* K12 MG1655. P1-facilitated gene deletion was repeated in strain W1 with the *tyrR* gene (JW1316), to obtain strain W2, a double knockout, and was also used to knock out the *tyrA* gene (JW2581) to create the Tyr auxotroph, strain Y1. The *yfp* gene was introduced into strain Y1 via the same method (host strain DS1-Y was obtained from the Balaban group, Hebrew University of Jerusalem) and was integrated into the *intC* locus with a *cat* selection cassette (strain Y2). This gene is under control of two λP_R promoters (*44*). The *trpE* and *tyrA* gene knockouts were confirmed via colony PCR, as well as phenotypically by growing the strains alone in unsupplemented M9 medium after each genetic manipulation. None of the auxotrophs grew without its partner strain (data not shown).

2.3.2 Plasmid construction

The arabinose-inducible promoter P_{BAD} was amplified from strain BW31003 (CGSC #8183) digested with restriction endonucleases NdeI and HindIII, and ligated to the pET17 expression vector (Novagen). The *yddG* gene was amplified from wild-type *E. coli* MG1655, digested with XhoI and HindIII, and ligated to the pET17-P_{BAD} construct

giving vector pAK1. This vector was transformed into the W2 strain, producing strain W3. The *trpEDfbr* gene cassette was synthesized (Geneart) and then cut with SalI and EcoRI and ligated to the pPro24-gfp vector behind the propionate-inducible promoter P_{prpB} with GFP removed (Addgene). This vector was then transformed into strain Y2, giving strain Y3. Both plasmids confer ampicillin resistance.

Table 2.1 Complete strain list for Chapter 2.

Auxotrophy	Name	Genotype	Vector genes
Tryptophan	W1	*K12 ΔtrpE::kanR*	/
	W2	*K12 ΔtrpE ΔtyrR::kanR*	/
	W3	*K12 ΔtrpE ΔtyrR::kanR pAK1*	P_{BAD}-yddG AmpR
	W4	*K12 ΔtrpE ΔtyrR::kanR pCFP*	P_{BAD}-cfp AmpR
	W5	*K12 bioA::λRed ΔtrpABCDE::cat pGFP*	P_{BAD}-gfp AmpR
Tyrosine	Y1	*K12 ΔtyrA::kanR*	/
	Y2	*K12 ΔtyrA::kanR intC::yfp*	/
	Y3	*K12 ΔtyrA::kanR intC::yfp pAK5*	P_{prpB}-trpEDfbr AmpR
	Y4	*K12 ΔtyrA::kanR intC::yfp pPro24-gfp*	P_{prpB}-gfp AmpR
	Y5	*K12 bioA::λRed ΔtyrA::cat pGFP*	P_{BAD}-gfp AmpR

2.3.3 Co-culture composition determination using YFP

Minimal M9 medium containing 0.2% glucose was used in all experiments. For circuit induction, either arabinose (20% w/v stock) or sodium propionate (1 M stock) was used at the indicated concentration. Frozen stocks were inoculated into rich LB medium and grown overnight to saturation. The cells were then washed and diluted by 1:800 into fresh minimal M9 medium and the appropriate inducers were added. Cultures were then pipetted onto a 96-well microplate (Grenier) to a volume of 200 µl per well. Unless otherwise stated, four replicates were conducted per sample. A Biotek Synergy 2 microplate reader was used to monitor co-culture growth and composition over time via reading the absorbance at 600 nm and the YFP fluorescence using filters for excitation (485/20) and emission (528/20). For each microplate growth experiment, calibration between the Y3 strain OD_{600} and the fluorescence (FL) was obtained by plotting the FL vs. the OD_{600} and fitting the data with a linear model (see Figure 2.6 for a sample calibration curve). The slope was then used to determine the Y3 density in the co-culture (note that we could have also considered the "fluorescence" of the W3 strain, but it did not significantly change the results). The W3 density was obtained by subtracting the Y3

density from the total OD_{600}. The ratio Y3:W3 is then equal to the density of Y3 divided by the density of W3. Cultures were grown for 48 hours at 37°C with shaking and measurements were taken every 15 minutes.

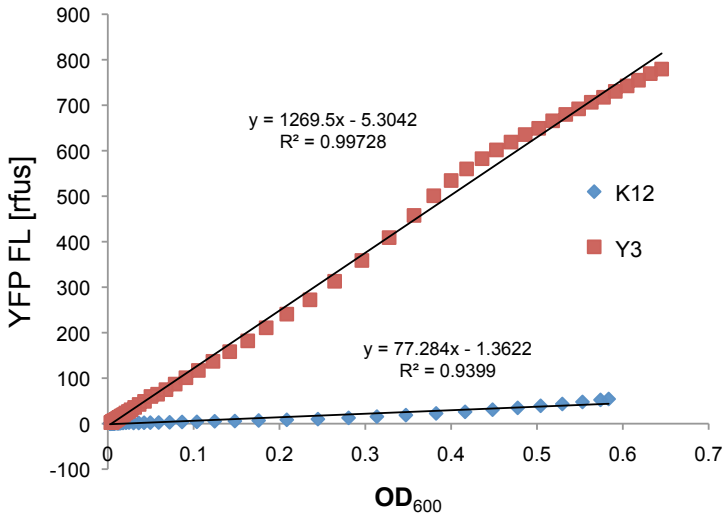

Figure 2.6 Sample YFP calibration. Four replicates of each of K12 and Y3 were averaged, and then the YFP FL readout was plotted against the OD_{600}. The calibrations are linear during the exponential phase of growth, which is shown in the graph. Excel was used to fit the data using linear regression.

To validate our method for determining the co-culture composition using YFP, we tested four co-culture samples and compared ratio results obtained via the above method and differential plate counting (i.e. using viable cell counts from minimal medium petri dishes supplemented with Trp or Tyr). The co-cultures were grown and monitored on a microplate reader. Based on manual inspection of the growth curve, each co-culture was stopped either in the middle or at the end of exponential growth whereupon samples were extracted for differential plate counting (note that it is virtually impossible to continue a microplate growth experiment once it is stopped and the lid removed, due to technical complications and the risk of contamination). Out of the four tested samples, three showed reasonable agreement between the ratio results from the two different methods (Figure 2.7). In addition, we observed that when the ratio is close to one and does not change rapidly, the result from YFP calibration is in excellent agreement with that from plate counting and the error bar is very small. However, when the ratio deviates substantially from one and fluctuates over time (e.g. Figure 2.9B, the condition of 0.15%

arabinose), the result from YFP calibration tends to be much less accurate and the error bar becomes much larger.

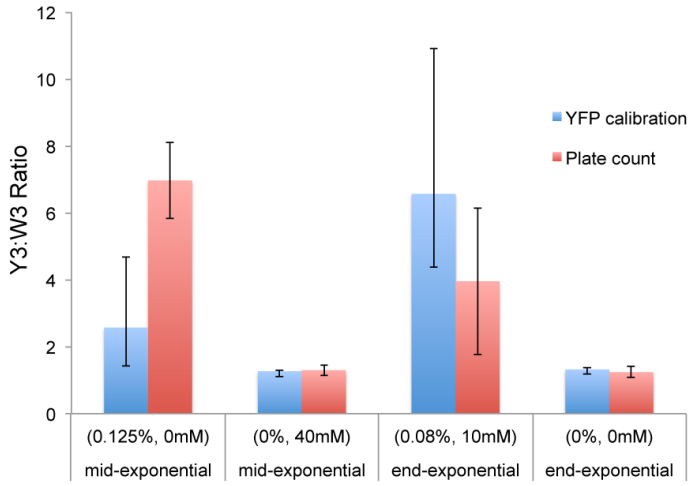

Figure 2.7 Comparison of Y3:W3 ratio results determined using YFP calibration vs. plate counting. For each co-culture condition, four wells (replicates) were used to determine the Y3:W3 ratio using the YFP calibration method. After a certain period of time, the microplate reader was stopped and the four wells were pooled and plated on M9 minimal plates with either Trp or Tyr. Each co-culture was diluted appropriately to give 30 - 300 colonies per plate for accurate counting. The ratio was then calculated using all combinations of the Y3 cell count from Tyr+ plates and that of W3 from Trp+ plates.

2.3.4 Measurement of Trp and Tyr concentrations in mono- and co-culture supernatants

Concentrations of Trp and Tyr in mono- and co-cultures were estimated using a bioassay similar to one previously reported (*21*). The cultures were grown in 10 ml M9 media in 50-ml falcon tubes. The monocultures were also supplemented with saturating amounts of Trp and Tyr (40 µg/ml). Inducers were added as needed. 1-ml samples were harvested at various time points over the course of growth corresponding to the early, middle and late exponential growth phases. The OD_{600} of the cultures was monitored over time to identify these points. The 1-ml samples were centrifuged at 12,000 rpm and the supernatants were sterile-filtered and stored at -20^{o}C. An auxotrophic test strain, W1 or Y1, was grown on the sterilized culture supernatants supplemented with concentrated M9 (400 µl supernatant and 100 µl 5X M9). The maximum OD_{600} reading was then used to determine the initial Trp or Tyr concentration in each supernatant, according to a

calibration curve. The Trp and Tyr calibration curves were prepared as follows. Standard dilutions of Trp or Tyr stocks were made with M9 media and then the corresponding auxotrophic test strain was grown on each standard for about 48 hours on a microplate reader at 37^{o}C with shaking. OD_{600} measurements were taken every 15 minutes, and the maximum OD_{600} of each sample was used to generate the calibration curve.

2.3.5 Measurement of Trp and Tyr Affinities

Each strain (either W3 or Y3) was grown alone in M9 with specified amounts of Trp or Tyr at various inducer concentrations to determine the effect of the inducer on the strain's affinity and maximum growth rate. More specifically, cells were first grown overnight in minimal M9 media with saturating amounts of Trp or Tyr (40 μg/ml). The cells were then washed three times in M9 and diluted to a final density of ~1000 cells/ml in 50 ml M9 in a 250 ml flask supplemented with the desired metabolite and inducer concentrations. The cultures were grown at 37^{o}C in a shaking water bath and the initial growth rate was measured via plate counting. The range and spacing of sampling times were dependent on the expected growth rate of the culture. For each initial Trp or Tyr concentration, after obtaining the cell counts, the exponential growth rate and goodness of fit (the error bar shown at each point in Figure 2.8) were determined using Excel. Finally, the Matlab curve-fitting tool was used to fit each curve of growth-rate vs. Trp/Tyr concentration to a Monod function and to obtain the μ^{max} and K_m values.

2.3.6 3D surface and design space plots

Experimental 3D surface results and design spaces were plotted using MATLAB. For the growth and ratio results, interpolation was carried out (griddata) and the results were used to plot the 3D surfaces. To create the design spaces, griddata was again used to obtain points across a continuous space and then a closed contour plot (contourf) was created using the interpolated results.

2.4 Results

2.4.1 Effect of inducers on metabolite secretion and growth properties of engineered strains

To verify the effect of increased metabolite secretion induced by the genetic circuit constructed above, we performed a bioassay (*21*) to determine the amount of Trp and Tyr in W3 and Y3 monocultures. Each of these engineered strains was grown alone in the minimal medium with and without the corresponding inducer. The culture supernatants were then harvested at times corresponding to the early, middle, and late stages of the exponential growth phase. A test strain, either a Tyr or Trp auxotroph, was then grown on the sterile-filtered supernatant to determine the concentration of the secreted amino acid using a similarly derived calibration curve (Methods). As summarized in Table 2.2 and Table 2.3, we observed that, overall, addition of the inducer did increase the secretion of Trp or Tyr when each strain was grown in mono-culture. More specifically, for strain Y3, when the propionate inducer concentration was raised from 0 to 40 mM the amount of secreted Trp per cell at the end of exponential growth decreased slightly at first and then more than tripled, leading to a maximum Trp concentration of 142 ± 9 μg/L in the supernatant, corresponding to a culture-averaged secretion of 0.33 ± 0.00 μg/L/OD. Interestingly, the amount of Tyr secreted by strain W3 was over 100 fold higher, in the range of a few to several tens of mg/L in the supernatant. When the arabinose inducer was added, the amount of extracellular Tyr accumulated in the mono-culture became so high that it was detectable starting in the early exponential growth phase and steadily increased both as growth proceeded and as the inducer concentration was raised to 0.15%, reaching concentrations > 31 mg/L, corresponding to a culture-averaged secretion level > 300 mg/L/OD (Table 2.2, Table 2.3).

Table 2.2 Culture-averaged secretion of Tyr and Trp in mono-culture growth experiments. Over the course of growth, W3 secretes more Tyr per cell with the addition of arabinose and Y3 secretes more Trp per cell with the addition of NaProp. Supernatants were harvested at the early, middle stages, and the end of the exponential growth phase. Note the different units of Trp and Tyr (i.e. μg/L/OD vs. mg/L/OD), which reflect the vast difference between the metabolite secretion capacities of the two strains. N/D: not detectable.

Secreted Metabolite	Culture	Time point	
		middle	end
Trp/OD [μg/L/OD]	Y3	N/D	0.095 ± 0.002
	Y3 + 10mM NaProp	N/D	0.063 ± 0.000
	Y3 + 40mM NaProp	N/D	0.33 ± 0.00
Tyr/OD [mg/L/OD]	W3	N/D	9.8 ± 0.0
	W3 + 0.08% ara	40.0 ± 0.0	56.2 ± 0.2
	W3 + 0.15% ara	**>300**	**>125**

In addition to the effect on metabolite secretion, it is also possible that inducing the genetic circuit constructed above may change the growth property of the engineered strains, in particular their nutrient uptake capabilities. For instance, since YddG can also export Trp to some degree (*25*), we suspected that the expression of this protein on the pAK1 vector may decrease its "affinity" for Trp and thereby increase the apparent K_m value of W3 for the molecule. Therefore, for each strain, we conducted a set of flask experiments to evaluate the inducer's effect on the strain's maximum growth rate and affinity for its essential metabolite (described in Methods, Section 2.3.5). It was found that for each strain, the corresponding inducer had a negative effect on the maximum growth rate (Figure 2.8). In particular, the observed growth rate of W3 and Y3 decreased from about 0.6 1/hr to 0.2-0.3 1/hr when the inducer of arabinose or propionate was added. Additional experiments at saturated Trp or Tyr concentrations confirmed these observations, including the unusual trend that the maximum growth rate of strain W3 decreases and then slightly recovers when the arabinose concentration increases (Figure 2.8A and Figure 2.12).

Subsequently, by comparing the growth of various strains at saturated Trp or Tyr concentrations, we found that the growth rate decrease of W3 is caused by the pAK1 plasmid, whereas the growth of Y3 is significantly reduced due to the over-expression of the *trpEDfbr* genes on plasmid pAK5 as well as slight inhibition by the propionate inducer (Figure 2.12). This substantial growth decrease of the individual strains caused by induction of the cross-feeding circuit, termed metabolic burden, had a significant impact on the co-culture's property, as will be discussed in the next section. On the other

hand, with the addition of inducers, the affinity parameters of the engineered strains appeared to have remained at comparable values, in the ranges of 2-4 µg/L Trp for W3 and 5-8 µg/L Tyr for Y3 (Figure 2.8).

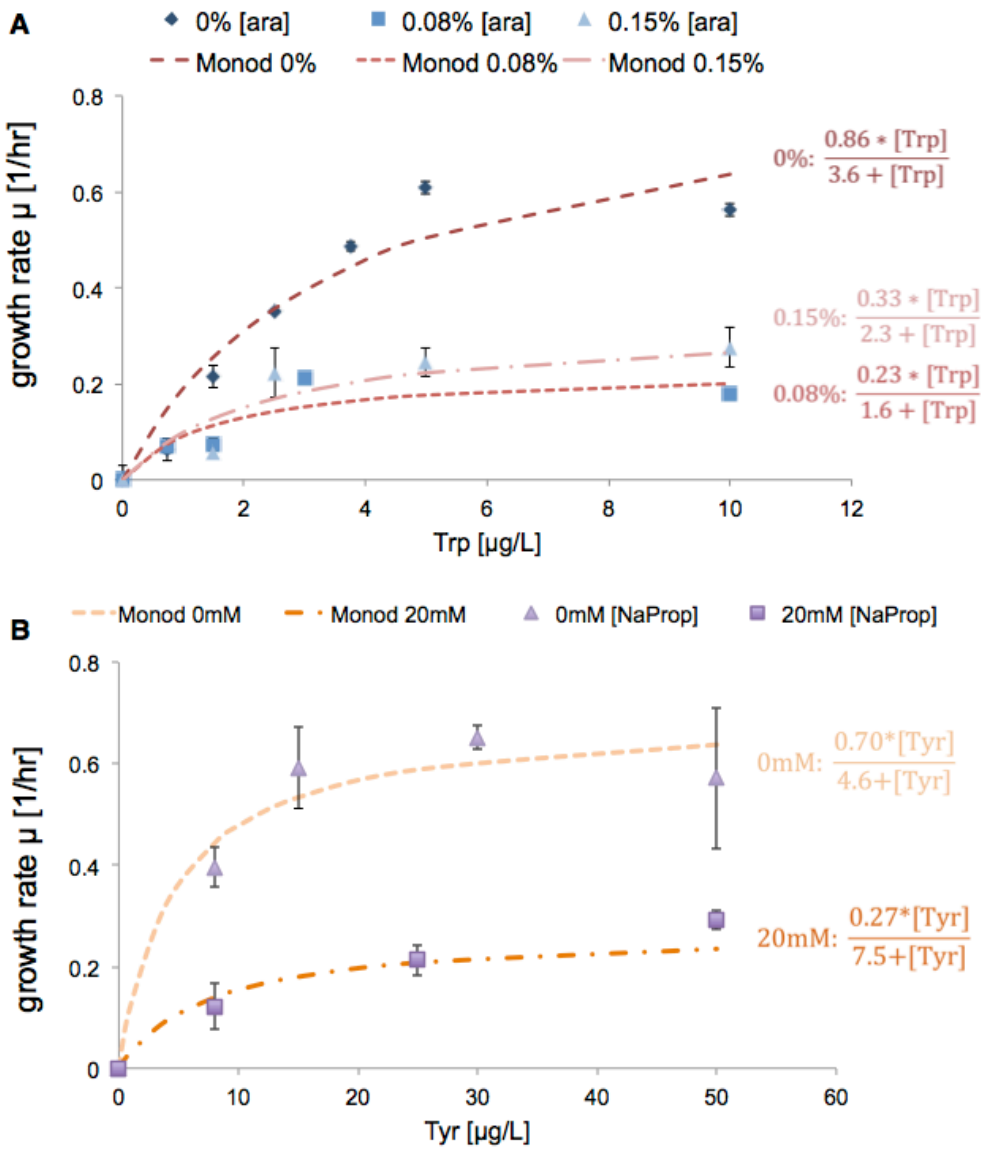

Figure 2.8 Growth rates of W3 and Y3 at various Trp and Tyr concentrations. The maximum growth rates and affinity of W3 for Trp (A) and of Y3 for Tyr (B) were measured under inducing and non-inducing conditions. The Matlab curve-fitting tool was used to fit each growth curve to a Monod function and to obtain the μ^{max} and K_m values. The error bars at each point on the growth curve represent the goodness of the exponential growth curve fit. The R^2 values for each Monod fit are as follows: W3 - 0%, 0.92; 0.08%, 0.82; 0.015%, 0.87; and Y3 - 0 mM, 0.96; 20 mM, 0.88.

2.4.2 Changes in the consortium growth and composition

The Trp and Tyr auxotroph pair constructed above was first grown in M9 minimal medium for examination of the baseline property without arabinose or propionate (Figure 2.9). The growth rate of the co-culture, inoculated with a 1:1 strain ratio, was found to be 0.45 ± 0.004 1/hr. To determine the ratio (Y3:W3) of the two auxotrophs, a constitutively expressed YFP gene was integrated into the chromosome of strain Y3. By combining total OD and YFP measurements, we were able to obtain the ratio of the two strains during growth (see Methods 2.3), however it was observed that the co-culture was not reaching a steady composition (Figure 2.9) as predicted by the model described in Section 2.2.1. This might be because the co-culture had entered the stationary phase before reaching the pseudo steady state.

Further experiments revealed that the co-culture exhibits various ratio dynamics when the inducers are added. An example is shown in Figure 2.9, in which arabinose was added at different concentrations when propionate was held constant. Depending on the concentration of arabinose, the ratio could monotonically change to a final steady value or exhibit more nonlinear behavior. After observing these complex dynamics, we decided that instead of choosing one value to represent the co-culture "ratio" it would be better to examine the Y3:W3 ratio in the middle and at the end of the exponential growth phase, henceforth referred to as the mid-exponential and end-exponential ratios, respectively. At the baseline without inducers, the mid-exponential Y3:W3 ratio was found to be 0.66 ± 0.02, and the end-exponential ratio to be about 4.41 ± 0.05.

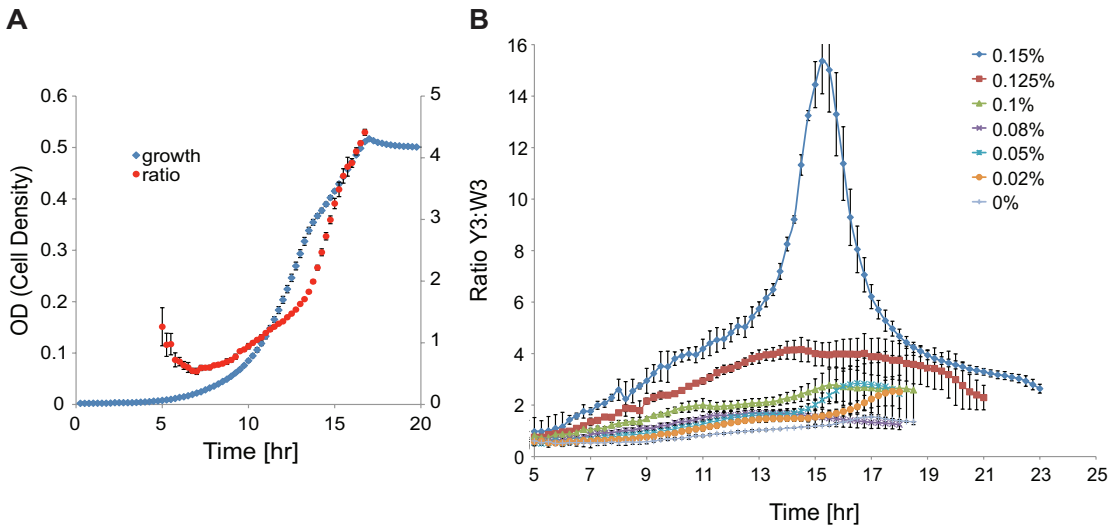

Figure 2.9 Co-culture growth and ratio dynamics: baseline and with tuning. (A) Co-culture density (measured by OD_{600}) and Y3:W3 ratio during growth in minimal medium without inducers. The ratio measurement is shown only for the exponential growth phase because the YFP calibration is not reliable after the cells enter the stationary phase. (B) An example of Y3:W3 ratio dynamics at various arabinose concentrations. Propionate concentration was held at 20 mM. Only the exponential growth phase is shown. Each curve represents the mean of four replicates. Note: the secondary y-axis label in (A), Ratio Y3:W3, is also the label for the primary y-axis in (B).

By simultaneously adding the two inducers that regulate the metabolic cross-feeding circuit, we were indeed able to change the growth rate and composition of the synthetic consortium (Figure 2.10). Overall we achieved a fairly large range of co-culture growth rate (0.16 – 0.59 1/hr, Figure 2.10A), mid-exponential ratio (13 to 0.6, Figure 2.10B), and end-exponential ratio (9.7 to 0.9, Figure 2.10C). Adding the inducers, however, does not affect these co-culture properties in the simple manner our basic model suggested. Instead, the relationship between the co-culture growth rate and inducer concentrations is highly nonlinear, which can be illustrated with the two edges where only one inducer is involved. When only arabinose is added (Figure 2.10D), increasing arabinose caused the co-culture growth rate to increase from 0.45 1/hr to 0.58 1/hr at 0.08% arabinose, supposedly due to increased secretion of Tyr by strain W3 as demonstrated by the bioassay described in the previous section. Further increasing the arabinose concentration to 0.15%, unexpectedly, decreased the co-culture growth rate sharply to 0.20 1/hr. On the other hand, when only propionate is added, the co-culture growth rate monotonically decreased from 0.46 to 0.30 1/hr (Figure 2.10E).

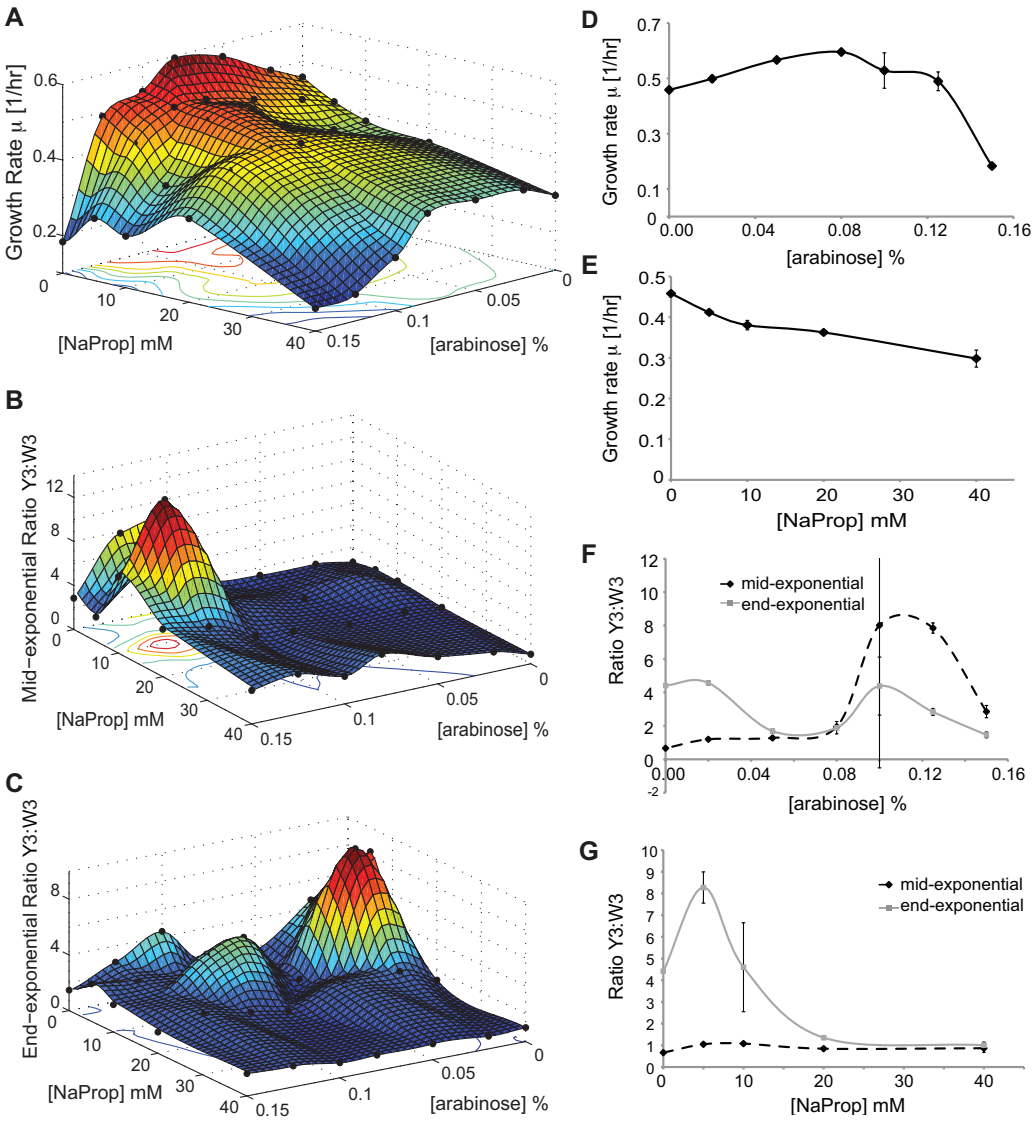

Figure 2.10 Range of co-culture growth rate and composition regulated by two inducers. Co-culture experiments were conducted over a grid of inducer concentrations. The experimental results (black dots) were then interpolated using Matlab to create a three-dimensional surface. Range of co-culture growth rate (A), mid-exponential Y3:W3 ratio (B), and end-exponential Y3:W3 ratio (C) that can be achieved using this circuit. (D, E, F, G) Edges of the 3D surfaces. Effect of tuning arabinose and propionate on the growth rate (D, E) and Y3:W3 ratios (F, G). (D, F) 0mM propionate (E, G) 0% arabinose. Both the mid-exponential and end-exponential ratio were determined using the YFP calibration.

We also observed highly nonlinear dependence of the co-culture composition on inducer concentrations (Figure 2.10). Interestingly, when two edges of the 3-D plots were examined more closely, tuning the W3 strain through arabinose seemed to have more of an effect on the mid-exponential ratio (Figure 2.10F), whereas tuning the Y3 strain

through propionate seemed to have more of an effect on the end-exponential ratio (Figure 2.10G).

The observed relationships between consortium properties (i.e. growth rate and strain ratio) and inducer concentrations are quite complex and nonlinear. This is likely due to multiple factors affecting the growth dynamics of our system, most importantly each inducer's double effect of increasing metabolite secretion while decreasing growth.

To verify the effect of regulated cross-feeding on the co-culture growth, we carried out two sets of negative control experiments in which the cross-feeding auxotroph pair was exactly the same as W3 - Y3 except that either the *yddG* gene in W3 or the *trpEDfbr* genes in Y3 was replaced by a negative control gene that does not participate in the cross-feeding circuit (i.e. CFP or GFP). It was observed that when *yddG* was not over-expressed in the tryptophan auxotroph, adding arabinose did not affect the co-culture growth (Figure 2.11A). Furthermore, at low concentrations of arabinose, the negative control pair grew more slowly than the pair with the full circuit. On the other side, when *trpEDfbr* was not expressed in the tyrosine auxotroph, adding propionate reduced the co-culture growth rate substantially (Figure 2.11B). Notably, the pair with the full circuit grew faster than this negative control pair when propionate is at medium to high concentrations. These results indicate that tuning the target genes in the designed circuit is indeed regulating the cross-feeding and hence the co-culture growth. Clearly there is a side effect of metabolic burden from this circuit, and regulation of the co-culture is more effective when the enhanced cross-feeding is not over-shadowed by the burden (for example when the arabinose concentration is not too high and propionate is at medium to high levels).

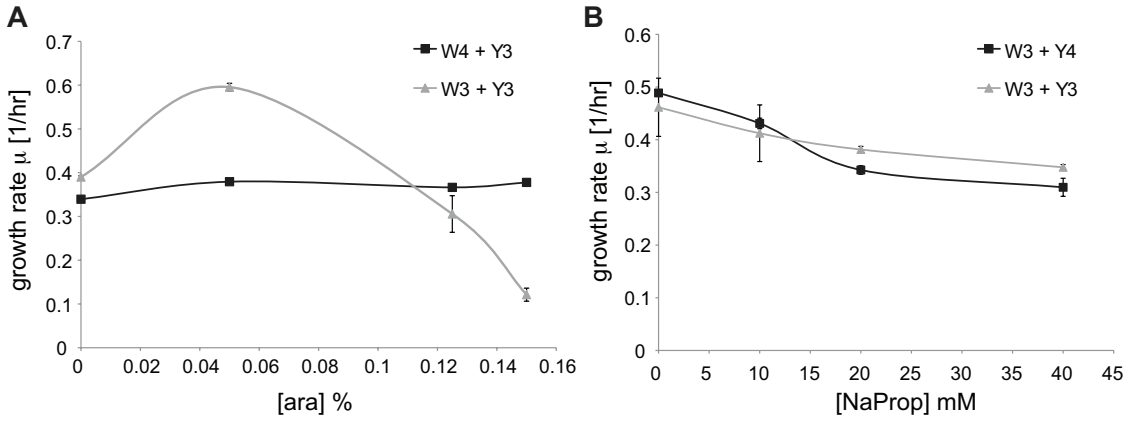

Figure 2.11 Negative control experiments. (A) Addition of arabinose has no effect on the growth rate of the negative tryptophan control strain (W4) and the positive tyrosine strain (Y3). (B) The growth rate of both cultures is decreased with the addition of increasing amounts of propionate, but the growth rate decreases less with the addition of the cross-feeding genes. For both (A) and (B) the negative control strain is either W4 or Y4. See Table 2.1 for the complete strain genotypes.

To understand further how the two strains W3 and Y3 interact in this co-culture, we also attempted to measure the amounts of Trp and Tyr in the co-culture supernatants at the grid "corners", namely the arabinose and propionate concentration combinations of (0%, 0mM), (0.15%, 0mM), (0%, 40mM), and (0.15%, 40mM). Using the same bioassay employed for the monocultures (Methods Section 2.3), we found that throughout the course of co-culture growth, the concentration of Trp remained below detectable levels (~10 μg/L) and Tyr could only be detected at the end of cultivation (~0.1 mg/L) (Table 2.3). This was in sharp contrast to their obvious accumulation in the monocultures (Table 2.3) and was in line with what we had initially hypothesized, i.e. that each amino acid is the limiting nutrient for the corresponding auxotrophic strain. Given the high affinity of each auxotroph for its required amino acid, with K_m in the range of several μg/L (Figure 2.8), it is very likely that the amino acid is taken up by the auxotrophic strain as soon as the molecule is secreted by the partner strain and hence does not accumulate in the supernatant. In fact, based on the observation that in a co-culture each strain's growth rate was largely below its maximum value associated with the saturated amino acid concentration (~10 μg/L Trp for W3 and ~50 μg/L Tyr for Y3, Figure 2.8), we could infer that the Trp/Tyr concentrations were indeed very low, up to a few μg/L for Trp and several tens of μg/L for Tyr.

Table 2.3 Trp and Tyr concentrations in the mono- and co-culture supernatants. Trp concentrations in the supernatant of Y3 growing alone with either 0, 10, or 40 mM NaProp and Tyr concentrations in the supernatant of W3 growing alone with 0, 0.08, or 0.15% arabinose over time. No Trp was detected in the co-culture supernatants. *: Not detectable, below range of the calibration curve (Trp: ~10 µg/L; Tyr: ~0.1 mg/L). **: Above range of the calibration curve, lower bound indicated.

Secreted Metabolite	**Monoculture**	**Time point**		
		early	middle	end
Trp [µg/L]	Y3	N/D*	N/D*	46.9 ± 16.4
	Y3 + 10mM NaProp	N/D*	N/D*	26.4 ± 1.2
	Y3 + 40mM NaProp	N/D*	N/D*	142 ± 9
Tyr [mg/L]	W3	N/D*	N/D*	4.38 ± 0.04
	W3 + 0.08% ara	0.174 ± 0.005	10.7 ± 0.2	21.0 ± 2.2
	W3 + 0.15% ara	2.18 ± 0.02	>31**	>31**
Secreted Metabolite	**Co-culture**	early	middle	end
Tyr [mg/L]	(0%, 0mM)	N/D*	N/D*	1.15 ± 0.39
	(0.15%, 0mM)	N/D*	N/D*	0.76 ± 0.96
	(0%, 40mM)	N/D*	N/D*	0.20 ± 0.01
	(0.15%, 40mM)	N/D*	N/D*	0.15 ± 0.04

2.4.3 Incorporation of metabolic burden in mathematical modeling

Our basic model predicted that increasing the inducer concentration would increase the growth rate of the co-culture. We observed the opposite result experimentally, however, and hypothesized that the effect might be caused by the metabolic burden of expressing the *yddG* and *trpEDfbr* genes. In single strain growth experiments it was observed that increasing the amount of inducer, arabinose or sodium propionate (NaProp), added to either the W3 or Y3 alone, would decrease the max growth rate (Figure 2.12). This was also the case in the "affinity" experiments discussed previously (Figure 2.8). We introduced a burden term, M, which would reduce the maximum growth rate (μ_{max}) giving an apparent maximum growth rate ($\tilde{\mu}_{max}$) and would be based on single-strain growth data (Figure 2.12). The general form is:

$$M = a \cdot [ind]^2 - b \cdot [ind] + c \quad [4]$$

$$\tilde{\mu}_{max} = \mu_{max} \cdot M \quad [5]$$

where the coefficients a, b, and c are determined from the single strain growth experiments shown in Figure 2.12A&C. The relationship between the maximum growth rate and the growth rate at a specific inducer concentration [5] was rearranged to give the burden, M, which was then plotted as function of the inducer concentration [4]. The quadratic fits are shown in Figure 2.12B&D, for the W3 strain with arabinose, and the Y3 strain with NaProp, respectively. The control strains are either not affected, or affected to a lesser extent, by the inducers.

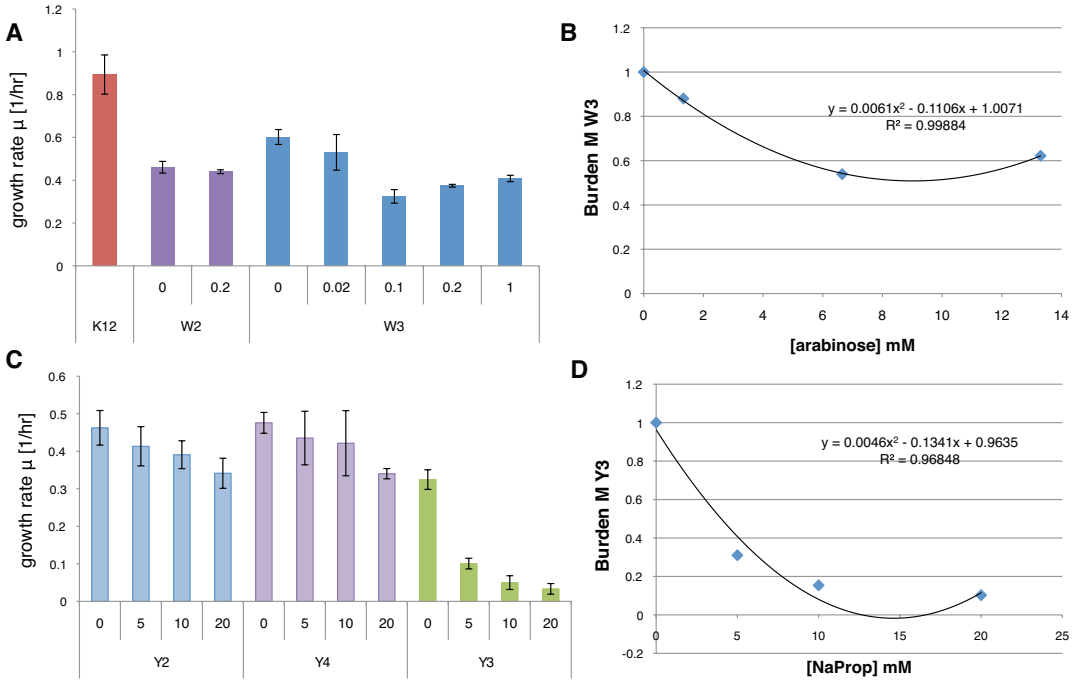

Figure 2.12 Effect of arabinose and propionate on single strain growth. (A) Arabinose (shown in % w/v) has a significant effect on W3, but not on W2. The effect on the growth is not straightforward: increasing arabinose seems to at first have a negative effect on the growth rate, and then a slight positive effect. (B) Burden effect on W3 due to YddG expression. (C) Propionate (in mM) decreases the growth rate of Y2 and Y4 at 20 mM. There does not seem to be any negative effect of adding a plasmid with gfp only. Expressing the trpEDfbr genes has a significant negative effect on the growth rate of Y3 even with 0 mM propionate and decreases sharply after addition of 5 mM propionate. (D) Burden effect on Y3 due to trpEDfbr expression. $M = \tilde{u}_{max}/u_{max}$.

We also hypothesized that expression of the YddG protein may be affecting the W3 strain's affinity for Trp, since this membrane protein has also been shown to export Trp from the cell. As discussed previously, the K_m value did not appear to change significantly, however we still tried to capture this effect in the model. In the future this could be further refined with more experiments, and/or perhaps altering the β parameter

instead of the K_m value. To capture the effect of YddG expression, we introduced a term "G", which is dependent on the yddG expression and arabinose concentration and increases the effective K_m value. The general form of this equation and the final growth relations are:

$$G = \left(\frac{[ind1]^{1.5}}{K_{ind1}+[ind1]^{1.5}}\right) \quad [6]$$

$$\mu_W = \frac{\widetilde{\mu}_{Wmax} \cdot C_{Trp}}{\left(\frac{K_W}{1-G}\right)+C_{Trp}} \quad [7]$$

$$\mu_Y = \frac{\widetilde{\mu}_{Ymax} \cdot C_{Tyr}}{K_Y+C_{Tyr}} \quad [8]$$

where C_{Trp} and C_{Tyr} are the concentrations of Trp and Tyr in the medium in mM and [ind1] is the concentration of inducer 1 in mM. K_{ind1} is the dissociation constant for inducer 1 and its corresponding activator, and K_W and K_Y are the "affinities" or K_m values -- the concentrations (in mM) of Trp/Tyr when the growth rate of the W or Y strain is half of its maximal value.

After incorporation of equations [7] and [8], the model now more accurately simulates the growth trends observed experimentally. As the inducers increase, the growth rate of the co-culture decreases due to the metabolic burden (Figure 2.13). The lowest points are at the highest inducer 2 concentrations (meant to mimic NaProp). The maximum growth rate is not at (0,0), but is along the [inducer 2] = 0 edge, as observed in the experiments (Figure 2.13A). The simulation results for the mid- and end-exponential ratio (Figure 2.13B&C) are very similar. They predict reduced ratios for higher [inducer 2] and exhibit local maxima at around [inducer 2] = 2 which is similar to the patterns seen experimentally.

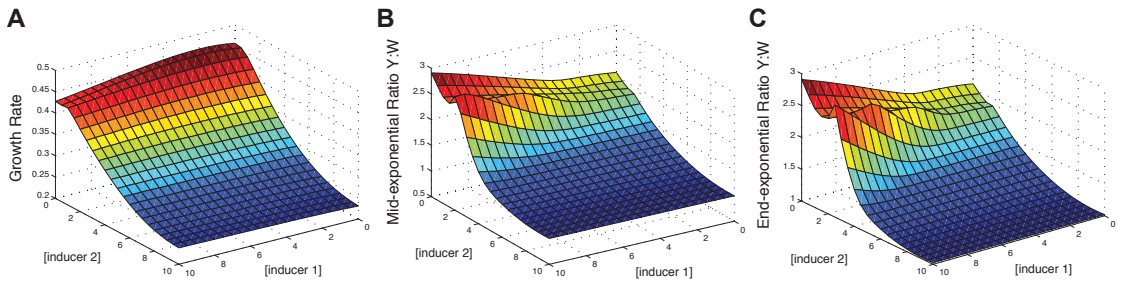

Figure 2.13 Simulation results with the updated burden model. Growth rate (A), mid-exponential (B), and end-exponential (C) Y:W ratio for general inducers 1 and 2. Here the strains are labeled as Y and W since the equations are meant to mimic the Y3 and W3 interaction and effect of actual inducers, but do not use actual inducer and α values.

Obviously this model still does not capture all of the interesting dynamics exhibited by the co-culture. In the Discussion, Section 2.5 we discuss options for refining the model, such as investigating potential changes in the cellular requirements (the β parameter) for Trp and Tyr of W3 and Y3, respectively.

2.4.4 Programming the synthetic consortium with the Design Space

To utilize the above results for programming the consortium, we reversed the relationships of growth rate/strain ratio versus inducer concentrations and defined a design space represented by two contour plots (see Methods 2.3.6 for details). For achieving a specific growth rate and end-exponential ratio combination, Figure 2.14A and Figure 2.14B show which arabinose and propionate concentrations should be used, respectively. Similarly, Figure 2.15 can be used to determine the inducer concentrations for achieving a specific growth rate and mid-exponential ratio combination. Due to the high nonlinearity of the dependence of growth rate and strain ratio on inducer concentrations (Figure 2.10), the design spaces are also very nonlinear and exhibit irregular shapes (Figure 2.14A&B, Figure 2.15A&B). For both arabinose and propionate, the two-dimensional contour plot has both "steep" areas featuring tight contour lines, where substantially varying the inducer concentration is required to change the growth/ratio, and almost "flat" regions, where small changes of inducer concentration correspond to large changes of growth/ratio. Additionally, higher concentrations of arabinose appear to produce lower end-exponential ratios and variable growth rate, while

higher propionate concentrations seem to produce lower growth (except the small region on the left, Figure 2.14B).

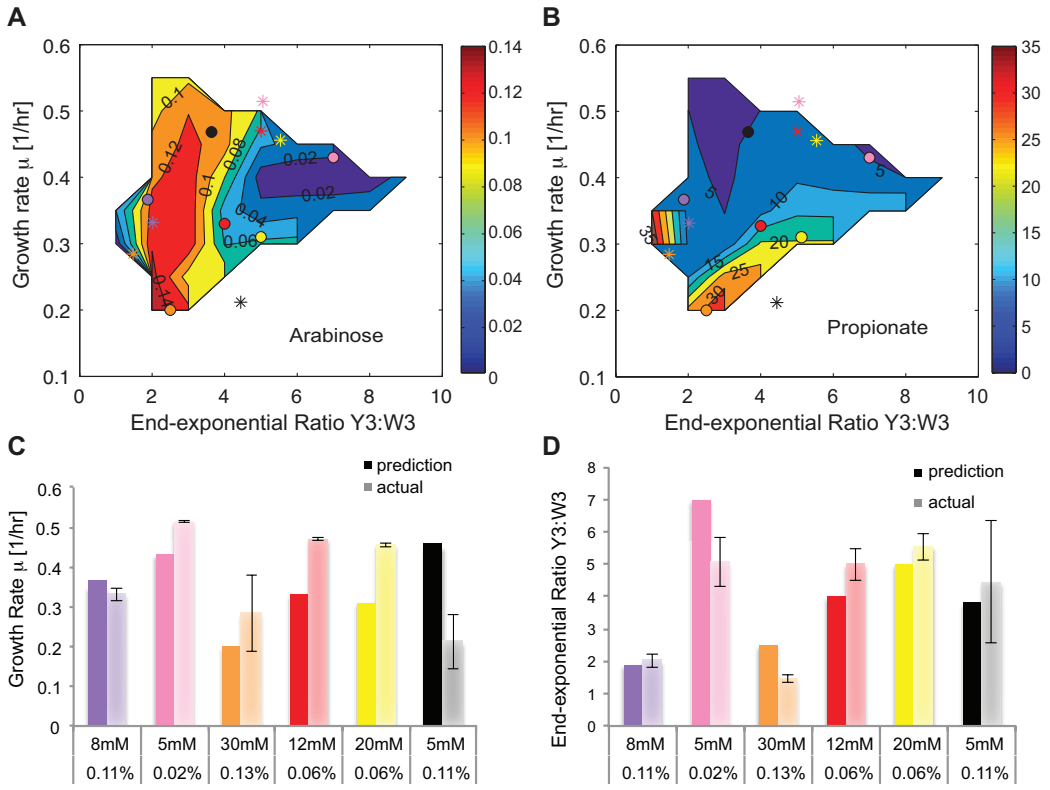

Figure 2.14 Design space and testing for the end-exponential ratio. (A, B) By inverting the relationships of growth rate/strain ratio vs. inducer concentrations, a design space was generated to represent the two-dimensional space of achievable growth rates and strain ratios, and to determine the arabinose (A) and propionate (B) concentrations for a desired growth rate and end-exponential ratio combination. The colored circles are "prediction" points and the asterisks of the same color are the "actual" results of using that combination of arabinose and propionate in the co-culture. The colors denote inducer combinations: purple (0.11%, 8mM); pink (0.02%, 5mM); orange (0.13%, 30mM); red (0.06%, 12 mM); yellow (0.06%, 20mM); black (0.11%, 5mM). (C, D) Comparing the predicted and actual outcome for growth rate (C) and end-exponential ratio (D) in bar graph form; the predictions are in darker colors and the actual (experimental) results are in lighter ones. Error bars: ± standard deviation. The mid-exponential ratio design space is shown in Figure 2.15.

To test the accuracy of the design space, a "prediction" point was first selected at the same position in both plots of Figure 2.14A&B, which would correspond to a particular growth rate and ratio. For example, the yellow circles correspond to a growth rate of ~0.31 1/hr and an end-exponential ratio of ~5. At this specific point, using the contour lines, the inducer concentrations can be estimated to be 0.06% arabinose (Figure 2.14A) and 20 mM propionate (Figure 2.14B). The auxotroph pair was then grown under

this specific combination of inducers and the resulting growth rate and ratio (the "actual" data) were compared with the "predicted" values. Results from six such tests are illustrated in Figure 2.14 (panels A&B: circles – predictions, asterisks – actual values from experiments; panels C&D: bar graph comparisons). For the growth rate, two out of these six tests showed good agreement between predicted and actual outcome (within two standard deviations, Figure 2.14C: 8 mM, 0.11%; 30 mM, 0.13%); for the end-exponential ratio, four of them are reasonably accurate (within two standard deviations, Figure 2.14D: 8 mM, 0.11%; 12 mM, 0.06%; 20 mM, 0.06%; 5 mM, 0.11%). These results confirm our expectation that the steeper regions of the design space are more accurate, while the flatter regions are more difficult to target. It is also worth noting that the contours could explain, at least partially, the deviation of the actual outcome from the prediction. For example, for the inducer concentration of 0.06% arabinose and 12 mM propionate, the predicted and actual values of growth rate are significantly different (Figure 2.14A, red circle and asterisk), but the plot illustrates how the point may have moved around the arabinose surface along the 0.06% contour.

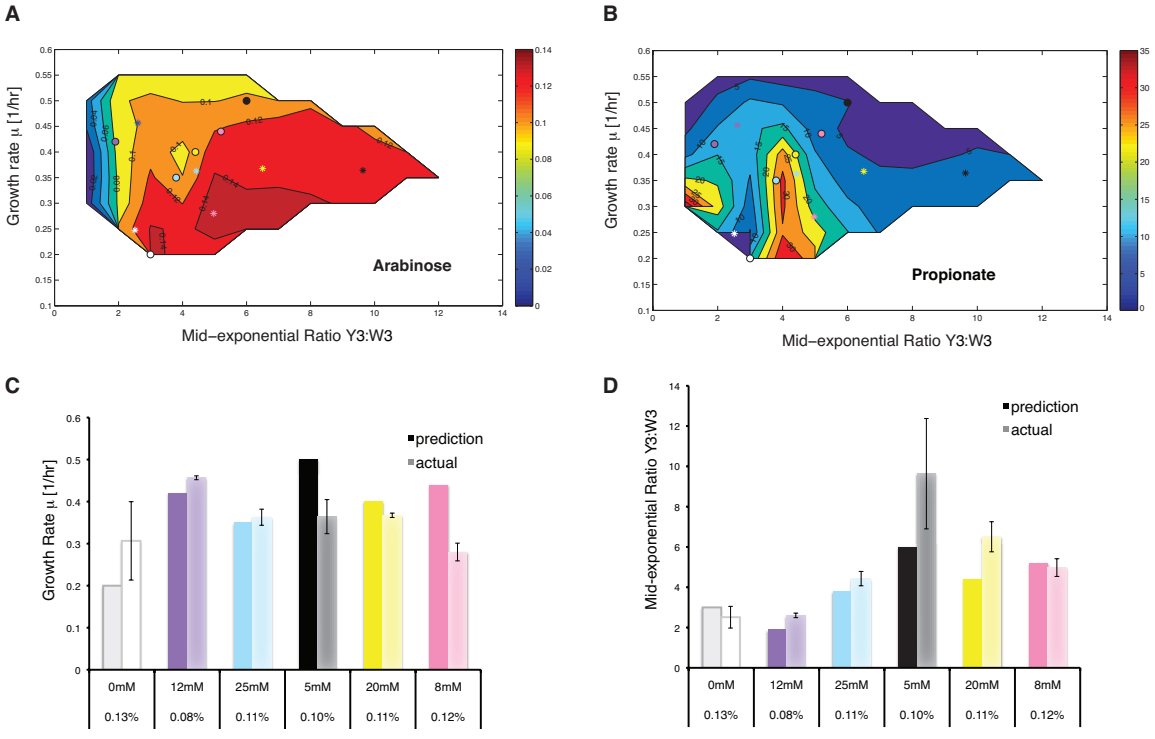

Figure 2.15 Design space and testing for the mid-exponential ratio. (A, B) Graphs created as for the end-exponential ratio above to determine the arabinose (A) and propionate (B) concentrations for a desired

growth rate and mid-exponential ratio combination. The colored circles are "prediction" points and the asterisks of the same color are the "actual" results of using that combination of arabinose and propionate in the co-culture. The colors denote inducer combinations: white (0.13%, 0mM); purple (0.08%, 12mM); blue (0.11%, 25 mM); black (0.10%, 5mM); yellow (0.11%, 20mM); pink (0.12%, 8mM). (C, D) Comparing the predicted and actual outcome for growth rate (C) and mid-exponential ratio (D) in bar graph form; the predictions are in darker colors and the actual (experimental) results are in lighter ones. Error bars: ± standard deviation.

2.5 Discussion and conclusion

As described above, we have constructed a proof-of-principle biological circuit to regulate the growth rate and composition of a two-member *E. coli* consortium based on tunable symbiosis. The resulting co-culture is able to achieve a continuous range of growth rate and composition; in addition, we show that the system can be "programmed" reasonably well for desired growth rate or strain ratio. The symbiotic scheme (two auxotrophic strains cross-feeding amino acids) has been proposed and examined in previous work, most notably with the yeast system by Shou *et al*. (*21*). Building on this basic concept in our work here, we have devised a novel approach for continuously *tuning* two important properties of synthetic consortia: the growth rate and community composition. Whereas previous work largely focused on using synthetic circuits to investigate the mechanism of microbial interactions such as mutualism, the main objective of this study has been developing a tool for engineering a synthetic microbial community, which can be deployed in various applications.

The main issue of our current system is that the metabolic burden partially masks the cross-feeding benefits with regard to the growth rate. This obstacle could potentially be overcome by using plasmids of lower copy number, by modifying the promoters to achieve more appropriate expression levels, or by transferring the system to the chromosome. On the other hand, since the gene expression level would be lower, the effect of activating the circuit might also become smaller. Nevertheless, we expect that eliminating or reducing the metabolic burden would lead to larger and more predictable ranges of growth rate and strain ratio upon addition of inducers. This would also improve the quality of the design space, which ideally would exhibit monotonic relationships between inducer levels and desired growth/ratio (as would be expected for the design

space corresponding to our basic model) and hence provide better estimates of inducer concentrations for generating the desired co-culture property.

In terms of our burden model, we had begun to capture some of the ratio dynamics but it could obviously be refined further. As illustrated in Figure 2.8, there is an interesting relationship between the inducer concentration and "affinity" parameter K_m. While the change in K_m did not appear to be as significant as we had hypothesized, especially for the Trp auxotroph, W3, there is a change in the K_m value that is observed when the arabinose and sodium propionate is varied. For the W3 strain, as arabinose is increased the affinity actually increases (K_m goes down) and then decreases (K_m goes up) as arabinose is increased from 0% to 0.08% to 0.15%. Although we originally focused on tuning the α value and the max growth rate decrease, the genetic changes may be affecting the β parameter, which is reflected in what was termed the "K_m", just based on the format of the Hill equation. In this case the "affinity" of the cells for the essential metabolite is probably very representative of the β parameter, defined as the cell's requirement for that specific amino acid. One way to test changes in this parameter would be to do a series of bioassays (as was done for Trp/Tyr -- see Methods, Section 2.3.4) combined with data from expanding the "affinity" experiments, Figure 2.8, to determine the lowest concentration of Trp/Tyr that would support growth for each auxotroph, with and without the tuning genes, and with varying amounts of inducer. Then an empirical expression could be derived for the relationship between inducer concentration and the β parameter, as was done for the metabolic burden. This could then be incorporated into the model to make the β tunable and dependent on inducer concentration, as well as the α value.

We also want to point out that our measurement of consortium composition (i.e. strain ratio), via a combination of absorbance and fluorescence readout, is not ideal and occasionally showed large variation among replicates when the ratio deviates substantially from one and changes rapidly over time. In addition to inherent variability of the biological system (e.g. due to gene expression), another possible source could be the population variances in YFP expression and maturation. In our current system, GFP variant eYFP is constitutively expressed on the chromosome in the tyrosine auxotroph

but its expression is not very high. Furthermore, YFP in its native state has a slow maturation time (*45*), which may be causing the inaccuracy and large variation. Using another fluorescent protein with higher signal/noise ratio and faster maturation time could potentially reduce or eliminate these issues and hence improve the measurement. It will also be worth exploring in the future alternative methods, such as qPCR and fluorescence-activated cell sorting (FACS), to achieve better accuracy.

Finally, we would like to emphasize that the approach reported in this work for regulating and programming a two-member synthetic microbial consortium and its extensions could be readily transferred to more complex systems consisting of different microbial strains or species. Two key components are required to construct such a regulatory circuit. First, the two consortium members need to form an inter-dependent relationship. Part of this inter-dependence might already exist when a synthetic microbial consortium is assembled (*46, 47*). If a complete cross-feeding loop is not in place, genetic manipulation such as the gene deletions we conducted in this work to generate auxotrophs will be needed. Second, genes that can affect the export of cross-fed metabolites need to be regulated, which can be achieved by various means, for instance through the usage of chemically inducible promoters as illustrated in this work. The resulting tunable microbial consortia can potentially be utilized for many applications. For example, complete and efficient co-fermentation of hexose and pentose sugars is one of the major obstacles in effectively converting lignocellulosic biomass into fuels (*48*). Existing strategies to optimize the sugar utilization using a bacterial co-culture include delaying the inoculation time of one of the strains or changing the inoculation ratio (*49*). Tuning the composition of the co-culture during growth might be easier and more efficient than either of the previous strategies.

Chapter 3 Engineering a two-member *E. coli* consortium for conversion of five- and six-carbon sugars to isobutanol

3.1 Summary

As described above, consolidated bioprocessing (CBP) of lignocellulosic biomass is a promising method for overcoming current and future liquid fuel shortages. Some of the challenges that remain in CBP are complete utilization of five carbon sugars such as xylose, as well as achieving high titers of next-generation biofuels on actual biomass rather than on defined laboratory media. To address this issue we have constructed a biculture of two *E. coli* specialists converting five- and six- carbon sugars into isobutanol that consumes both types of sugar and can achieve relatively high titers and yields of isobutanol on defined laboratory media and on AFEX-pretreated corn stover hydrolysate. We have also engineered the C5 specialist to consume xyloligosaccharides by introducing a xylodextrin transporter and xylosidase, *xynTB*, from *Klebsiella oxytoca*. These genes were assembled onto the isobutanol production plasmid, pSA55, for simultaneous xylodextrin utilization and isobutanol production. We demonstrate the consumption of xylodextrins on minimal media and the growth of the xynTB-containing strain on the corn stover hydrolysate.

The materials presented in this chapter are currently in preparation: Kerner A*, Minty J*, Kistler S, Singer M, Faulkner I, Balan V, and X. N. Lin. A synthetic *Escherichia coli* consortium for efficient conversion of hexose and pentose monomers and oligomers to isobutanol. *: Equal contributions.

3.2 Introduction

The current energy crisis and environmental sustainability of our liquid fuel reserves remains a global obstacle with no clear and immediate solution. Particularly in the United States, the dependence on foreign oil has become an environmental, political, and ethical dilemma. Biofuels can be a potential solution to this problem, but corn- and starch-derived fuels are not sufficient on their own; even if all the corn produced in the U.S. were used instead for fuel production it would only make up about 15% of our country's fuel needs (*50*). Cellulosic biofuels, which are biofuels derived from lignocellulosic biomass such as grasses, woods and crop residues, could potentially displace our petroleum dependency. There are many advantages to using cellulosic biomass as a feedstock, including renewability, abundance, wide geographic distribution, and low greenhouse gas emissions (*51*). Additionally, these feedstocks avoid competing with the food supply, unlike corn- and starch- based feedstocks (*50*); current estimates for U. S. production are 1.4 billion tons of cellulosic biomass annually (*52*).

Production of biofuels from cellulosics is a three-step process (*51*). First, plants store solar energy in the form of cellulose and hemicellulose; next, these compounds are separated from lignin and other macromolecules and broken down by physical or chemical pre-treatment and enzymatic saccharification. Finally, the five- and six-carbon sugars that are produced during saccharification are fermented into biofuels. Although the general process seems straightforward, it is still a long way from being optimized for large-scale production.

Cellulosic biomass is made up of three main components: cellulose, hemicellulose, and lignin, but the ratio of these three components varies between plants and between parts of the plant (*53*). To solve this problem, researchers have already begun to use novel genomic techniques to identify organisms and genes that could be useful in standardizing the feed composition (*51*). Additional issues include the high cost of removing the lignin by pre-treatment and the high cost of cellulase and hemicellulase production (enzymes used to degrade cellulose during saccharification) (*50*). Efforts to decrease the costs of pretreatment are discussed in the next section. In order to overcome the second issue, the cost of enzyme production, one could look to mimic natural

microbial consortia such as those found in the cow rumen (*54*), which are naturally able to break down grasses and recalcitrant plants and produce such enzyme *in situ*. These consortia could then be used as the enzyme producer and/or production strain in the previously discussed system, consolidated bioprocessing (CBP).

3.2.1 Pretreatment methods and next-generation biofuels

Pre-treatment of lignocellulosic biomass is necessary to allow enzymes such as cellulases and xylanases access to substrates, which are often physically blocked by the presence of lignin and the tight packing of cellulose microfibrils. Cellulose makes up the largest component of the cell wall, at 35-50% of the plant dry weight, and is arranged in bundles of microfibrils surrounded by hemicellulose (20-40%) (*50*). Additionally, lignin (10-25% plant dry weight) is also present to give the cell wall rigidity and also protect against invading species. Thermochemical pretreament is needed to remove and/or rearrange the lignin and macromolecular structure to make fibers available for hydrolysis – this can increase the rate of hydrolysis from 3-10X depending on the method used (*55*). However, pretreatment can be quite expensive, contributing as much as 16-19% to a biorefinery's total capital investment (*55*).

Recently, more economical means of pretreatment have been developed, such as Ammonia Fiber Expansion (AFEX) (*56, 57*), a low temperature, dry-to-dry process where annhydrous ammonia is added to the prewetted biomass. This process retains the macromolecular structure of the cellulose and hemicellulose, but reduces the degree of polymerization to increase substrate availability (*57*). The polymers then still need to be enzymatically hydrolyzed, but less inhibitors are produced than in other methods so the feedstock can be used directly in fermentation experiments without further detoxification (*58*). Improved ammonia recovery methods have also reduced cost estimates -- in simulations by Sendich *et al*. that took into account these improvements and by using the minimum amount of water and ammonia possible, the minimum ethanol selling price (MESP) was predicted to decrease from the previous estimate of $1.41 per gallon to about $1.03 per gallon if simultaneous saccharification and fermentation is used for corn stover conversion (Figure 3.1) (*56*). For a CBP process, however, this is decreased even further to about $0.80 per gallon (*56*).

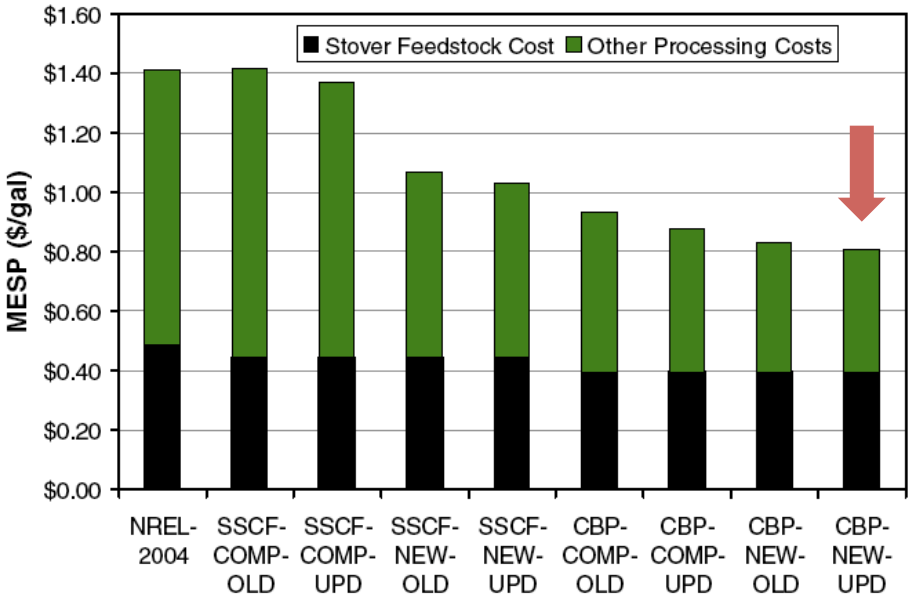

Figure 3.1 Comparison of the predicted MESP for various process simulations on corn stover, adapted from (*56*). Old data from a 2004 NREL study are compared with updated AFEX parameters and various configurations. Red arrow indicates the MESP of AFEX with the new parameters incorporated, for a CBP approach. Abbreviations not previously explained: new NH_3 recovery (NEW), NH_3 recompression (COMP), old AFEX parameters (OLD); updated AFEX parameters (UPD).

In our case, AFEX has been demonstrated as an efficient pretreatment method for our chosen feedstock, corn stover, which is pretreated and enzymatically hydrolyzed by the Biomass Conversion Research Laboratory (BCRL) at Michigan State University using a commercial enzyme mixture (see Methods for AFEX conditions and further details). This process results in glucose and xylose titers up to ~58 and ~29 g/L, respectively, though this may vary slightly from batch to batch (Venkatesh Balan, BCRL, personal communication).

In order to reach recent energy goals and reduce the impact of petroleum use, it will be necessary to find other sources of liquid fuel substitutes other than corn- and sugarcane-derived ethanol or biodiesel. Several issues with 1st-generation ethanol include: competition with land used for food crops, contribution to increasing food and energy prices, and high cost of production which necessitates the use of subsidies to be competitive (*59*). Vegetable oil-derived biodiesel, used widely in Europe, only contains 91% of the energy of D2 diesel and suffers from distribution issues in cold climates, where low temperatures may cause waxes to form in the fuel (*60*). A solution to these

problems may be 2nd-generation biofuels, which are derived from lignocellulosic sources such as forest residues, grasses, and sugarcane bagasse. Depending on the type of biomass, higher energy yields may be obtained than from 1st-generation feedstocks, and when wastes from other processes are utilized they will then also not compete with food crop production (*59*). However, we are currently much less experienced at producing fuels from these feedstocks, so it will likely be some time before the switch can be made from corn or sugarcane ethanol to fuels produced from lignocellulosic sources.

There are many feedstock and fuel alternatives to corn-derived ethanol (Table 3.1) the difficult part will be finding or designing either a synthetic or natural microbe capable of producing industrially-relevant yields (*60*). One promising fuel alternative to ethanol is butanol, which has a higher energy content than ethanol (84% vs. 65% of the energy contained in gasoline) and, unlike ethanol, is less hygroscopic and can therefore more easily become part of our current fuel infrastructure (*5*). Isobutanol and 1-butanol have also been produced in *E. coli* in relatively high titers *(61-63),* making these fuels a good starting point for further process optimization. We have chosen to focus on the production of isobutanol in particular.

Table 3.1 Properties of 2nd-generation fuel alternatives. Adapted from (*60*).

Fuel type	Major components	Properties	Potential advanced biofuels
Gasoline	C_4-C_{12} hydrocarbons; Linear, branched, cyclic aromatics	Octane number (87-91); Energy content	Butanol, isobutanol, short-chain alcohols, short branched-chain alkanes
Diesel	C_9-C_{23} hydrocarbons; Linear, branched, cyclic aromatics	Cetane number (40-60); Good cold properties	Fatty alcohols, alkanes, linear or cyclic isoprenoids

3.2.2 Isobutanol production in *E. coli*

E. coli is not a natural producer of 1-butanol or isobutanol, however Atsumi *et al.* were able to engineer isobutanol production by co-opting the L-valine biosynthesis pathway and expressing a heterologous 2-keto acid decarboxylase and alcohol dehydrogenase (Figure 3.2) (*61*). The L-valine biosynthesis pathway produces 2-

ketoisovalerate from pyruvate, which is then converted into L-valine (*64*). The final steps in the Erlich pathway (*65*) can then be used to convert the 2-keto acid into an alcohol using a 2-keto acid decarboxylase (KDC) and alcohol dehydrogenase (ADH) (Figure 3.2). In this case, the KDC used was Kivd from *Lactococcus lactis* and the ADH was Adh2 from *Saccharomyces cerevisiae* – both were placed under the control of an inducible promoter, $P_L lacO_1$. To further increase isobutanol production, several genes from the L-valine pathway were also overexpressed on a plasmid, *ilvIHCD*, under control of the same promoter. However, the *ilvIH* genes (encoding the isoenzyme acetohydroxy acid synthase) were then replaced by the *alsS* gene of Bacillus subtilis, which has a higher affinity for pyruvate (*61*) and would then direct product formation towards L-valine/isobutanol rather than towards other products such as L-isoleucine. Six chromosomal genes were also knocked out to decrease byproduct formation and competition for pyruvate: *adhE* (ethanol), *ldhA* (lactate), *frdAB* (succinate), *pta* (acetate), *fnr*, and *pflB*. The final rationally-designed strain JCL260 was able to produce up to ~300 mM isobutanol (22 g/L, 86% theoretical yield) after 120 hours with one round of glucose-feeding (*61*).

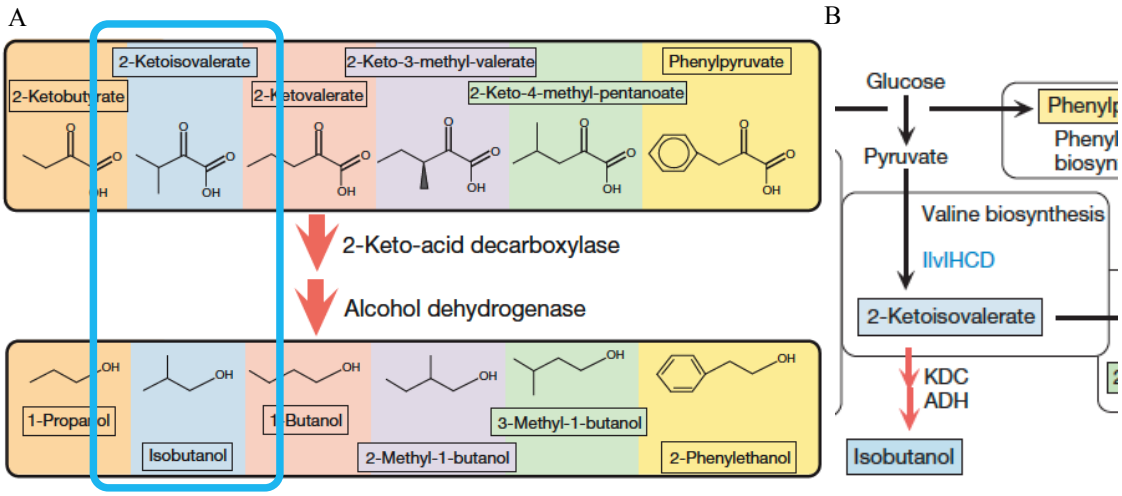

Figure 3.2 Isobutanol production in *E. coli* using the valine biosynthesis pathway, adapted from (*61*). (A) Converting 2-ketoisovalerate into isobutanol via the Erlich pathway. (B) Conversion of glucose to isobutanol, overall schematic.

Isobutanol production was also achieved by the same group using evolution as opposed to rational design (*63*). The precursor strain to the above-mentioned JCL260 (JCL16), which does not contain the chromosomal mutations, was evolved for increased

isobutanol production by selection on a L-valine analog, norvaline, which in high concentrations is normally toxic (*63*). If a strain could grow well in media containing this analog, then it is likely that it contains mutations favorable for norvaline and valine secretion from the cell. Since the valine and isobutanol pathways are intertwined when the KDC and ADH genes are introduced, then increased valine secretion should also lead to increased isobutanol secretion. To test this, the JCL16 strain was mutagenized using N'-nitro-N-nitrosoguanidine (NTG) and then evolved on liquid media containing norvaline. Resistant mutants were selected on plates containing norvaline, screened for increased isobutanol production, and then the process was repeated. After transforming with the relevant plasmids, the resultant NV3 strain was found to produce up to 13.6 g/L isobutanol compared to JCL260 which produced 21.0 g/L isobutanol (*63*). After "repairing" a key mutation in *rpoS*, the titer could be increased to 21.2 g/L isobutanol (strain NV3r1). A full list of the mutations in strain NV3 is shown below in Appendix Table 1.

In our own hands, the NV3 strain produced more isobutanol than NV3r1 with plasmids pSA55 and pSA69 and only one round of glucose feeding, so we chose this as our base strain for the two-member consortium. It should also be noted that we used the plasmids pSA55 and pSA69 for isobutanol production, whereas in the evolution study, plasmid pSA69 was combined with plasmid pSA65 (*66*), which encodes a different alcohol dehydrogenase gene from *L. lactis*, *adhA*. This newer plasmid, pSA65, showed better performance than the pSA55 plasmid, so this might be one of the reasons the strains performed differently in our hands. This is discussed further in the Discussion and conclusion, Section 3.5

The highest titer so far reported for isobutanol is 50.8 ± 1.1 g/L by the JCL260 pSA65/pSA69 strain, which was achieved under aerobic conditions in a 1L bioreactor in 72 hours on 55 g/L glucose with intermittent glucose feeding cycles (*67*). Interestingly, the JCL260 strain outperformed the evolved isobutanol-tolerant strain SA481 (*68*) which produced only 23 ± 4.4 g/L isobutanol under the same conditions. A gas-stripping mechanism was used to remove the isobutanol from the fermentation broth, which can be toxic at titers over 8 g/L. Two condensers were attached to the bioreactor, and then

oxygen was sparged in to help remove the isobutanol, which was condensed into water in receiver B and D (Figure 3.3). This product removal strategy allowed the production of much higher levels of isobutanol than had been previously reported in shake flasks (22 g/L, (*62*)). These results suggest that the gas stripping process was an effective removal strategy and that such a process will be necessary in order to reach industrially relevant levels of isobutanol production. Additionally, these production strains perform much differently depending on whether or not the toxic product is removed, so care should be taken when scaling up such bench-scale processes since the results are likely to be much different.

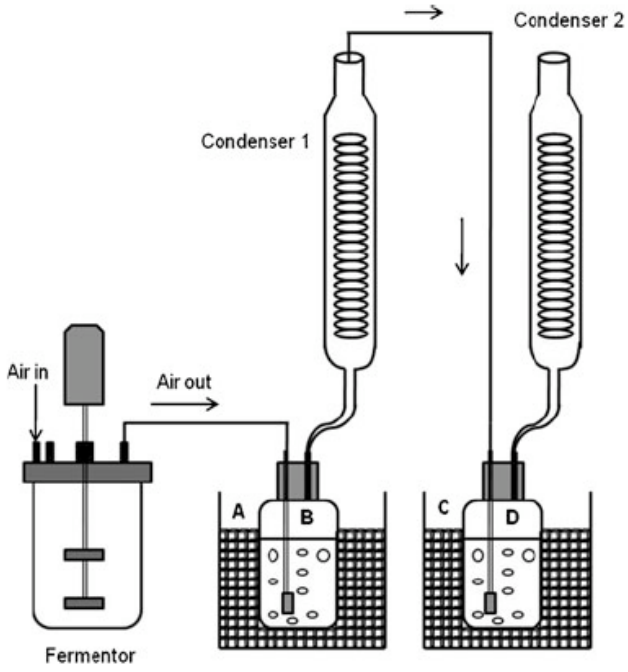

Figure 3.3 Diagram of fermentation and removal of isobutanol via gas stripping, adapted from (*67*).

3.2.3 Consortia vs. "Superbug" for fuel production and sugar co-utilization

It remains to be seen whether a microbial consortia or a "superbug" will be the best option for biofuel production, but both strategies have been thoroughly investigated. Recent work suggests that a co-culture may be more efficient than a monoculture with regard to alternative fuel production in general. When a cellulolytic, hydrogen-producing bacterium, *Clostridium thermocellum*, was cultured with a non-cellulolytic hydrogen

producer, *Clostridium thermopalmarium*, the overall titer of H_2 on filter paper from a 1:0.05 co-culture was much higher (~400 ml/L) than that produced by the *C. thermocellum* alone (176 ml/L), even though this strain can produce hydrogen from cellulose on its own (*69*). The increased benefit may result from the reduced ethanol and acetate production; the concentration of both of these byproducts decreased when the strains were cultured together (*69*).

One of the remaining challenges for CBP systems is complete utilization of five-carbon sugars (e.g. xylose or arabinose) when six-carbon sugars (e.g. glucose) are also present, since the six carbon sugars will naturally be utilized first and may also inhibit utilization of the five carbon sugars (*48, 70*). In sequential utilization, by the time the glucose is used up, the product titers (such as ethanol) have already reached levels that may reduce xylose utilization to extremely slow rates, further complicating the problem (*70*). There are various examples of attempts to engineer one strain to co-utilize six- and five-carbon sugars, as well as examples of consortia designed for the same purpose. Co-utilization of cellobiose (a glucose disaccharide) and xylose was completed in an engineered *E. coli* strain adapted for growth on cellobiose (*71*). Although rates of xylose utilization reached ~0.13 g/L/hr, it was not clear how this strain would perform with glucose present as well. Similarly, a *Saccharomyces cerevsiae* strain was also engineered to co-utilize cellobiose and xylose, achieving higher yields of ethanol on the sugar mixture as opposed to each sugar alone in the same time frame (0.39 g/g vs. 0.31-0.33 g/g) (*70*). This result indicates that co-utilization, as opposed to sequential utilization, might be more effective with regard to isobutanol production in *E. coli* as well. Although the researchers did test this strain on a "simulated" hydrolysate containing glucose, xylose and cellobiose, it is not clear that it would be able to perform as well on an actual hydrolysate. It would be interesting to see how a co-culture would perform compared to this strain in the same conditions.

In contrast, co-utilization of sugars by a microbial consortium has also been demonstrated extensively (*6, 72, 73*), although so far there have been no studies, to our knowledge, that also demonstrate this co-utilization on an actual lignocellulosic biomass coupled to isobutanol production. As briefly described earlier, Eiteman *et al.* were able to

achieve simultaneous consumption of both glucose and xylose by engineering two *E. coli* strains to preferentially use either one sugar or the other (*6*). In an aerobic batch culture, the co-culture completely consumed each sugar in about 15% less time than the separate processes. Also, the co-culture demonstrated an ability to adapt to changing culture conditions, as the ratio of the specialists changed depending on the composition of the feed stream in a fed-batch process (*6*). This also demonstrates one of the advantages of a co-culture over a monoculture: the ability to adapt to a changing extracellular environment.

In another interesting report by the same group, a four-member co-culture was designed to consume three sugars (glucose, xylose, and arabinose) and one waste product (acetate) by engineering specialists that would each utilize only one of these carbon sources (*73*). In a bioreactor containing 14 g/L glucose, 11 g/l xylose, 7 g/L arabinose, and 3 g/L acetate, all of the sugars and acetate were consumed within 10 hours (*73*). While these concentrations are low, this demonstrated the ability of a consortium to simultaneously consume three sugars, as well as remove a possibly detrimental waste product as may be produced in a lignocellulosic fermentation.

Lastly, as described above in Section 1.2, the yeast consortium engineered by Tsai *et al*. to produce a synthetic cellulosome is an excellent example of a situation in which a modular consortium is vastly preferable to a monoculture or "superbug" (Figure 1.4) (*8*). Up to 93% of the theoretical yield of ethanol on cellulose was obtained with the optimized consortium, as compared to previous studies with one strain secreting all four components (62% of theoretical yield). With the consortium, the metabolic burden of expressing three different enzymes and one scaffold was spread across four separate engineered strains, and each could be manipulated individually. For example, the exoglucanse was switched out in one of the partners, in favor of an enzyme with better scaffold-docking properties. This would be much more difficult to achieve with one strain, where the genetic manipulations needed to swap out genes might affect the expression or sequence of the heterologous genes that have already been added.

3.2.4 C5 specialist construction and xylodextrin utilization

Since *E. coli* is naturally a hexose specialist, it is necessary to knock out several genes in order to engineer preferential xylose utilization. It has been shown in several studies that knocking out the genes for glucose uptake and phosphorylation will render the cell unable to use glucose (*6, 74*). To achieve this, we first knocked out *ptsG* which encodes the glucose-specific transporter (enzyme $IICB^{Glc}$) of the glucose phosphotransferase system (PTS) (*75*). The cell can still transport glucose via the mannose PTS (*75*), so *manX*, a subunit of the mannose permease (enzyme $IIAB^{Man}$) that participates in the phosphorylation of exogenous mannose, as well as glucose, was also knocked out. This protein complex is localized to the cytosolic side of the membrane. Previous work has shown that knocking out *manZ* is also an effective strategy (*6*). Lastly, the glucokinase gene, *glk*, should be removed in order to prevent utilization of intracellular glucose. Glucokinase uses one ATP molecule to phosphorylate β-D-glucose to β-D-glucose-6-phosphate. It is not necessary for growth on glucose but can be utilized when the PTS system can no longer transport and phosphorylate glucose or there are low extracellular concentrations of glucose (*76*). Removal of all three of these genes was necessary and sufficient for preferential xylose utilization in a glucose and xylose-containing medium, as demonstrated in the Results, Section 3.4.1 below. Description of the process for removing these genes in discussed in the Methods, Section 3.3.1.

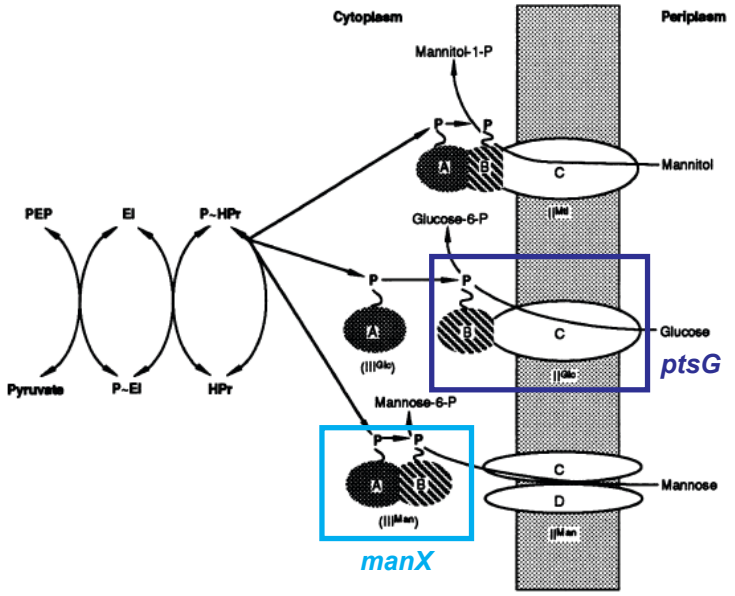

Figure 3.4 Phosphotransferase system (PTS) highlighting participation of the pstG and manX genes, adapted from (*75*). General PTS proteins are shown on the left, wherease the substrate specific proteins, I, II, or III, are shown on the right, where some are membrane-associated and some are cytosolic.

As discussed above, after enzymatic hydrolysis the CS hydrolysate still contains oligomers of glucose and xylose that have not been completely hydrolyzed to their monomeric forms (*58*). *E. coli* is not naturally able to utilize oligomers of either sugar, though it does contain two cryptic operons for utilization of cellobiose (*chb* and *asc*) (*77*). The xylodextrin utilization operon from *Klebsiella oxytoca*, *xynTB*, contains a xylodextrin transporter (*xynT*) and a xylosidase (*xynB*) (*74*)--a schematic is shown in Figure 3.5. When expressed in *E. coli* this operon allowed for utilization of xylodextrins up to a degree of polymerization of six (xylobiose to xylohexaose) (*74*). We obtained a plasmid containing these genes under control of the lactose-inducible promoter (pLOI3708) from this previous study, and then cloned the operon behind the *ADH2* gene in plasmid pSA55 to couple the isobutanol production and xylodextrin utilization. A map of the completed plasmid is shown below (Figure 3.5) and a strain list is given in the Results section (Table 3.2). Details of the plasmid construction are given in the Methods, Section 3.3.2 of this chapter.

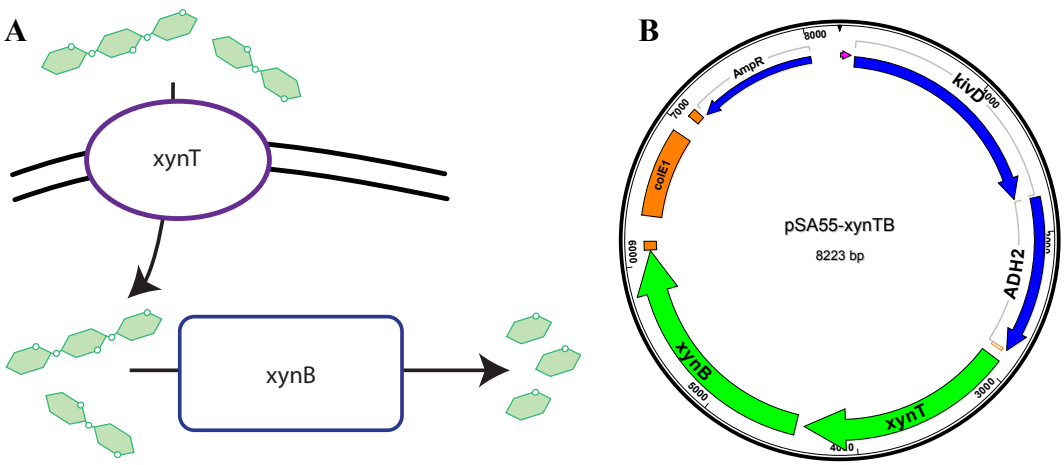

Figure 3.5 (A) Xylodextrin uptake and hydrolysis by the *K. oxytoca xynTB* genes. (B) *xynTB* insertion onto the pSA55 plasmid for isobutanol production and xylodextrin utilization

3.3 Methods

3.3.1 Strain construction

Our base strain for the *E. coli* hexose specialist is NV3 (*63*), and was termed "NC6". A full strain list is given in Table 3.2. The pentose specialist was constructed by knocking out genes for glucose transport and utilization: *ptsG*, *glk*, and *manX* (*78*), and was named "NC5". Each gene was knocked out via P1 transduction (*42*) using lysate grown on the corresponding Keio collection strain (JW1087-2, JW2385-2, JW1806-1) obtained from the CGSC (*43*). After each transduction the *kanR* selection cassette was removed using the heat-sensitive FLP recombinase (*42*) and then the next gene was deleted. Each specialist was then transformed via electroporation with plasmids pSA55 and pSA69 (*61*) and the results were confirmed via ethidium bromide (EtBr) gel electrophoresis (see Table 3.2). The plasmid pSA55 contains genes *kivd* and *ADH2* under control of the $P_L lacO_1$ promoter, induced via the addition of IPTG. The plasmid pSA69 contains genes *alsS*, *ilvC*, and *ilvD* also under control of the $P_L lacO_1$ promoter. To create the NC5 xylodextrin utilization strains, the NC5 strain was transformed via electroporation with either plasmid pLOI3708 (*74*) or pAK6 (see construction details below). The results were confirmed on an EtBr gel and by sequencing.

3.3.2 pAK6 (pSA55-*xynTB*) plasmid construction

Plasmid pAK6 was constructed via the one-step isothermal assembly method, or the "Gibson Assembly" method (*79*). Primers were designed to amplify either the *xynTB* genes from plasmid pLOI3708 or the pSA55 backbone with 20 bp overhang flanking regions with a total overlap of 40 bp. Each template was amplified via PCR using the Phusion High-fidelity Master Mix from New England Biolabs (NEB), and then the fragments were assembled using the Gibson Assembly Master Mix (NEB). After the 1 hour incubation at 60C, the reactions were diluted 3X and transformed via electroporation into NEB 10β electrocompetent cells (NEB). Transformants were screened by selection on ampicillin plates (100 μg/ml), miniprepping, and digestion with restriction enzymes to check for the correct length. Plasmids were analyzed on an EtBr gel and also confirmed via sequencing. The constructed vector was named "pAK6". Once the plasmids were confirmed, the NC5 strain was then transformed with the constructed pAK6 vector.

3.3.3 Microplate and flask cultivations using M9IPGX+YE media

For the microplate and flask cultivations, mono- and co-cultures were cultivated in minimal M9IP medium (1X M9 salts, 0.01 mM $FeSO_4$, 0.1 mg/L Thiamine HCl, 0.13 mM $CaCl_2$, 1 mM $MgSO_4$, 0.2 ml/L MOPS micronutrients) with either 18, 36, or 48 g/L glucose or 18, 36, or 12 g/L xylose as indicated and 5 g/L yeast extract (YE, final medium termed M9IPGX+YE). IPTG was added to a final concentration of 0.1 mM for induction of gene expression. Ampicillin and kanamycin were added to final concentrations of 100 and 30 μg/ml, respectively. Frozen stocks were inoculated into rich LB medium with antibiotics and grown overnight to saturation, then washed twice with minimal M9 medium without yeast extract. Cultures were then diluted by 1:100 and pipetted onto a 96-well microplate (Costar) to a volume of 200 μl per well, which was then covered with an adhesive Mylar film to prevent isobutanol evaporation. Unless otherwise stated, four replicates were conducted per microplate sample. Cultures were grown for 48 or 72 hours at 30^{o}C on a VersaMax (Molecular Devices) plate reader with shaking, and OD_{600} measurements were taken every 15 minutes. For the microplate experiments with NC5 pLOI3708, no kanamycin was added and the IPTG concentration was raised to 0.1 M for induction of pLacZ. M9 medium without sugar was used as the

base medium, to which the various xylodextrins (Megazyme) were added to a concentration of 2 g/L. For the flask experiments, cultures were inoculated in the same manner, and then washed with M9IP+YE medium without sugar. They were then diluted to a total cell density of 1:100 and grown for 48 hours at 30^{o}C with shaking at 225 rpm in 250 ml screw-top shake flasks with a total medium volume of 50 ml M9IPGX+YE with the sugar and antibiotic concentrations as described. IPTG was again added at 0.1 mM at the beginning of the cultivation. 0.5 – 1 ml samples were taken throughout the fermentation for OD_{600} and HPLC measurements. The final biomass yield was determined from a 1 ml sample washed and dried overnight.

3.3.4 Determination of isobutanol and sugar concentrations via HPLC

Glucose, xylose, and isobutanol concentrations were determined via High-performance liquid chromatography (HPLC). 1 ml aliquots were taken throughout cultivation and then frozen until all samples were ready for processing. The aliquots were centrifuged and then the supernatant was removed and filtered through 0.2 μM filters. Sample volumes of 5 μl were run on a Rezex ROA column (Phenomenex) with a mobile phase of 0.005 N H_2SO_4 at 0.5 ml/min. Standard calibration curves were made by diluting 40% glucose or xylose or 15 g/L isobutanol stock in diH_2O and filter sterilizing through 0.2 μM filters. Xylodextrin standards were obtained from Megazyme and were resuspended to a final concentration of 30 g/L with diH_2O, then diluted to make a standard calibration curve. For determination of xylodextrin concentrations, the diluted standards and samples were filtered through 0.2 μM filters and run on the Rezex RSO column with diH_2O as the mobile phase, at 0.3 ml/min.

3.3.5 Corn stover hydrolysate preparation

The corn stover hydrolysate was pretreated by ammonia fiber expansion (AFEX) as described previously (*57*). The enzymatic hydrolysis was performed at 6% glucan loading for 3 days with 15 mg enzyme per gram glucan using a combination of Ctec2, Htec2 and Multifect Pectinase enzymes (Ratio: 66.67%+16.67%+16.67%) by the Biomass Conversion Research Laboratory (Michgan State University, Lansing, MI) and sterile filtered and stored at 4 ^{o}C. Before each microplate or 50 ml falcon tube experiment, an adequate amount of hydrolysate was neutralized by addition of 5 M

NaOH to a pH of 7 and then re-filtered. If the hydrolysate was diluted with diH_2O, the water was added and then the pH was adjusted. Antibiotics and IPTG were added in the same concentrations as with the M9IP medium.

3.3.6 Growth experiments with CS hydrolysate

Frozen stocks were inoculated into rich LB medium with antibiotics and grown overnight to saturation, then washed twice with minimal M9 medium without yeast extract. Cultures were then diluted by 1:100 and pipetted to a volume of 200 µl per well onto a 96-well microplate (Costar) covered with an adhesive Mylar film. Three to four replicates were conducted per microplate sample. Cultures were grown for 60 - 72 hours at 30^{o}C on a VersaMax (Molecular Devices) plate reader with shaking, and either OD_{600} or OD_{650} measurements were taken every 15 minutes. For the 50 ml falcon tube cultivations, cultures were inoculated in the same manner, and then washed once with minimal M9 medium and then washed again and resuspended in neutralized hydrolysate. The cultures were diluted to a total cell density of 1:100 in 10 ml hydrolysate in 50 ml falcon tubes with the sugar and antibiotic concentrations as described. IPTG was again added at 0.1 mM at the beginning of the cultivation. Cultures were grown for 96 hours at 30^{o}C with shaking at 225 rpm. Samples were taken throughout the fermentation for OD_{650} and HPLC measurements (0.2 – 0.5 ml sample volume).

3.4 Results

3.4.1 Two bacterial strains engineered to co-convert hexose and pentose sugars to isobutanol

A diagram of the proposed two-member consortium is shown in Figure 3.6, wherein two *E. coli* strains are co-utilizing pentose mono- and oligosaccharides and glucose mono-saccharides to isobutanol. Each specialist preferentially consumes xylose or glucose, as well as xylodextrins in the case of the C5 strain. The strains are first grown on defined minimal media, which contains only glucose or xylose sugars, and then on lignocellulosic biomass (corn stover). The corn stover is pretreated using AFEX (ammonia fiber expansion) and then enzymatically hydrolyzed using a commercial

enzyme mixture (see Methods 3.3.5). The hydrolysis reaction produces monomers and oligomers of glucose and xylose, the latter of which can be utilized by the C5 specialist strain (containing either pLOI3708 or pAK6, Table 3.2) in this work. In the future gluco-oligosaccharide utilization will also be engineered into the C6 partner.

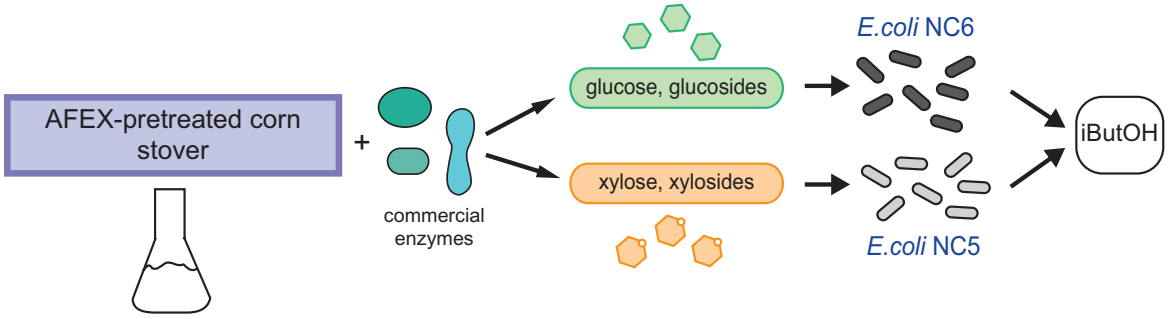

Figure 3.6 Process for converting AFEX-pretreated corn stover into isobutanol using *E. coli* specialist strains. The enzyme mixture breaks down the AFEX-pretreated corn stover, producing an enzymatic hydrolysate. The *E. coli* specialists then convert the sugars into isobutanol. Although the enzymes can hydrolyze the corn stover into glucose and xylose mono- and oligosaccharides, the glucose oligosaccharides are currently not utilized by the consortium.

To construct the two-member consortium we first selected a promising base strain, the *E. coli* NV3, a strain derived from evolution on a L-valine analog, norvaline (*63*). NV3 has been shown to produce high titers of isobutanol--comparable to other rationally designed strains (*61*) (see above descriptions of JCL260 and NV3 design and creation). Since *E. coli* is a natural hexose-utilizer, we did not further engineer this strain to be a C6 "specialist" as it will preferentially consume glucose without any further manipulation. The NV3 hexose specialist was termed "NC6". A full strain list is given in Table 3.2. The pentose specialist was constructed by knocking out genes for glucose transport and utilization: *ptsG*, *glk*, and *manX* (*78*), and was named "NC5" (Methods 3.3.1). We found that all three knockouts were necessary to eliminate growth on glucose (data not shown). Next we transformed each specialist with two plasmids that will allow for isobutanol production, pSA55 and pSA69 (*61*), (see Table 3.2). The plasmid pSA55 contains genes from the Erlich pathway that convert 2-keto acids to alcohols via heterologous genes from *L. lactis* and *S. cerevisiae* under control of the $P_L lacO_1$ promoter, induced via the addition of IPTG. The plasmid pSA69 overexpresses three

genes from the valine pathway under control of the $P_L lacO_1$ promoter, with two native *E. coli* genes and one homologous gene from *B. subtilis*.

Table 3.2 Strains and plasmids used in this chapter

Strain/plasmid	Genotype	Reference
NC6	NV3 evolved strain, various point mutations, see supplementary information	(*63*)
NC5	NV3 *ptsG glk manX*	This work
pSA55	ColE1 ori; AmpR; $P_L lacO_1$-*kivd-ADH2*	(*61*)
pSA69	p15A ori; KanR; $P_L lacO_1$-*alsS-ilvC-ilvD*	(*61*)
pLOI3708	pNEB193 derivative; AmpR; pLacZ-*xynTB*	(*74*)
pAK6	ColE1 ori; AmpR; $P_L lacO_1$-*kivd-ADH2-xynTB*	This work

3.4.2 Co-culture performance on mixed-sugar defined media

After constructing the specialists, we first investigated the growth, sugar consumption, and isobutanol production profile in defined minimal medium with glucose, xylose, or both sugars to confirm that the monocultures were indeed either pentose- or hexose-utilizing specialists and that they could make isobutanol. As seen in Figure 3.7 and Table 3.3, the NC5 strain was able to preferentially utilize xylose (Figure 3.7 A&B), while the NC6 strain preferentially used glucose (Figure 3.7 A&B). The growth profile is shown in Figure 3.7A. After about two days of growth on the mixed sugar media (18 g/L each of glucose and xylose), each monoculture produced 2.77 ± 0.06 and 5.80 ± 2.36 g/L isobutanol for the NC5 or NC6 strain, respectively (Figure 3.7D, Table 3.3).

When grown in co-culture at a ratio of 1:1 NC5:NC6, however, 6.57 ± 3.00 g/L isobutanol was produced (Figure 3.7D and Table 3.3), more than either monoculture even though the NC6 strain is still diauxic and has the ability to consume both glucose and xylose. However, with the high variability of the NC6 and NC5:NC6 co-culture taken into account, the titers were not significantly different (Figure 3.7C, Table 3.3). After 48 hours the cultures did not appear to be producing appreciably more isobutanol, so we examined the yield and productivity parameters at this point. The yield of isobutanol on the total amount of sugar consumed for the NC5, NC6 and NC5+NC6 co-culture was 0.201 ± 0.014, 0.339 ± 0.033, and 0.334 ± 0.007 g/g, respectively, and the productivities were 0.058 ± 0.001, 0.121 ± 0.049, and 0.137 ± 0.062 g/L/hr (Table 3.3). For the co-

culture, this corresponds to 81.5% of the theoretical yield (0.41 g/g). Looking at these values, it seems as if the co-culture was not significantly better than either monoculture, however the isobutanol produced per cell was much larger in the 1:1 co-culture, 4.03 ± 0.007 g/gDM vs. 0.201 ± 0.014 or 0.339 ± 0.033 g/gDM, suggesting that the cells in the co-culture may have been significantly more efficient at converting sugar to isobutanol on a per cell basis (Table 3.3).

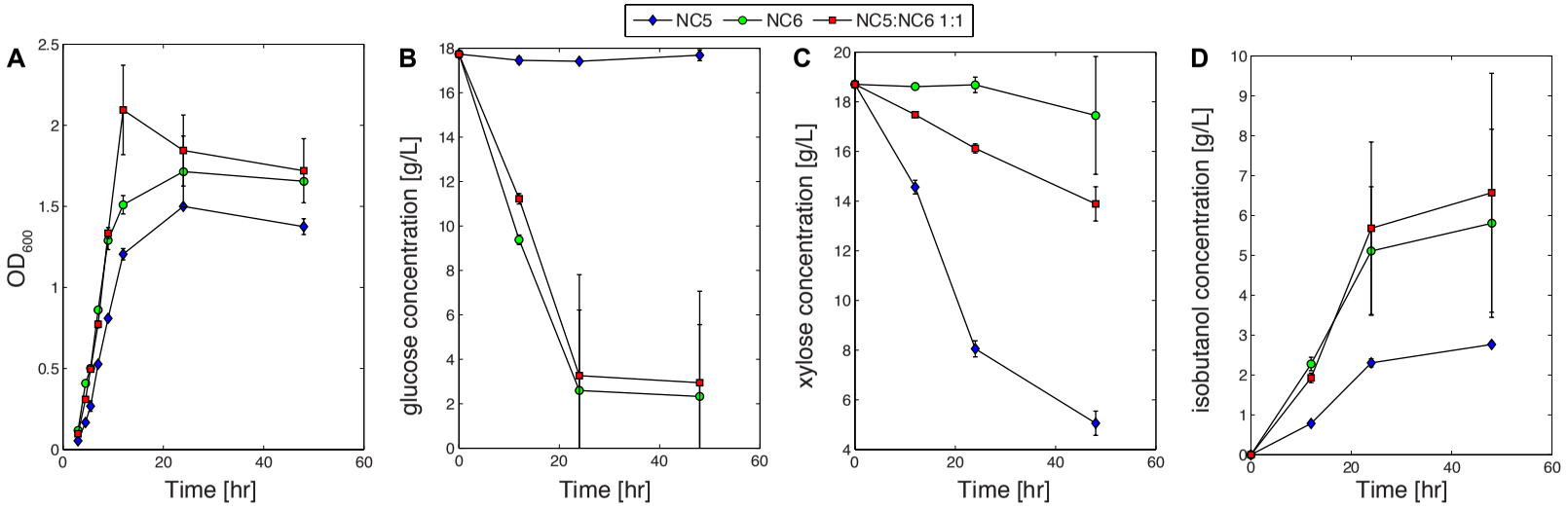

Figure 3.7 Mono- and co-culture growth profile (A), glucose (B) and xylose (C) consumption, and isobutanol production (D) on defined media containing both glucose and xylose (concentration of each sugar is 18 g/L, 36 g/L total).

Table 3.3 Sugar consumption and isobutanol production in mono- and co-culture on 18 g/L glucose and 18 g/L xylose. Data shown at 48 hours.

Strain	Glucose consumption [g/L]	Xylose consumption [g/L]	iButOH titer [g/L]	iButOH titer/cell [g/gDM]	iButOH $Yield_{P/S}$ [g/g total sugar]	iButOH Productivity q_P [g/L/hr]
NC5	0.05 ± 0.25	13.64 ± 0.49	2.77 ± 0.06	1.84 ± 0.04	0.201 ± 0.014	0.058 ± 0.001
NC6	15.41 ± 3.24	1.25 ± 2.37	5.80 ± 2.36	1.09 ± 0.25	0.339 ± 0.033	0.121 ± 0.049
NC5 + NC6	14.79 ± 4.12	4.81 ± 4.46	6.57 ± 3.00	4.03 ± 0.45	0.334 ± 0.007	0.137 ± 0.062

Unexpectedly, the NC5 strain was the least variable in the mixed-sugar media (previous C5 specialist test strains had shown poor performance and high variability). It also consumed 13.64 ± 0.49 g/L xylose over 48 hours, demonstrating that it is indeed an efficient C5 consumer (Figure 3.7C and Table 3.3). When grown in co-culture with the NC6 at a ratio of 1:1, more xylose was utilized than in the NC6 monoculture, illustrating that the use of a co-culture when co-utilization is the desired outcome is, in this case, the better option. Interestingly, increasing the ratio of the NC6 partner (NC5:NC6 = 1:5) did not increase the isobutanol titer over that of the 1:1 co-culture in the mixed sugar medium with 36 g/L total sugars (Figure 3.8D), even though NC6 produces more isobutanol then the NC5 as a monoculture. Also, increasing the NC5 fraction to 5:1 did not result in more xylose utilization (Figure 3.8C).

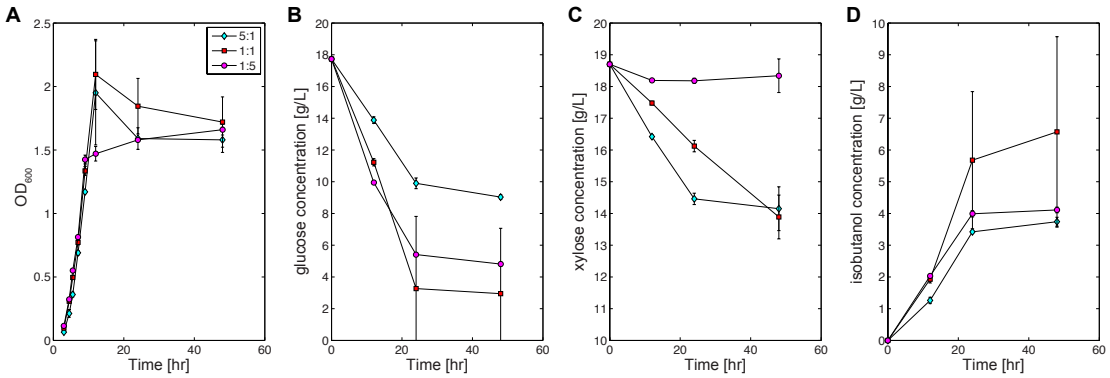

Figure 3.8 Growth profile (A), sugar consumption (B, C), and isobutanol production (D) on 18 g/L each of glucose and xylose defined media for co-culture combinations 5:1, 1:1, and 1:5 NC5:NC6.

Additionally the amount of total sugar seems to greatly affect the final isobutanol titers. In contrast to above, previous studies with increased amounts of total sugars (36 g/L each, 72 g/L total) showed that the co-culture produced significantly higher titers than either monoculture, however only one biological replicate of the NC6 strain was tested in this experiment (see Figure 3.9 and Table 3.4). The experiment was then repeated with lower sugar (36 g/L total) since much of the sugar was not consumed, and the above result was obtained (Figure 3.7). Interestingly, in the experiment with 72 g/L total sugar, the NC6 strain produced the least isobutanol, but with 36 g/L total sugar the NC5 has much lower titers than either NC6 or the co-culture (Table 3.3, Table 3.4).

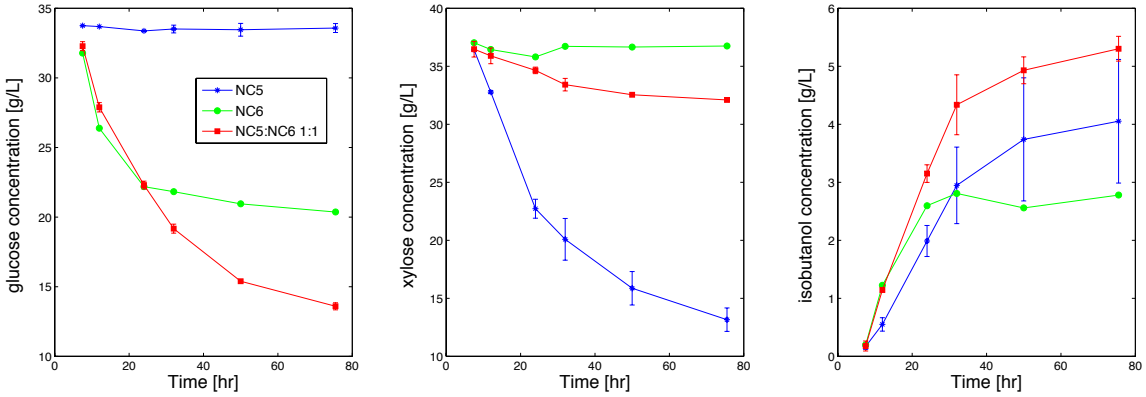

Figure 3.9 Mono- and co-culture sugar consumption and isobutanol production on defined media containing both glucose and xylose (36 g/L each, 72 g/L total)

Table 3.4 Sugar consumption and isobutanol production of the NC5, NC6, and co-culture after about 2 days (48 or 50 hr) on 36 g/L of each sugar (72 g/L total).

Strain	Glucose consumption [g/L]	Xylose consumption [g/L]	iButOH titer [g/L]	iButOH Yield$_{P/S}$ [g/g total sugar]	iButOH Productivity q_P [g/L/hr]
NC5	0.22±0.46	21.01±1.44	3.74±1.06	0.175±0.041	0.075±0.021
NC6	12.72	0.22	2.56	0.198	0.051
NC5 + NC6	18.28±0.09	4.33±0.01	4.93±0.23	0.218±0.011	0.099±0.005

There was also some growth inhibition and inhibition of product formation observed when both sugars were present in the media, which may be part of the reason there are such variable dynamics depending on the total sugar content. The growth rates of the strains in monoculture on the microplate were reduced when grown with both sugars present (Figure 3.10) and the NC6 strain produced more isobutanol when grown in glucose alone (Figure 3.10 and Table 3.5, 6.64 ± 0.15 vs. 2.56 g/L for 36 g/L total glucose).

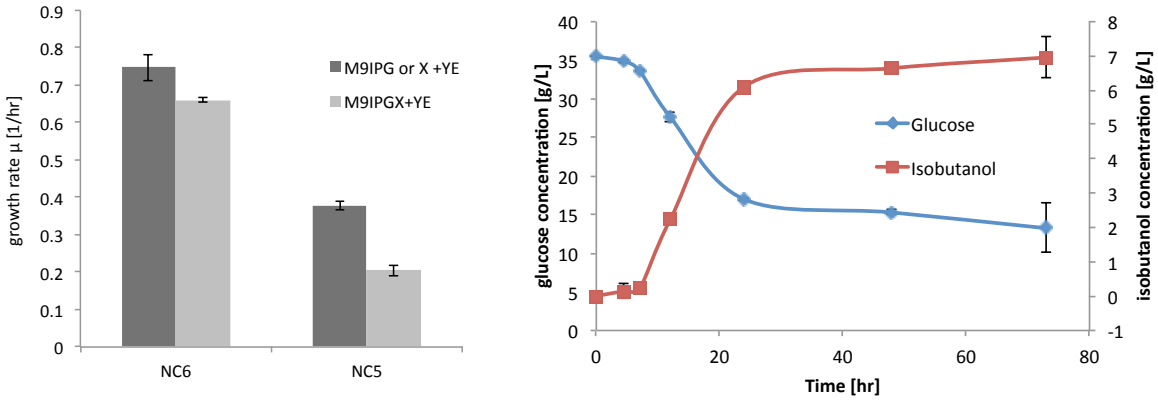

Figure 3.10 (Left) Growth rate inhibition when two sugars are present in the media (M9IPGX) vs. when only one sugar is present (M9IPG or X). YE = yeast extract. (Right) Glucose consumption and isobutanol production of the NC6 strain in 36 g/L glucose media.

Table 3.5 Glucose consumption and isobutanol production for the NC6 strain on glucose only (36 g/L).

Strain	Glucose consumption [g/L]	iButOH titer [g/L]	iButOH yield P/S [g/g total sugar]	iButOH productivity qP [g/L/hr]
NC6	20.19 ± 0.32	6.64 ± 0.15	0.329 ± 0.002	0.138 ± 0.003

Part of the observed variability may have been due to the plasmid loss over the course of the culture growth. On the defined media we often observed that the pSA69 plasmid (KanR, counts on LB Kan plates) was often lost to large degree by 48 hours, and the pSA55 plasmid (AmpR, counts on LB Amp plates) was either lost to a lesser extent or occasionally the colony count was even higher than for the LB plates without antibiotic (Figure 3.11). Since we only added antibiotics and inducer to the culture at the beginning of growth, this problem could be overcome by addition of antibiotics at a later time point, or by moving the plasmid genes onto the chromosome, an idea which will be discussed further in the Discussion, Section 3.5.

While the titers of the NC6 strain on glucose alone are slightly higher, the results still demonstrate that a co-culture of specialists can outperform a monoculture even when compared to a diauxic strain such as the NC6 on a mixed-sugar defined media, which better approximates an actual biomass feedstock than a single-sugar media.

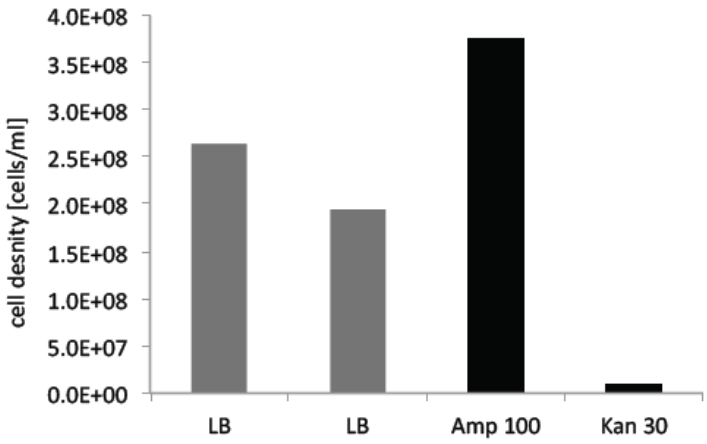

Figure 3.11 Example of plasmid loss at the end of the cultivation. Cell density was determined via plate counting. Two LB plates and one plate for each antibiotic, either LB ampicillin 100 μg/ml or LB kanamycin 30 μg/ml, were counted. The pSA55 plasmid confers resistance to ampicillin (AmpR), and the pSA69 plasmid to kanamycin (KanR).

3.4.3 Sugar variation in defined media

Before testing the co-culture on a lignocellulosic substrate, we wanted to determine if the optimal ratio for isobutanol production differed depending on the media composition, and if so, if there is an optimal ratio that might work well on the hydrolysate. We chose to look at two media compositions: 1:1 and 1:2 xylose to glucose (X:G), to mimic the approximate sugar concentrations of our chosen feedstock. We also investigated various ratios of specialist strains, from 5:1 to 1:5 NC5:NC6, on each media. The 5:1 culture was not included on the 1:2 media since it was not likely that this would be better for production. The total amount of sugars in these experiments was kept constant at 72 g/L, which is closer to the approximate hydrolysate composition. For the 1:1 X:G media, that is 36 g/L of each sugar, and for the 1:2 X:G that is 48 g/L glucose and 24 g/L xylose.

Overall there was not a vast difference among the co-culture mixtures on the 1:1 media with 72 g/L total sugar (Figure 3.12A-C). Not much sugar was utilized in these co-cultures, though the 5:1 co-culture consumed almost as much xylose as glucose, illustrating that if utilization of the different substrates is a main concern then modifying the partner ratio is a way to achieve that goal; oddly, the isobutanol titers were not as high

as in the experiments above (Figure 3.12C, Table 3.6). These experiments were not performed in duplicate due to the large number of flasks run simultaneously, so that may explain why the results are so different in this case. However they do give some insight into the co-culture dynamics—interestingly, although the 1:5 co-culture had the highest isobutanol yield at at 0.226 g/g, the 2:1 culture achieved the highest isobutanol titer and titer per cell at 3.98 g/L and 1.97 g/gDM (Table 3.6). It was surprising that the 2:1 NC5:NC6 co-culture did better than the others on 1:1 media in several categories, as the NC5 often did not perform as well as the NC6 in monoculture. This illustrates the fact that the co-culture dynamics are often difficult to predict, but it would be best to repeat these experiments with more biological replicates, seeing how the variation from the other experiments affects the outcome.

On the 1:2 xylose:glucose (X:G) media, the results were much different (Figure 3.12D-F). The 1:2 co-culture was now producing the most isobutanol at 5.58 g/L (Figure 3.12F, Table 3.7). This is not too surprising, since the co-culture ratio matches the sugar ratio in the medium. This culture also had the highest isobutanol yield (0.257 g/g total sugar) and highest titer per cell (3.03 g/gDM) (Table 3.7). Clearly, the optimal ratio for the 1:2 X:G sugar combination was also 1:2 NC5:NC6, which informed our choices for ratios on the corn stover hydrolysate, discussed in the next section.

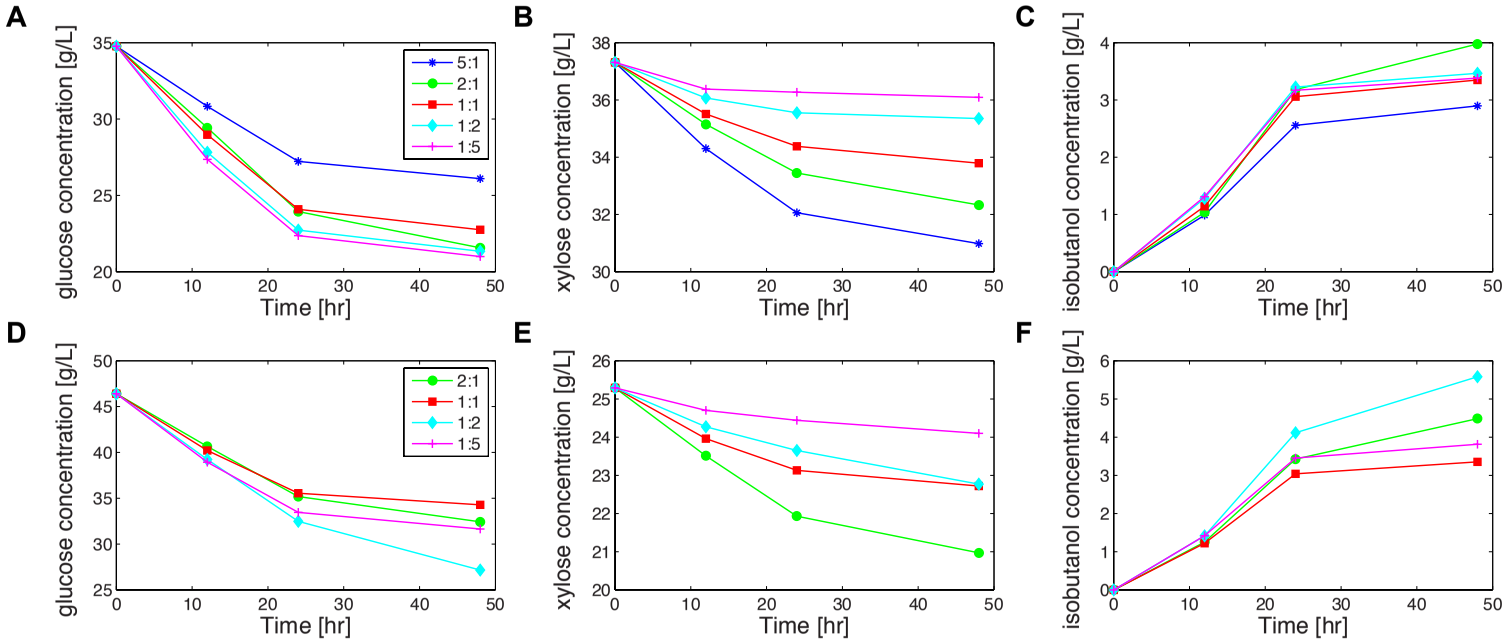

Figure 3.12 Glucose (A, D) and xylose (B, E) consumption and isobutanol production (C, F) in 1:1 xylose:glucose (X:G) media (A-C) and 1:2 (D-F) xylose:glucose (X:G) media, 72 g/L total sugar. Culture ratios are all NC5:NC6. Legend is the same for (A-C) and for (D-F).

Table 3.6 Sugar consumption and isobutanol production in 1:1 xylose:glucose (X:G) media, 72 g/L total sugar.

Culture ratio NC5:NC6	Glucose consumed [g/L]	Xylose consumed [g/L]	Isobutanol titer [g/L]	Isobutanol $yield_{P/S}$ [g/g total sugar]	Isobutanol titer per cell [g/gDM]	Isobutanol productivity [g/L/hr]
5:1	8.67	6.32	2.90	0.193	1.57	0.060
2:1	13.2	4.98	3.98	0.219	1.97	0.083
1:1	12.02	3.52	3.35	0.215	1.82	0.070
1:2	13.44	1.95	3.47	0.225	1.75	0.072
1:5	13.78	1.22	3.38	0.226	1.68	0.070

Table 3.7 Sugar consumption and isobutanol production in 1:2 X:G media, 72 g/L total sugar

Culture ratio NC5:NC6	Glucose consumed [g/L]	Xylose consumed [g/L]	Isobutanol titer [g/L]	Isobutanol $yield_{P/S}$ [g/g total sugar]	Isobutanol titer per cell [g/gDM]	Isobutanol productivity [g/L/hr]
2:1	13.97	4.32	4.49	0.245	2.02	0.093
1:1	12.12	2.57	3.35	0.228	2.07	0.070
1:2	19.24	2.52	5.58	0.257	3.03	0.116
1:5	14.76	1.19	3.81	0.239	1.70	0.079

3.4.4 Isobutanol production on AFEX-pretreated corn stover hydrolysate

Next we investigated the growth of the pair on an actual lignocellulosic feedstock. Our chosen feedstock is corn stover (CS) that has been pretreated using ammonia fiber expansion (AFEX) which was then enzymatically hydrolyzed to monomeric and oligomeric sugars using a commercial enzyme mixture (BCRL, MSU). A description of the enzymes used is given in the Methods, Section 3.3.5. The measured sugar concentrations for glucose and xylose in this batch of hydrolysate were ~55 g/L glucose and ~34 g/L xylose. The strains were first grown on the undiluted CS hydrolysate (titrated to a neutral pH of ~7) in microplate studies to ensure that these strains would indeed grow on the unsupplemented hydrolysate, which may contain some inhibitory compounds especially with regard to xylose utilization (*58*). The strains grew surprisingly well, achieving comparable growth rates compared to the control strain, wildtype K12 MG1655, of up to 0.29 ± 0.19 1/hr for the NC5+NC6 co-culture vs. 0.37 ± 0.03 1/hr for the control, and maximum OD_{600} values up to 0.47 ± 0.10 vs. 0.37 ± 0.06 for the control (Figure 3.13) although the lag phases were longer and the growth more variable, as evidenced by the large error bars.

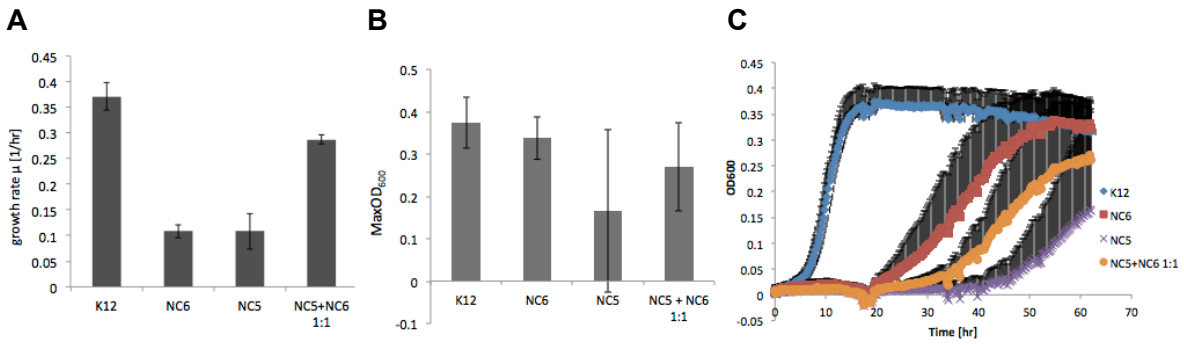

Figure 3.13 Growth rate (A), maximum OD_{600} (B) and growth profile (C) of mono- and co-cultures in undiluted hydrolysate on the microplate. Error bars are ± standard deviation of four replicates for (A, B) and + standard deviation only for (C).

We next grew the strains on the undiluted CS hydrolysate in 50 ml falcon tubes to investigate the sugar consumption and isobutanol production, if any, on this complex feedstock. The hydrolysate was not supplemented with any nutrients, salts, or extra sugars beyond that which was produced via enzymatic hydrolysis. Each strain was grown in monoculture (two biological replicates) and in co-culture at ratios 2:1, 1:1, and 1:2 NC5:NC6 (one biological replicate each). Although we saw variable growth on the microplate with some samples, we only tested one biological replicate for each co-culture since we were limited by the total amount of hydrolysate available. Again the strains grew quite well on the CS hydrolysate, with growth rates up to 0.242 1/hr for the 1:1 co-culture (data not shown), which grew faster than either monoculture. In terms of sugar consumption, oddly not much sugar was utilized in any of the cultures, but we were able to obtain up to 2.29 g/L isobutanol with the 1:2 co-culture, which produced much more isobutanol than either of the other co-cultures and the mono-cultures (data not shown).

The lignocellulosic biomass and the CS hydrolysate in particular have compounds that have may be inhibitory towards cells, especially with regard to xylose utilization (*58*), so we tried diluting the hydrolysate to 75% with sterile deionized water. Since the strains were barely utilizing all of the sugars present in the unmodified hydrolysate, we reasoned that the hydrolysate could be further diluted without a decrease in substrate availability and that the dilution might even increase isobutanol production and sugar utilization rates. Figure 3.15 shows the results on the 75% diluted CS hydrolysate after 4 days (96 hours) of growth in 50 ml falcon tubes. The growth rates were higher when diluted with water and the growth patterns changed -- now the NC5 strain was growing

slightly faster than the rest at 0.294 ± 0.002 1/hr followed by the 2:1 co-culture (Figure 3.15A). The lag phases were also shortened by about 6 hours (Figure 3.15A) and were much shorter than the lag phases in the microplate experiment with undiluted hydrolysate (Figure 3.13C). The strains were also fairly stable in the diluted hydrolysate, as the error bars are quite small. In terms of sugar consumption, again not much glucose nor xylose was consumed; the 1:1 culture consumed the most glucose at 9.89 ± 0.37 g/L and NC5 the most xylose at 3.98 ± 0.62 g/L (Figure 3.15B&C). The co-cultures outperformed the monocultures with regard to isobutanol production, with the 1:1 co-culture producing the highest titer at 2.95 ± 0.05 g/L isobutanol, though all of the co-cultures achieved titers above 2.8 g/L (Figure 3.15D, Table 3.8). With regard to isobutanol yield the NC6 strain performed similarly to the co-cultures, although the 1:2 co-culture was again the most efficient at isobutanol production, producing 0.267 g/g total sugar on both glucose and xylose, corresponding to ~65% theoretical yield (Table 3.8).

The NC5 strain was again performing better than expected, as the growth rates and titer were higher than the parental NC6 (NV3) strain without modification. We also examined the ratios at the end of the growth (96 hours) using differential plate counting and found that the ratios changed to favor the NC5 strain (Figure 3.14). The ending ratios for the 2:1, 1:1, and 1:2 co-cultures were 4.59 ± 0.55, 1.98 ± 0.38, and 1.41 ± 0.41 NC5:NC6. This may be due to some synergy between some of the NV3 base strain mutations (Appendix Table 1) and the genes knocked out to create the NC5.

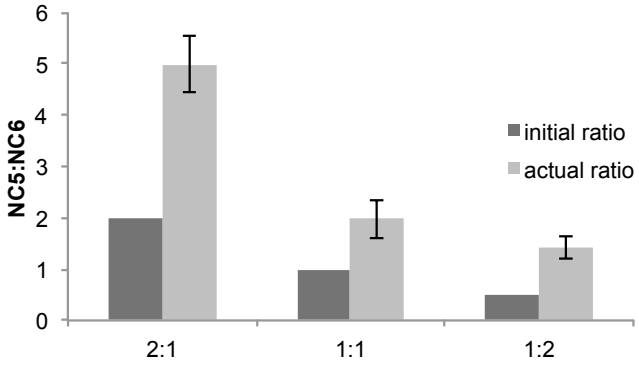

Figure 3.14 NC5:NC6 ratios at the end of cultivation on the diluted 75% hydrolsyate ("actual" ratio) determined via differential plate counting. X-axis labels denote the inoculation ("initial") ratio. MacConkey-glucose plates were used to differentiate the NC5 from the NC6 strain.

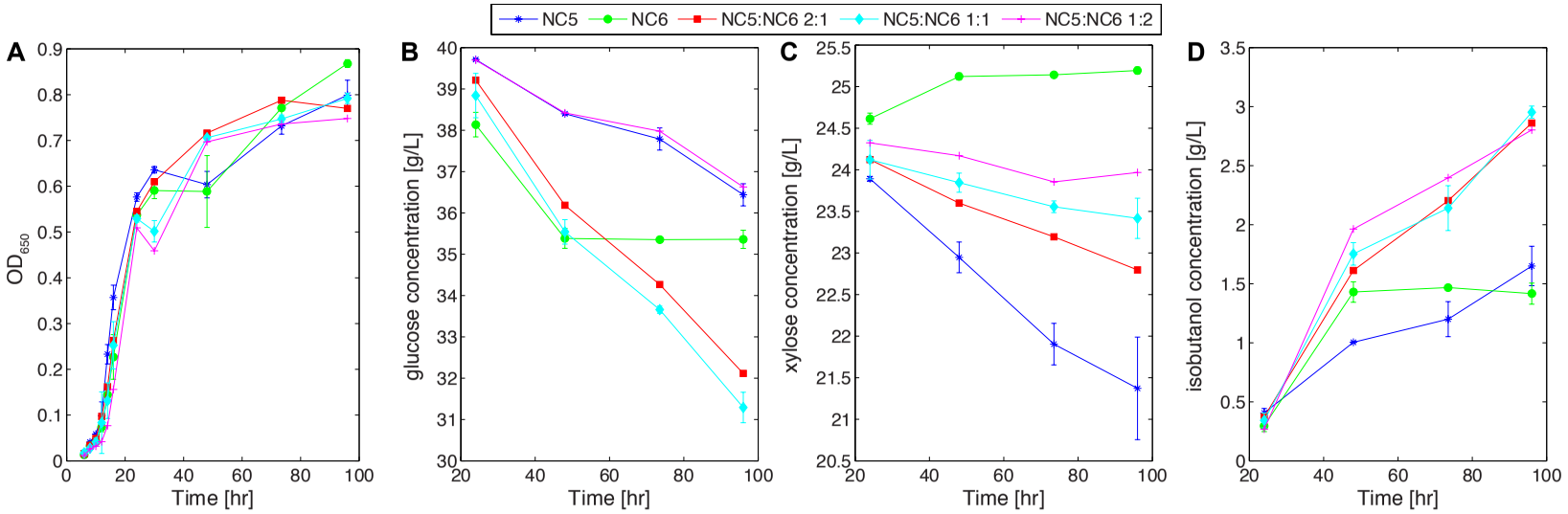

Figure 3.15 Growth profile (A), glucose (B) and xylose (C) consumption and isobutanol production (D) on diluted 75% CS hydrolysate after 96 hours. Error bars are ± standard deviation of four replicates.

Table 3.8 Isobutanol yields and productivity on diluted 75% CS hydrolysate after 96 hours.

Sample	iButOH titer [g/L]	iButOH yield$_{P/S}$ [g/g] G+X	Average iButOH Productivity q_P [g/L*hr]
NC5	1.65 ± 0.17	0.189 ± 0.012	0.017 ±0.002
NC6	1.42 ± 0.09	0.237 ± 0.008	0.015 ±0.001
2:1	2.86	0.246	0.030
1:1	2.95 ± 0.05	0.250 ± 0.002	0.031 ±0.001
1:2	2.80	0.267	0.029

3.4.5 Xylodextrin utilization by NC5 pLOI3708

It had been previously found that the CS hydrolysate contains up to 9.89 g/L xylose oligosaccharides and up to 2.75 g/L glucose oligosaccharides resulting from incomplete enzymatic hydrolysis (Venakatesh Balan, *personal communication,* BCRL, MSU). In order to utilize this significant portion of oligomers left in the feedstock, we engineered the NC5 strain to utilize xylodextrins by introducing genes for xylodextrin transport and metabolism from *Klebsiella oxytoca*, *xynTB* (*74*), as discussed above in the Introduction, Section 3.2.4. These genes were amplified from plasmid pLOI3708 (*74*) and then assembled to pSA55 behind the *ADH2* gene under control of the $p_L lacO_1$ promoter, creating vector pAK6 (see Table 3.2). We then transformed the NC5 strain with the completed pAK6 and pSA69 to allow for simultaneous xylodextrin utilization and isobutanol production (Methods). Plasmid pLOI3708 was also transformed into NC5 as a control and test strain.

To test the functionality of the *xynTB* operon, we first grew the NC5 xynTB-containing test strain NC5 pLOI3708 in minimal M9 medium with only xylodextrins or xylose as a carbon source. With 2 g/L of each xylodextrin present (xylobiose – xylohexaose, X_2 – X_6) the cells were able to grow as well or better than the positive control, M9 + 5 g/L xylose (Figure 3.16). Although the maximum optical density values are low (the plate was accidentally left without shaking for the first ~21 hours, so there was less aeration) it can still be concluded that there is a definite difference between the growth on xylodextrins and the growth on the M9 medium without additional sugar (negative control), and that the *xynTB* operon allows utilization of the xylodextrins up to X_6.

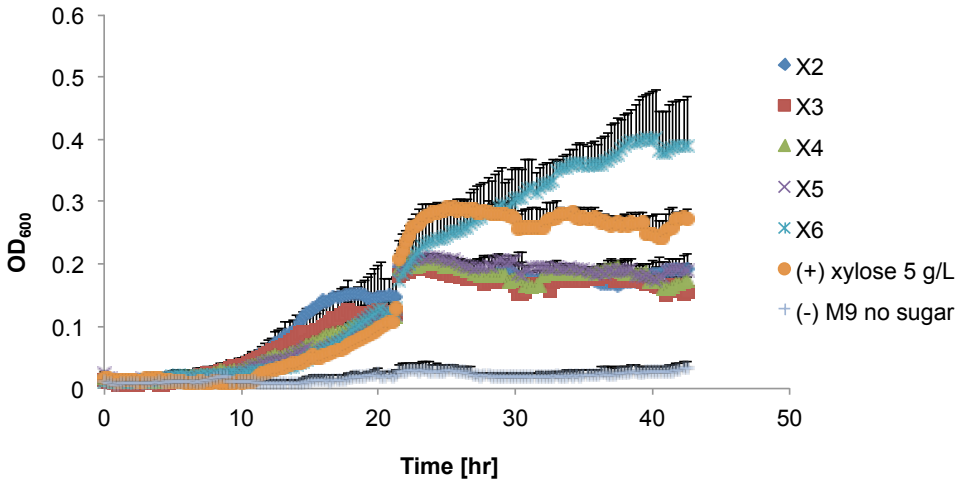

Figure 3.16 Growth profile of the NC5 pLOI2708 strain on 2 g/L xylobiose (X2), xylotrioise (X3), xylotetraose (X4), xylopentaose (X5), and xylohexaose (X6). For comparison growth is shown on 5 g/L xylose, (+) control, and on M9 with no sugar (-) control. Positive error bars show the standard deviation of three replicates.

Next we grew the NC5 xynTB-containing strain NC5 pLOI3708 on the hydrolysate and examined the changes in xylodextrin concentration vs. the NC5 strain without *xynTB* as measured by HPLC. As shown in Figure 3.17A, the growth of the NC5 pLOI3708 strain was comparable to the NC5 strain without any plasmids, in contrast to the isobutanol–producing strains which grow more slowly. Very little glucose or xylose was utilized by these cultures, and the profiles were similar between the two strains (data not shown). However there is a clear difference in the consumption profiles of several HPLC peaks (Figure 3.17B,C,D), which we have preliminarily identified via HPLC as xylobiose (X_2), xylotriose (X_3), and xyloheaxose (X_6). We did not see a change in the peaks identified as possible xylotetraose and xylopentaose peaks. At this time these peaks have been only identified preliminarily as xylodextrin peaks, since the retention times of the xylodextrins seem to be shifted when in the hydrolysate. For this reason, only the peak areas are plotted, rather than the xylodextrin concentrations, however, there is a clear difference between the NC5 strain without the plasmids and that with the *xynTB*-containing pLOI3708. This result combined with the microplate study just discussed indicates that there is some utilization of the xylodextrins occurring when the *xynTB*

genes are expressed. Other methods which will be used in the future to confirm the xylodextrin consumption are discussed below.

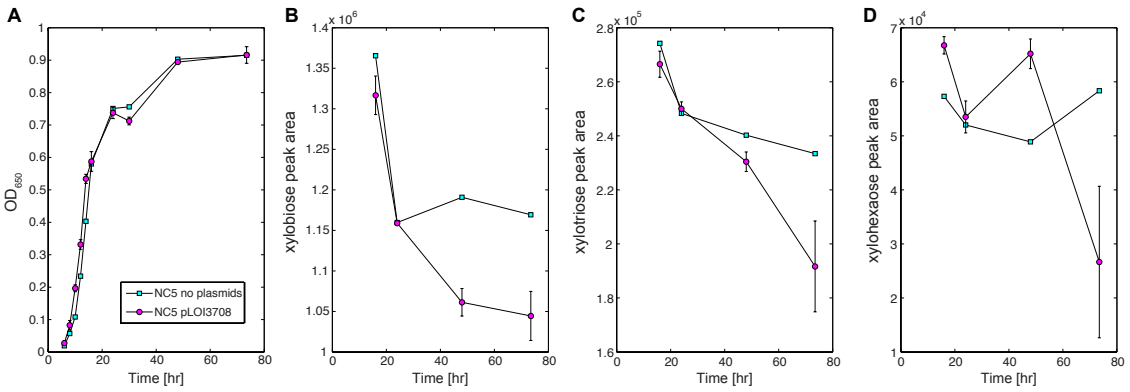

Figure 3.17 Xylodextrin utilization of the NC5 pLOI3708 strain on 75% hydrolysate. (A) Growth profile and utilization of xylobiose (B), xylotriose (C) and xylohexaose (D) on 75% CS hydrolysate. Results are shown for the NC5 strain with no plasmids incorporated and the NC5 pLOI3708 (two biological replicates). Peak areas are shown for the xylodextrins instead of concentrations. HPLC results are from the Rezez-RSO oligosaccharide column.

3.5 Discussion and conclusion

In conclusion, we have designed a two-member *E. coli* consortium that is capable of converting hexose and pentose monosaccharides (and potentially pentose oligosaccharides) into isobutanol. We have shown that the co-culture of a five- and six-carbon specialist (NC5/NC6) produces higher titers of isobutanol than a diauxic strain (NC6) under the same conditions (6.57 vs. 5.8 g/L), at a yield of about 82% of theoretical. We have also demonstrated that this co-culture grows well on AFEX-pretreated corn stover (CS) hydrolysate and produces almost up to 3 g/L isobutanol (at ~65% of the theoretical yield) without supplementation, and that diluting this hydrolysate with diH_2O increases titers and improves growth (Figure 3.15). This work addresses some of the remaining challenges that remain in the conversion of lignocellulosic feedstocks to next-generation biofuels: complete utilization of five-carbon sugars and achieving high titers on actual biomass as opposed to defined laboratory media.

It is important to consider our results in the context of other isobutanol production schemes. In terms of overall titers on *defined* media, ours are much lower than that obtained by Baez *et al*. (*67*), which used a gas stripping mechanism for isobutanol removal from a much larger 1 L bioreactor. Since isobutanol is toxic at about 7-8 g/L (*67*) high titers of isobutanol are unlikely to be achieved without some mechanism to remove the product. If we compare our process with other work using the same strain in 250 ml shake flasks on defined media, we again see that our titers are lower, but are yields are comparable or even higher. In previous work with the NV3 strain, it was reported to produce 8 g/L after 24 hours with no glucose feeding and 13.6 g/L after 99 hours with glucose feeding, achieving an isobutanol yield of 0.24 g/g (productivity 0.0024 g/L/h, calculated from (*63*)), vs. our yield of 0.33 g/g after only 48 hours. This shows that our co-culture process is more efficient with regard to isobutanol yield. We could increase the titer by feeding more sugar as in these other processes, however, in our experiments the sugar was not completely consumed, so it is not clear that feeding cycles would further increase the isobutanol titer in our case.

In selecting a promising base strain for the C5 and C6 specialists, we examined the isobutanol production and yields of various isobutanol producers, such as JCL60, NV3, and NV3r1 (*62, 63*) under our preliminary culture conditions. Although in previous work the JCL260 strain exhibited the highest isobutanol yield, and the NV3r1 strain the highest isobutanol titer under the same conditions (*63*), in our hands the NV3 was the least variable and produced the highest isobutanol titer when grown on xylose, suggesting that it would make a good C5 specialist (data not shown). For these reasons we chose the NV3 as our base strain over the JCL260 or NV3r1. Differences between our culture conditions and those of the previous study (feeding cycles, induction time, etc.) may have contributed to the exhibited differences in the best producer. Additionally, we used plasmids pSA55 and pSA69, whereas plasmids pSA65 and pSA69 were used in the previous study (*63*). Since pSA65 contains a better ADH enzyme, AdhA from *L. lactis*, (*66*), this will certainly affect the final titers achieved and each ADH may perform differently depending on the host strain. Switching from pSA55 to pSA65, therefore, may be one way to further increase our titers, as this enzyme has shown better production than ADH2 is previous work (*66*).

We observed much variability in isobutanol production, especially with the NC6 and NC5+NC6 cultures. We hypothesized that most of this variability was due to plasmid loss during the fermentation, as plate counting revealed that the cells often lost the larger pSA69 plasmid in defined medium. A possible solution to this problem could be to supplement antibiotics throughout the co-culture growth, however this would not be useful in an industrial setting due to the cost and would increase the chance of contamination. We could instead move the plasmid-borne genes onto the chromosome using λRed phage recombination or a similar method. This would likely need further optimization as the chromosomal expression level of these genes (which corresponds to one copy) would then be much lower than that on multi-copy plasmids.

Although our process is aerobic, we did observe some fermentation byproduct formation in the NC5, NC6, and NC5+NC6 cultures, perhaps as a result of oxygen depletion during the course of growth. The cultures were grown at a volumetric flask to culture ratio of at least 5:1 and the flasks were opened every 12-24 hours to retrieve samples (the ratio would increase over time due to decreases in culture volume as a result of sampling). As shown in Figure 3.18 below, for the fermentation with 36 g/L of each sugar (72 g/L total) a significant amount of ethanol was produced in the monocultures and co-cultures, as well as some acetate and succinate. These byproducts may have led to the cessation of growth and lessened overall isobutanol titers. Since the flasks must be closed to prevent isobutanol evaporation, the best way around this problem is to eliminate the pathways for byproduct formation, as demonstrated previously (*62*). This can be achieved by knocking out genes such as *adhE* for ethanol, *pta* for acetate, and *frdAB* for succinate formation.

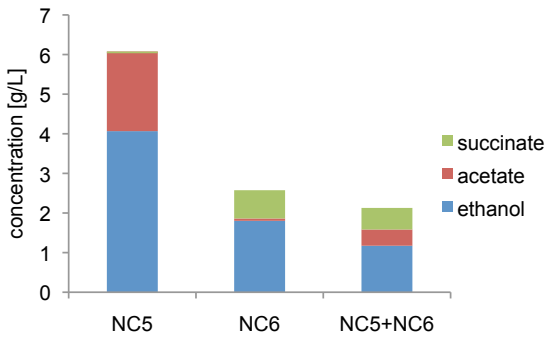

Figure 3.18 Byproduct formation on M9IPGX+YE 36 g/L each sugar (72 g/L total). Only one biological replicate is shown for each culture.

In contrast to our chosen aerobic system, the maximum isobutanol yield would be obtained via an anaerobic process (*80*). This is not possible with the current setup, as two enzymes in the pathway (IlvC and ADH) require the cofactor NAD(P)H which cannot be regenerated anaerobically (*80*). To resolve this issue, in a recent article by Bastian *et al*., the IlvC (ketol-acid reductoisomerase) was engineered via evolution and targeted mutagenesis to use the cofactor NADH instead of NAD(P)H (*80*) which is generated via glycolysis. By combining this engineered enzyme with another version of the alcohol dehydrogenase that can utilize NADH (LdhA from *L. lactis*) isobutanol production at 100% of the theoretical maximum under anaerobic, NADH-producing conditions, was achieved (*80*). To improve our system, we could then utilize these enzymes in place of the IlvC on plasmid pSA69 and the ADH on plasmid pSA55, and convert our setup to an anaerobic process. This would likely change our results and experimental process a great deal.

An obvious next step for our system is to combine the NC5 pAK6/pSA69 strain with the NC6 and grow these in co-culture on the hydrolysate. From preliminary cultivations on the diluted hydrolysate it is not clear whether or not the addition of the *xynTB* genes allows for increased isobutanol production. This may be due to the high concentration of xylose that still remains unutilized at the end of the cultivation. Also, there will likely be several rounds of optimization necessary in order to see acceptable results. Utilization of the xylodextrins should also be confirmed with other methods besides HPLC, since we have observed that the retention times of the xylodextrins seem to have shifted in the hydrolysate. Other qualitative methods include thin-layer

chromatography (TLC) (*81*), which has been used in the past to measure the consumption of xylodextrins (*74*). Additionally, we could do an acid hydrolysis of the culture supernatants before and after cultivation to measure the total oligosaccharide content. This method, however, would not identify the usage or presence of individual oligosaccharides.

Lastly, we would like to combine these two *E. coli* specialists with a fungal cellulolytic specialist, *Trichoderma reesei*, to create a truly "one-pot" production system whereby the fungus acts in place of the enzyme mixture to break down the corn stover directly into fermentable sugars. This idea is discussed further in the Future Directions, Section 5.2.2.

Chapter 4 Use of microbial consortia in high-throughput screening for over-production of L-valine and isobutanol

4.1 Summary

In this work, we have designed a two-member microbial consortium consisting of a secretor-sensor pair to detect highly-secreting L-valine production strains. This will be part of a larger effort to develop a new high-throughout screening (HTS) method for automated production strain development and identification. We have identified a partner strain that exhibits synergistic growth with the L-valine auxotroph, ΔpanB, a pantothenate auxotroph. We then engineered a secretor "proof-of-concept" strain with mutation capabilities incorporating several mutations for L-valine over-production (*panB*$^-$, *ilvNfbr*), and demonstrated that when grown with the L-valine auxotroph the co-culture growth is increased with *panB* deletion, however additional secretor strain characteristics that are beneficial for engineering mutations (such as *mutS*$^-$) may overshadow growth benefits conferred on the L-valine auxotroph (the sensor strain, ΔilvE). The composition of the co-culture, however, is altered to favor the sensor strain, indicating increased L-valine secretion. We also investigated optimal conditions for growth by titrating the concentration of L-leucine that is added to the medium.

The materials presented in this chapter will be reported as part of a future manuscript: Kerner A, Park J, Minty J, Rossion M, Burns MA, and Xiaoxia (Nina) Lin. A high-throughput screening system for microbial overproduction based on cross-feeding and droplet cultivation.

4.2 Introduction

4.2.1 High-throughput microbial screening techniques

Traditional methods of strain engineering – rational design and random mutagenesis – are time-consuming and extremely low-throughput, and do not allow for vast combinatorial interactions to be easily investigated (*82, 83*). However, recent advances in high-throughput genome engineering (*84-86*) have brought about the need for much faster and more efficient screening techniques in order to utilize the large mutant libraries generated through automation (*83*). There exist various screens for easily detectable, colorimetric products, but so far traditional methods of detecting small molecules, such as gas chromatography or mass spectrometry, lag far behind the advances in strain development in time and scope--current library screening size is about 1000 mutants (*82*). There is a critical need, therefore, for high-throughput screens that are fast, can handle large numbers of variants, can detect low concentrations of non-colorimetric molecules, and ideally are not molecule-specific. Especially lacking are screens that detect actual *secretion* of desired small molecules. A possible solution to this problem are biosensors (*82*), which can convert the undetectable molecules into readable outputs (Figure 4.1). In particular, "whole-cell" biosensors are useful for detecting secretion of desired compounds, one of which we have designed and constructed in this work. Following is a brief discussion of various recent advances with regard to microbial detection of small molecules.

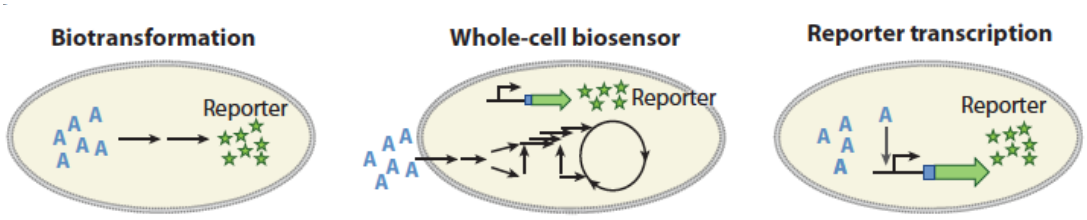

Figure 4.1 Different types of biosensors, adapted from (*82*). Small molecule A is detected intracellularly by conversion into a reporter protein, extracellularly by import into the cell, or intracellularly by activating transcription of a reporter protein.

Earlier examples of microbial screens used colorimetric assays to detect production of desired compounds. One interesting example is the use of a tyrosinase to couple the over-production of tyrosine to that of melanin, which is a brownish-black pigment that can be easily detected by visual inspection (*87*). Cells that carry a plasmid carrying a mutant *melA* gene (encoding the tyrosinase) would turn brown when also producing large amounts of tyrosine. After creating a random knockout library, production strains carrying the tyrosinase were visually selected on agar plates and then subcultured for two rounds at 120 - 144 hours each to allow for melanin synthesis. After subculturing and plasmid-curing of the tyrosinase vector, two mutants were isolated that produced up to 57 and 71% more tyrosine than the base strain (*87*). While this example highlights the simplicity of colorimetric assays, it also illustrates the low-throughput nature of visual inspection and is also time-consuming (in part due to the nature of the melanin synthesis process).

More recently, several studies have used transcriptional regulators coupled with fluorescence-activated cell sorting (FACS) to detect small-molecule production intracellularly (*88, 89*). Single-cell intracellular detection of metabolites was demonstrated through the use of a lysine-responsive promoter in front of a reporter protein, YFP, which allowed mutant lysine over-producers to be identified and detected using FACS, and then sorted *(89)*. However, direct processing of the mutant library was not possible using FACS alone, and the post-processing isolation of mutants took over two days. Also, intracellular detection of lysine production resulted in two groups of strains being identified, those that synthesized and exported a large amount of lysine and those that exhibited large amounts of fluorescence but did not have a high extracellular concentration of lysine. This second group may be false positives or may produce higher amounts of lysine but not export it. This issue can be avoided by detecting the extracellular metabolite concentration, or metabolite secretion, instead of cytosolic concentrations. While it can be argued that some producers might be missed via this latter method, if the cells cannot secrete the desired metabolite then they will not very useful on an industrial scale. Also, as in our case, some metabolites and byproducts would be toxic if accumulated intracellularly in high amounts.

In a similar work, the transcriptional regulator Lrp of *Corynebacterium glutamicum* was used as a biosensor to detect intracellular concentrations of L-methionine and other branched-chain amino acids by placing a fluorescent readout protein (YFP) behind the promoter P_{brnFE} which binds the Lrp-amino acid complex (*88*). When exogenous dipeptides were added to the system, a linear fluorescent response was observed via FACS and the minimal detection limit was in the millimolar range, suitable for detection of physiological amounts of small molecules (*88*). The biosensor was also used for the detection and sorting of L-valine production strains that had been generated by random mutagenesis. As demonstrated in Figure 4.2, cells were mutagenized and then cultivated in tubes, sorted, enriched via FACS (up to 10,000 cells/sec), and then screened on agar and microtiter plates. The amounts of amino acids produced were analyzed by HPLC. The top five mutants selected produced from 4.6 to 8.7 mM L-valine (*88*). Although this sensor has lower rates of false positives than the above report, regions where only 2 and 6% of fluorescent cells actually produced increased amounts of L-valine were still identified by FACS as fractions of over-producers (Figure 4.2C). Additionally, this system suffers from the same problem as the previous biosensor of not actually detecting secretion of the desired metabolite and it also takes several days to enrich and select for strains that show increased production. The amount of branched-chain amino acids that were excreted is not very high, which may be due to the fact that the sensor is selecting for intracellular accumulation and not extracellular.

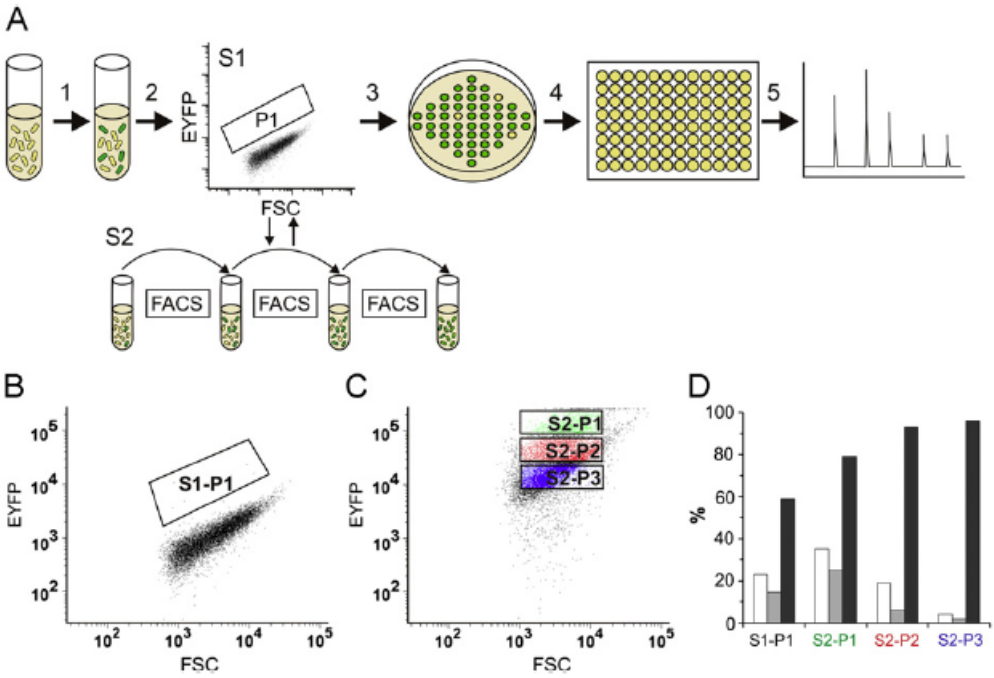

Figure 4.2 High-throughput screening approach used in (*88*). (A) Cells were mutagenized, sorted, re-cultivated and re-sorted, and then screened by agar plates and cultivated on a microtiter plate. (B-C) Changes in YFP levels after re-sorting and cultivation. (D) Percentage of positive clones shown in white, >2mM in grey, and viability in black.

Designing mutations rather than random mutagenesis avoids the decrease in cell viability associated with mutations in essential genes and may reduce the library size required to see significant increases above baseline (*82*), which may have been a problem in both of the previous single-cell studies. On the other hand, our consortia method may not make these deficiencies immediately apparent, as the sensor strain may complement some auxotrophies, however it is likely that we would obtain more viable cells since we will be able to direct the mutation to specific target genes.

There has been at least one example of a microbial pair used as a biosensor, in this case for detection of mevalonate (*90*). An *E. coli* mevalonate auxotroph was engineered by introducing a heterologous pathway to convert exogenous mevalonate to isopentenyl pyrophospahte (IPP) and dimethylallyl pyrophosphate (DMAPP), which are necessary for growth, after removing the native IPP and DMAPP synthesis pathways. Therefore, the cell could only grow if exogenous mevalonate was supplied--this strain was also tagged with GFP, and was used as the biosensor strain. Next this biosensor was

grown on the spent media from cultures of various mevalonate producers in 96-well plates. The entire process took about 1.5 - 2 days to first grow the producers, and then to grow the sensors on the spent media for mevalonate detection. Out of 600 pre-screened clones, 18% showed fluorescence that was significantly higher than baseline and four clones were eventually identified with 7X more mevalonate production than the baseline (*90*). While this is a very significant result in terms of production strain isolation, it is not very high-throughput since only 96 clones can be screened at once and also takes more than a day to grow up the producing strains. Also, it is not clear how much the pre-screen contributed to the selection of the high-producers. Growing the sensing strain and production strain in co-culture might be one way to decrease the screening time.

4.2.2 Detection of L-valine and isobutanol production using a secretor-sensor pair

We propose to detect secretion of the amino acid valine by employing two cross-feeding auxotrophs, one of which will be a L-valine auxotroph (the "sensor") whose growth will depend on the level of L-valine excreted by the "secretor" strain, here a pantothenate auxotroph (see Figure 4.3, a more complete description of the strains follows in the Results, Section 4.4.3). In contrast to the aforementioned work, the auxotrophs will be grown together in co-culture, allowing rapid detection of the amount of extracellular L-valine in the form of a growth response by the sensor. We predicted that increased L-valine production and export by the secretor strain would increase the growth rate of the co-culture as a whole, and possibly the fraction of the sensor as well, which can be distinguished by tagging with constitutively-expressed fluorescent protein YFP. This has been previously demonstrated in the previously described work and in our first project, where increased growth rate and/or ratio could be determined using fluorescent (FL) readout (*19, 90*).

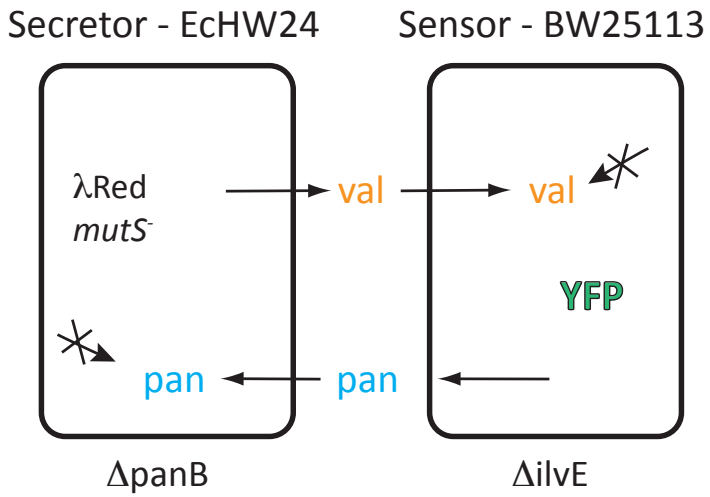

Figure 4.3 Schematic of the secretor-sensor pair. The sensor, a L-valine auxotroph (ΔilvE), secretes pantothenate for the secretor, a pantothenate auxotroph (ΔpanB), and vice versa. The sensor is tagged with a fluorescent protein, base strain BW25113. The secretor base strain is EcHW24 (*84*), a "mutator" strain with λRed homologous recombination capabilities.

The reason we are particularly interested in L-valine production is its link with isobutanol production, as described above in Section 3.2.2 (a schematic is shown in Figure 4.4). To briefly reiterate, the L-valine biosynthesis pathway produces 2-ketoisovalerate from pyruvate, which is then converted into L-valine (*64*). The final steps in the Erlich pathway were used to convert 2-ketoisovalerate into isobutanol using a 2-keto acid decarboxylase (KDC) and alcohol dehydrogenase (ADH) introduced into *E. coli* isobutanol production strains that were constructed via rational design (*61*) or evolution and random mutagenesis (*63*). It was demonstrated in the evolutionary approach, which selected for increased growth on a L-valine analog, norvaline, that increased secretion of L-valine does, in fact, correlate to increased isobutanol production once the plasmids containing the KDC and ADH have been introduced (*63*). For this reason, we predict that combining the mutations found by the random mutagenesis approach with those that have been shown to increase valine production via rational design (*64*) (discussed further below) will produce mutants that can secrete large amounts of L-valine and isobutanol.

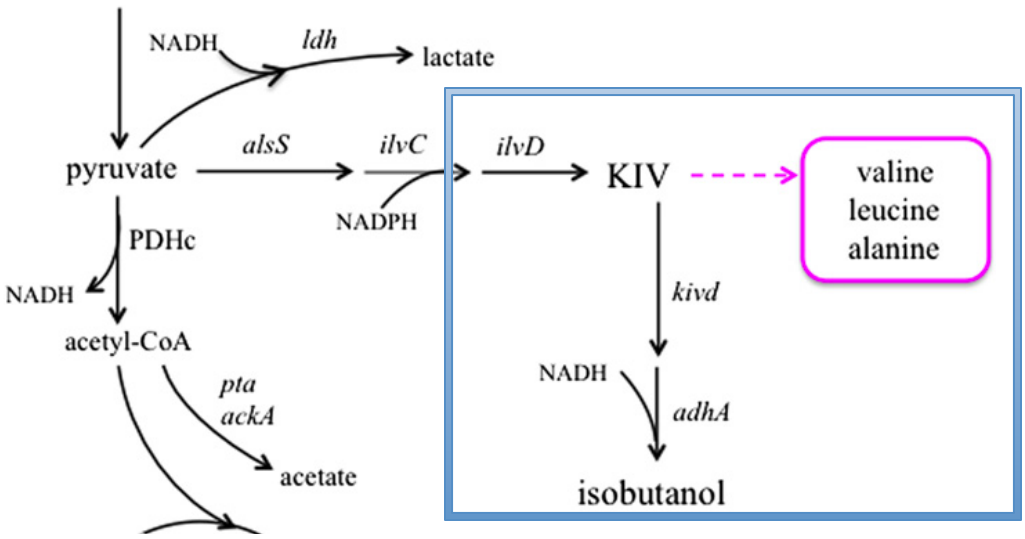

Figure 4.4 Schematic of the pyruvate to L-valine and isobutanol pathway created by the addition of the plasmid-borne *kivd* and *adhA* genes. The branch point between isobutanol and valine is highlighted. Adapted from (*63*).

To convert this microbial detection system into a high-throughput process for overall strain development and screening, we plan to use methods such as the recently-developed genome manipulation technique Multiplex Automated Genome Engineering, or MAGE (*84*), to simultaneously and rapidly introduce various mutations throughout the secretor chromosome, creating a large library of variants that secrete various levels of L-valine. Then we plan to cultivate the secretor mutants with the sensor strains in droplets on a microfluidic device. A diagram of the entire process is shown in Figure 4.5. The device will allow us to isolate one pair per droplet, and after cultivation, to sort the droplets by their level of growth (i.e. fluorescence). The strains can then be tested off-chip to confirm that those that have faster-growing pairs do indeed contain secretor strains that produce more L-valine, and hopefully, isobutanol, once they are transformed with the relevant KDC- and ADH-containing plasmids.

Here we discuss the design and construction of a proof-of-concept microbial secretor/sensor pair and demonstrate that by introducing a few preliminary mutations that have been known to increase valine production, the secretor strain is able to compensate for the valine auxotrophy. Also, the co-culture composition changes to indicate increased valine secretion, however growth defects may overshadow the growth rate benefit from the additional mutations beyond the first *panB* knockout.

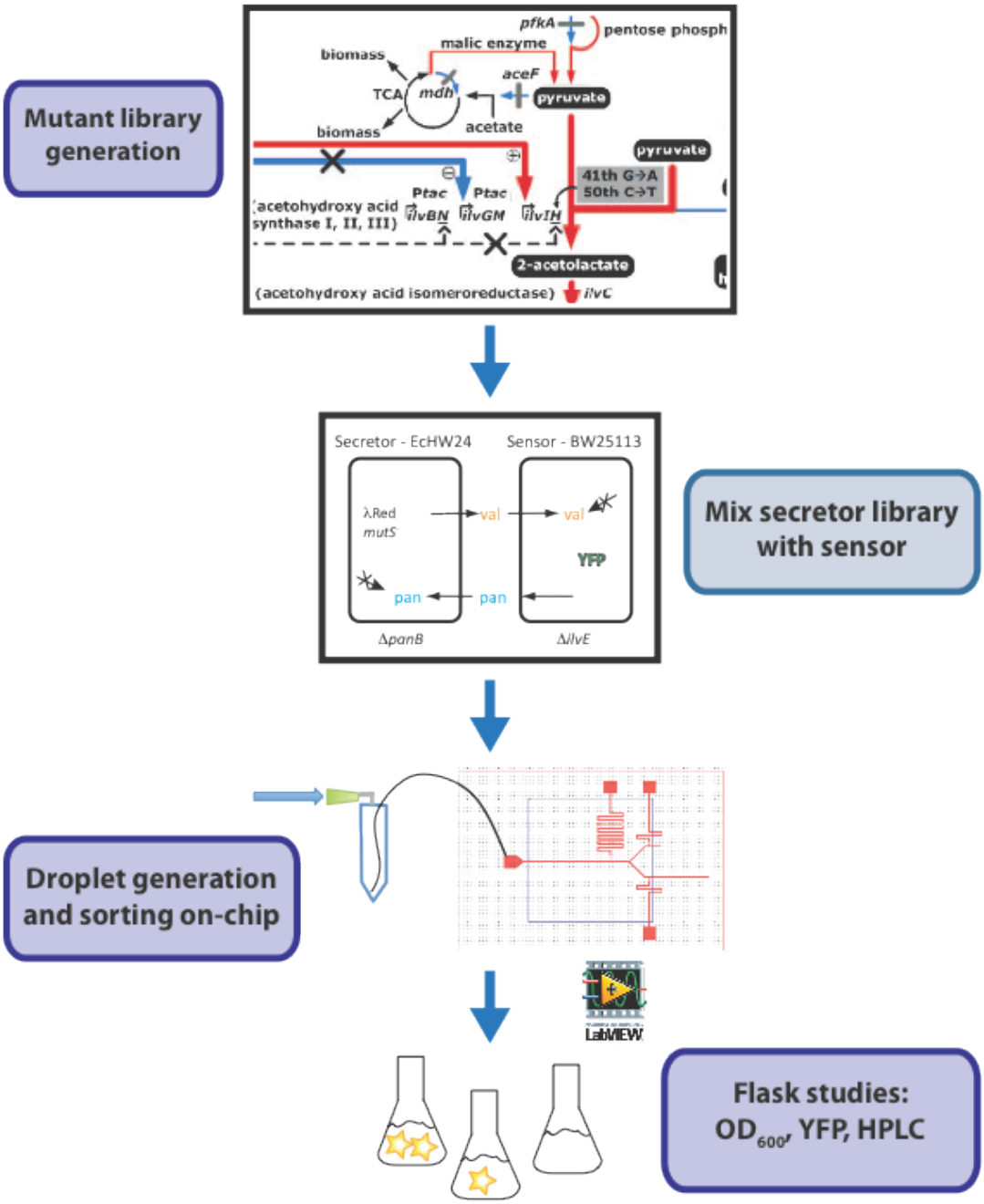

Figure 4.5 Proposed method for high-throughput production strain development and screening utilizing the microbial consortium as a secretion detection mechanism.

4.3 Methods

4.3.1 Microplate growth studies for auxotroph selection and leucine titration

For the microplate cultivations to determine the best secretor base strain, mono- and co-cultures were cultivated in minimal M9 medium with 0.2% glucose as a carbon source. L-Leucine and L-isoleucine were added to a final concentration of 2 mM unless otherwise indicated. L-valine was added to a working concentration of 150 mg/L where indicated, and sodium pantothenate to 1.5 mM. No antibiotics were added to the medium. Frozen stocks were inoculated into rich LB medium with 30 μg/ml kanamycin and grown overnight to saturation, then washed twice with minimal M9 medium. For the auxotroph determination, Keio collection (*43*) strains were used in all experiments. The strains used were: ΔilvE (JW5606-1), ΔpanB (JW0130-1), ΔpanD (JW0127-2), ΔproC (JW0377-1), ΔtrpE (JW1256-1), and ΔpheA (JW2580-1). Cultures were then diluted by 1:100 and pipetted onto a 96-well microplate (Costar) to a volume of 200 μl per well. Unless otherwise stated, four replicates were conducted per microplate sample. Cultures were grown for 48 hours at 37 ^{o}C on an VersaMax (Molecular Devices) plate reader with shaking and OD_{600} measurements were taken every 15 minutes.

4.3.2 Secretor and sensor strain construction

The Keio collection mutant BW25113 *ilvE::kan* (Keio collection strain JW5606-1) (*43*) was used as a base strain for the sensor (L-valine auxotroph, here called ΔilvE). The strain was then tagged with a fluorescent protein, YFP, for visualization of the ratio in microplate studies and the growth rate on-chip. The YFP cassette, *intC::yfp-cat*, was inserted into the L-valine auxotroph via P1 transduction. P1 lysates were grown on the donor strain DS1-Y (*91*) and were then mixed with the recipient strain, ΔilvE, to allow infection and recombination. YFP was integrated into the *intC* locus with a *cat* selection cassette. This gene is under control of two λP_R promoters (*44*).

To create the secretor strain, we started with base strain EcHW24 (*bioA::λRed-bla-tet mutS*$^{-}$) which was developed for the specific purpose of ssDNA recombination (*84*). The the pantothenate auxotrophy was then created by inactivating the *panB* gene by inserting two premature stop codons using λRed-mediated ssDNA recombination (*86*),

creating strain EcLSB. The sequence of the oligo for inserting the stop codons is as follows, with the mutated bases highlighted in blue:

panB_stop: 5'-T*A*C*A*AACAGGAAAAAAAACGTTTCGCGACCATCACCGC

TTA**G**GACTA**A**AGCTTCGCCAAACTC TTTGCTGATGAAGGGCTTAACGTCATG-3'.

The mutations were confirmed via sequencing the *panB* locus and allele-specific PCR (asPCR) (*92*), as well as via plating on minimal M9+biotin (or "N") plates. Without sodium pantothenate added, the strains did not grow on the minimal plates.

Next we introduced the following mutations into the *ilvN* gene: G59A, C60T, T62A, A63C, A64T, G66C (corresponding to amino acids substitutions: G20D, V21D, M22F) again using ssDNA recombination mediated by the λRed proteins, creating EcHW24 *panB*$^-$ *ilvNfbr*, or EcLSBN. The oligo used was:

ilvN_fbr_mut: 5'-T*C*A*A*CGTTAAAAGCGCGGCGGGCAAAAAGGCCACAAACGT

GGGT**G**A**AGT**C**AT**CCGGATGGTTGCGAACGGTGAGCTCCAGAATTACGTTG-3'

The mutations were confirmed by asPCR and by sequencing the *ilvN* locus.

4.3.3 Microplate growth cultivation with the secretor/sensor pair and ratio determination via plate counting

For the microplate experiments with the EcLSB and EcLSBN strains, mono- and co-cultures were cultivated in minimal N medium (M9 + biotin) with 0.2% glucose as a carbon source. L-valine was added to a final concentration of 150 mg/L where indicated, and sodium pantothenate to a concentration of 1.5 mM. No antibiotics were added to the medium. Frozen stocks were inoculated into rich LB medium with 50 μg/ml ampicillin for EcLSB/EcLSBN and 30 μg/ml kanamycin for ΔilvE and grown overnight to saturation. Cultures were then diluted by 1:100 in N medium and pipetted onto a 96-well microplate (Costar) to a volume of 200 μl per well. Unless otherwise stated, four replicates were conducted per microplate sample. Cultures were grown for 72 hours at 30 ^{o}C (so as not to induce the temperature-sensitive λRed proteins) on an M5 (Molecular Devices) plate reader with shaking. OD_{600} measurements were taken every 15 minutes. The co-culture composition was determined via differential plate counting. At 72 hours, the cultures were diluted by $1x10^4$ and 50 μl was plated on N + 2 mM sodium pantothenate plates (to select for the pantothenate auxotroph, contains biotin) and on M9 + 150 mg/L L-valine + 2 mM L-isoleucine plates (to select for the valine auxotroph). The

colonies were then counted after two days of incubation at 30 ^{o}C to determine the co-culture ratio at the end of cultivation.

4.4 Results and Discussion

4.4.1 Selection of a secretor base strain and microplate studies

In order to create a L-valine auxotrophy, the branched chain amino acid transferase-encoding gene, *ilvE*, was replaced with the kanamycin reisistance cassette in strain BW25113 (Keio collection strain JW5606-1, CGSC). This L-valine auxotroph, the sensor strain, is paired with another auxotrophic strain to create the metabolic dependency. It would be beneficial to find a suitable partner strain by looking for auxotrophs that grow well with the L-valine-deficient strain, since increased growth will be our metric for increased L-valine production. A good place to begin the search for a partner strain is previous data on the growth of auxotroph pairs, illustrated in Figure 4.6 below (*93*). In this work, various auxotrophs were grown together in minimal media to identify synergistic mutations (specifically, knockouts), by looking at the increase in co-culture growth over the baseline for either strain or for the pair (indicated by either red, blue, or purple in the heat map below, and inset). The results for the L-valine auxotroph (*ilvE*) when it is the mCherry-tagged partner strain are highlighted in yellow.

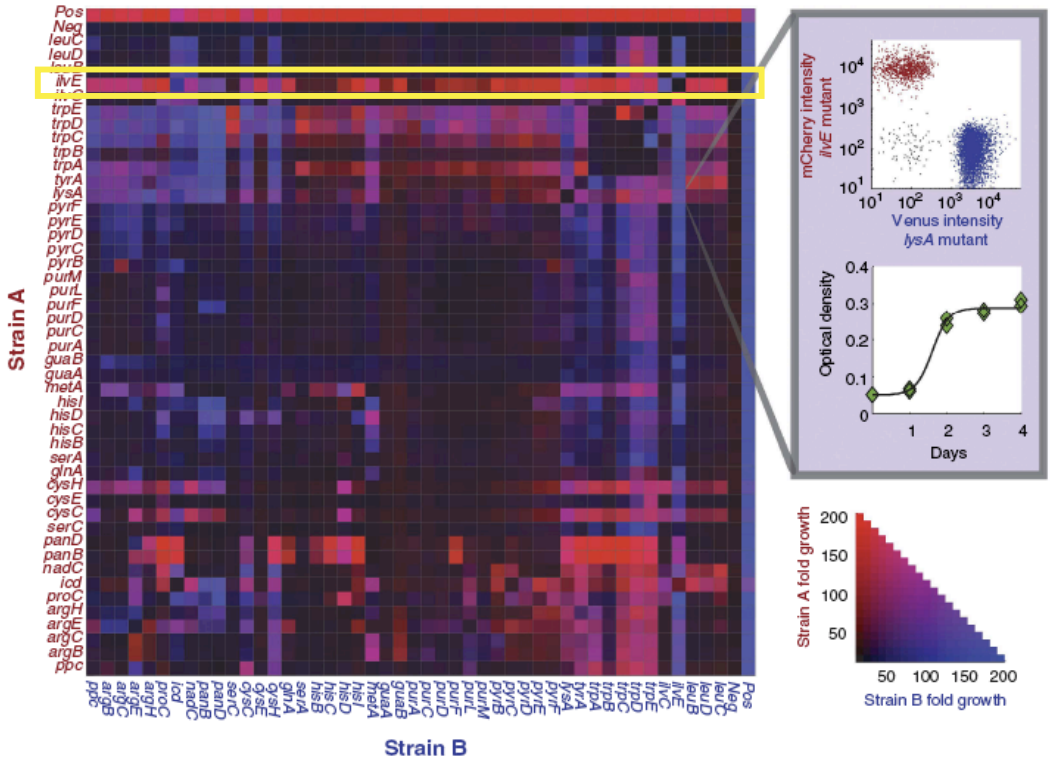

Figure 4.6 Heat map of synergistic interactions between auxotrophs, adapted from (*93*) to highlight the beneficial interactions for the valine auxotroph, *ilvE*, outlined in the yellow box. Red denotes increased growth of strain A, and blue denotes increased growth of strain B. The colors should be opposite and symmetrical about the diagonal.

From the above plot, we selected eight partners to test with the valine auxotroph in microplate studies, and then narrowed these down to the five with the highest growth rate and/or maximum optical density (OD_{600}) values: ΔpanB, ΔpanD, ΔproC, ΔtrpE, ΔpheA. Keio collection knockout strains were used in all microplate growth experiments (Methods). Several of these knockout are intuitive: knocking out *panB*, which encodes3-methyl-2-oxobutanoate and causes pantothenate auxotrophy, has been shown to increase valine production (*64*) and a *proC* point mutation (A98T) was also discovered in the norvaline-resistant mutant NV3 (Appendix Table 1, *63*). To ensure that any increases in growth are due to complementation of the valine auxotrophy and not to other auxotrophies caused by removal of the IlvE protein, we added L-isoleucine and L-leucine to the growth medium (2 mM each). However, the valine auxotroph was able to grow on its own when isoleucine is added (data not shown), so this was removed in the final experiments.

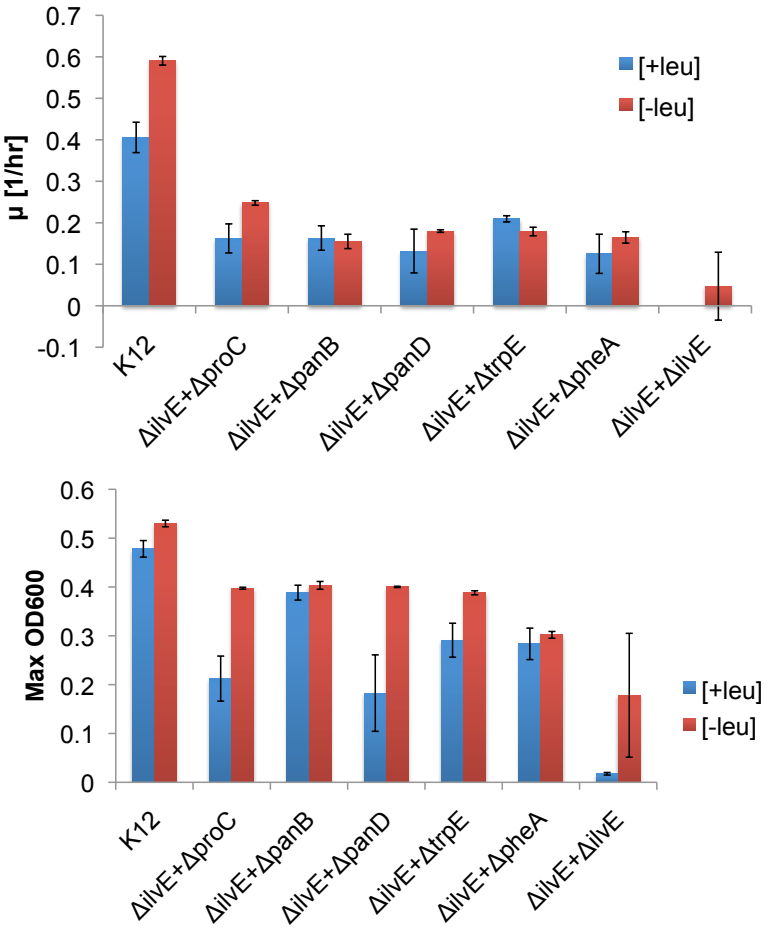

Figure 4.7 Growth rate (top) and maximum optical density (bottom) for the five auxotrophic pairs and control strains. Strain K12 MG1655 is used as a control. Error bars show the ± standard deviation of three replicates.

Microplate experiments with the auxotroph pairs in minimal media indicated that either ΔpanB or ΔtrpE would be the best growth partner for the L-valine auxotroph, ΔilvE. ΔtrpE + ΔilvE had the highest growth rate in minimal medium with L-leucine at 0.21 ± 0.01 1/hr, though all were fairly low. Without L-leucine, ΔproC + ΔilvE exhibited the fastest growth rate at 0.25 ± 0.01 1/hr, but the lag time was much longer with this pair, which is not reflected in the plots. ΔpanB + ΔilvE grew to the highest maximum OD_{600} with L-leucine added at 0.39 ± 0.05 a.u. which was significantly higher than the rest of the cultures (Figure 4.7). Without L-leucine, ΔpanB + ΔilvE also grew to the highest maximum OD_{600} though this value was not much larger than several of the other co-cultures. From these results we selected ΔpanB as the optimal partner, since knocking

out this gene has been known to increase valine production by shutting down formation of pantothenate (*64*).

We noticed that adding L-leucine sometimes negatively affected growth in the co-cultures and with the positive control, K12 MG1655 (see Figure 4.7 above). This may be due to the antagonistic affect of the transcriptional regulator leucine responsive protein (Lrp) when bound to excess L-leucine (*94*). The Lrp regulon is quite varied, including pathways for amino acid biosynthesis (depicted in Figure 4.9 below), degradation, transport, and pilin synthesis, and can act as a transcriptional activator or repressor depending on the operon and cellular conditions (*94*). For example, Lrp normally activates the *ilvIH* genes, but when L-leucine is present it antagonizes this activation.

Because of this, we investigated titrating the L-leucine concentration via microplate experiments to determine the optimal concentration of L-leucine for the growth and production of L-valine. As shown in Figure 4.8A, increasing the L-leucine concentration decreases the growth rate even for the control strain, K12 MG1655. The fastest co-culture growth rate was observed with the ΔpanB + ΔilvE strains and 0.2 mM L-leucine (0.38 ± 0.02 1/hr). A slightly higher maximum optical density at 600 nm was observed for the co-culture with 0.6 mM L-leucine, however it was not significantly better than either 0 or 0.2 mM L-leucine (Figure 4.8B). Since the lag phase for 0.2 mM was longer than either 0.6 mM (Figure 4.8C), on-chip this might not be best concentration since we will want to determine the cultures with the highest level of growth (fluorescence) at a particular point in time. Therefore, the optimal concentration will probably be somewhere between 0.2 and 0.6 mM. These experiments will be repeated with the final permutations of the secretor and sensor base strains before performing the automated mutant library generation (i.e. MAGE).

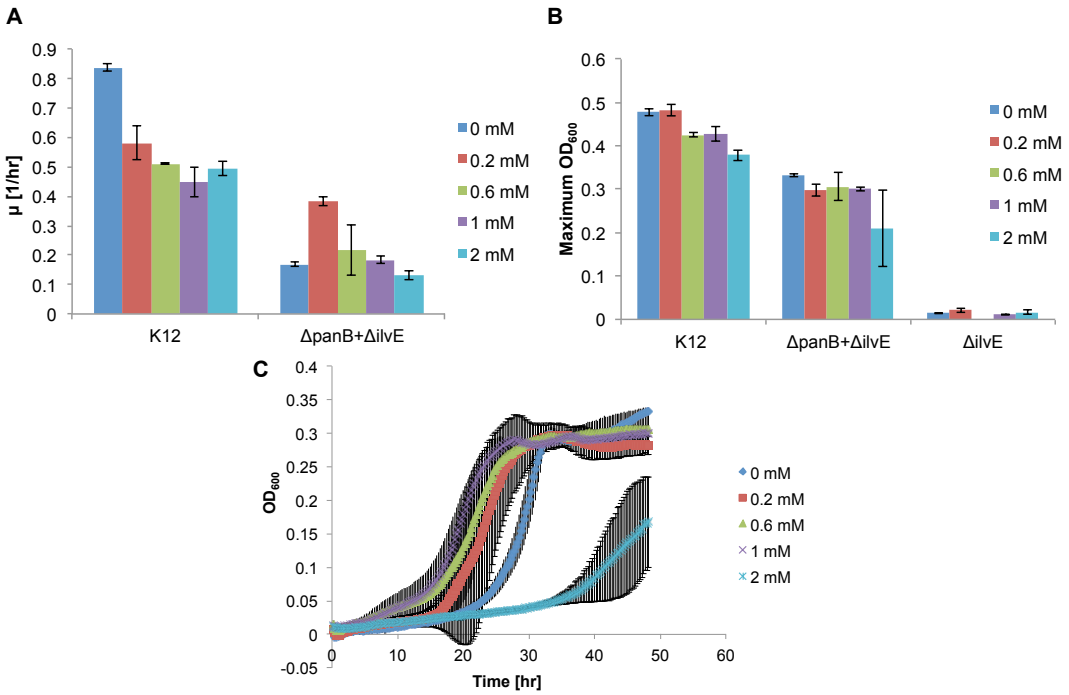

Figure 4.8 Leucine titration in microplate growth experiments. (A) Growth rate (1/hr) and maximum optical density at 600 nm (B) for the K12 control strain and the ΔpanB+ΔilvE or ΔilvE cultures with varying amounts of L-leucine. The ΔilvE monocultures did not grow out and so a growth rate was not calculated. (C) The growth curves for the ΔpanB+ΔilvE co-culture show large variation with 0.2 and 2mM L-leucine and a much longer lag phase with 2mM. Data shown is the average of three biological replicates.

4.4.2 Identification of target mutations for L-valine over-production

Over-production of L-valine and the other branched chain amino acids (BCAAs), L-leucine and L-isoleucine, has been very well-studied and annual production levels are currently around 400-500 tons (*95*). These amino acids may be used in various applications such as in animal feed (*95*) and as precursors for antiviral drugs and herbicides (*88*), so there has been much interest in their large-scale production (*64, 96-98*). There are therefore various reports in which we may find favorable mutations that we can use to create a L-valine and isobutanol over-producer.

A schematic of the L-valine and BCAA biosynthesis pathway is shown in Figure 4.9, which includes mutations that were introduced in the rational design methodology from (*64*). The BCAA synthesis from pyruvate begins with three acetohydoxy acid synthase isoenzymes (AHAS I, II, and III) encoded by *ilvBN*, *ilvGM*, and *ilvIH* which are transcriptionally regulated by some or all of the BCAAs (*95*). The larger subunits contain

the sites of each enzyme's catalytic activity (encoded by *ilvB*, *ilvG*, and *ilvI*) (*96*) whereas two of the smaller subunits (*ilvN* and *ilvH*) contain known sites for feedback inhibition. Excess L-valine and L-leucine can inhibit AHAS I and III production through transcriptional attenuation of the *ilvGMEDA* and *ilvBN* operons; the former can also be regulated by L-isoleucine as well (*94-96*). L-Valine can also allosterically inhibit these enzymes by binding to sites in the *ilvH* (*64*) and *ilvN* (*96*) genes (see Figure 4.9). The *ilvGM* protein AHAS II is not normally expressed in *E. coli* due to a frameshift mutation in *ilvG*, and this can lead to what is referred to as "valine toxicity" (*95*). If L-valine is over-expressed, it will inhibit expression of the AHAS I and III, causing an excess of 2-ketobutyrate, which is toxic to the cells. For this reason it is important to mutate either the ilvN or ilvH genes as one of the first steps when attempting to over-produce L-valine.

Park *et al.* were able to achieve high titers of L-valine in shake flasks by introducing mutations to relieve feedback inhibition and transcriptional attenuation, as well as remove byproduct formation by knocking out competing pathways (Figure 4.9) (*64*). First, feedback inhibition in the *ilvH* gene was removed by inserting the point mutations G41A and C50T. Next, transcriptional attenuation was removed by placing the chromosomal *ilvGM* and *ilvBN* genes under control of the *tac* promoter. To reduce formation of competing byproducts, the *ilvA*, *panB*, and *leuA* genes were knocked out, which encode enzymes that participate in L-isoleucine, pantothenate, and L-leucine synthesis, respectively. For over-expression of key enzymes in the biosynthetic pathway, *ilvBNCED* were cloned onto a plasmid, again behind the *tac* promoter. Lastly, since the protein Lrp was found to be down-regulated via transcriptome analysis, likely due to the addition of L-leucine to the medium, it was also placed on a separate plasmid for over-expression along with the putative valine exporter *ygaZH* (*64*) (Figure 4.9). As discussed above, Lrp activates transcription of the *ilvIH* genes (*94*) and also plays a role in activating *ygaZH* expression (a valine exporter) (*64*). This strain (Val pKBRilvBNCED, pTrc184ygaZHlrp) was able to produce up to 7.61 ± 0.24 g/L L-valine on 50 g/L glucose, an increase of 113% over the control strain (*64*).

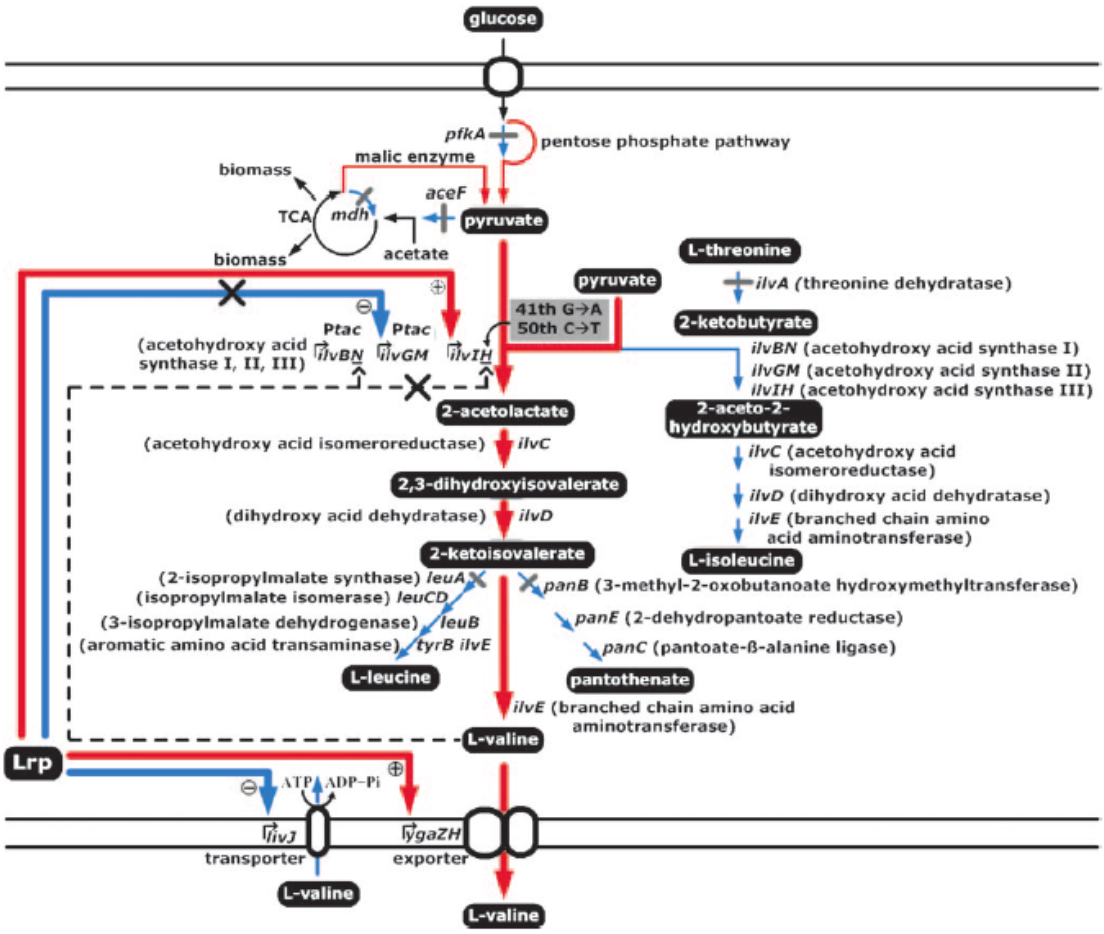

Figure 4.9 Pathway for synthesis of L-valine and the other BCAAs, adapted from (*64*). Knockouts are shown by gray bars, increased flux is indicated by thick red arrows. Thick blue arrows are inhibition by Lrp. Mutations in the ilvH gene are listed. Additional sites of L-valine inhibition in *ilvN* are not shown.

In the same report, three other genes (*aceF*, *pfkA*, and *mdh*) were identified for removal by *in silico* gene knockout analysis, giving strain VAMF. Although VAMF produced more L-valine in 20 g/L glucose media than the previous Val strain (both with the plasmids added), these last three mutations decreased the growth rate of the strain significantly. Therefore for our purposes these last three knockouts may not be as useful. More recent work by the same group introduced a feedback-resistant *ilvN* gene with amino acids substitutions G20D, V21D, and M22F, which conferred resistance to increasing amounts of L-valine (*98*). Similar mutations had previously demonstrated increased resistance to all three BCAA's and increased L-valine production in *C. glutamicum* (*96*). In the previously described Val strain, incorporation of the feedback-

resistant *ilvN* (Val pKBRilvBNfbrCED, pTrc184ygaZHlrp) resulted in 18.4 g/L L-valine being produced, a 22% increase over the control strain (*98*).

4.4.3 Design of secretor and sensor strains

Our end goal is to select around 30-40 mutations from both the rational design methodologies mentioned above, as well as the evolutionary study performed by Smith *et al.* (*63*) that we will then introduce into our secretor base strain in a combinatorial manner using techniques for automated genome library generation. We predict that there will be various benefits that may arise from the combinatorial interactions between some of these mutations, which we would not otherwise have come across from rational design. In order to demonstrate the utility of using a microbial consortium as a secretion detection mechanism, we will first introduce a set of preliminary mutations into the secretor base strain EcHW24 *(84)* to increase L-valine production (genotype *bioA::λRed-bla-tet mutS⁻*).

Once we chose the pantothenate auxotroph as the partner for the sensor strain, we first re-created the pantothenate auxotrophy in the EcHW24 strain by inactivating the *panB* gene via the insertion of two premature stop codons using λRed-mediated ssDNA recombination (*86*) (Methods). To determine the second proof-of-concept mutation, we looked at the most favorable mutations from the previous reports (*64, 98*). Since we did not know the benefit of each of the mutations that resulted from the evolution and random mutagenesis study by Smith *et al.* (*63*), we looked to the rational design methodology first. Below is a table showing some of the mutations that either occur early on in the synthesis pathway or result in a large increase in L-valine production (Table 4.1). For some mutations there were no data available on the increase in L-valine due to that mutation alone. Since the efficiency of recombination is greater with a point mutation than an insertion or deletion when using the ssDNA recombination system (*84*), and since excess L-valine is "toxic" to the cells unless the feedback inhibition is removed for either AHAS I or II, we decided to mutate one of these enzymes first. The AHAS I has a greater affinity for pyruvate than AHAS III (*95*), which has a higher affinity for 2-ketobutyrate, so we decided to try mutating this gene first since that would lead to more L-valine production rather than L-isoleucine. We introduced the following mutations into the *ilvN* gene: G59A, C60T, T62A, A63C, A64T, G66C (corresponding to amino acids

substitutions: G20D, V21D, M22F) again using ssDNA recombination mediated by the λRed proteins, creating EcHW24 *panB*⁻ *ilvNfbr*, or EcLSBN.

Table 4.1 Various mutations to increase valine production and the level of increase, if available. ND: no data.

Gene	L-Valine increase	Mutation type	Notes	Reference
ilvH (AHAS III)	ND	Point; G41A, C50T	Relieves allosteric inhibition, but still inhibited by transcriptional attenuation	(*64*)
ilvN (AHAS I)	22%	Point; G20D, V21D, M22F (aa)	May create a lot of acetic acid Higher affinity for pyruvate	(*98*)
aceF	2X (100%)	deletion	May slow secretor growth	(*64*)
ygaZH	47.1%	Over-expression	Putative valine exporter	(*64*)

To create the base sensor strain, we started with the Keio collection mutant ΔilvE (Methods). We then tagged the strain with a fluorescent protein, YFP, for visualization of the ratio in microplate studies and the on-chip growth rate. The YFP cassette, *intC::yfp-cat*, was inserted into the L-valine auxotroph via P1 transduction (Methods). Preliminary growth studies with these strains are discussed below.

4.4.4 Preliminary growth studies with the proof-of-concept strains

After constructing the secretor and sensor strains with the preliminary mutations, we grew the strains in mono- and co-culture on the microplate to examine the growth rate changes and changes in composition (Figure 4.10). In this experiment the sensor strain (ΔilvE) does not contain YFP. The different strains used were the Keio collection pantothenate auxotroph, ΔpanB, and the EcHW24-derived strains EcLSB and EcLSBN. When paired with all three secretors the sensor strain can grown in N medium without valine added, demonstrating that the deletion of *panB* function can compensate for the valine auxotrophy in the sensor. However, to our surprise, the lag time is still quite long with the *ilvNfbr* mutations incorporated, and the co-culture growth rate is slower for ΔilvE paired with EcLSBN than either of the other pantothenate auxotrophs without *ilvN* mutated (ΔpanB or EcLSB, Figure 4.10B). This was rather unfortunate, as we had hoped

to use the increase in growth rate to monitor the rate of cross-feeding. However, since the EcLSB + ΔilvE co-culture does not exhibit the same growth dynamics as the ΔpanB + ΔilvE co-culture, the problem may be with the parental EcHW24 or something that occured when inserting the premature stop codon into *panB*. Since EcHW24 contains the *mutS*⁻ genotype, it is prone to mutations and may have incorporated a deleterious growth mutation. It also contains the λRed cassette, which we have found can significantly decrease the growth rate (data not shown). When pantothenate is added to the medium, the strain grows but does not grow as well as the Keio strain ΔpanB (data not shown). Ideally, we would remove these genes and revert the *mutS*⁻ genotype after all of the valine secretion mutations have been incorporated.

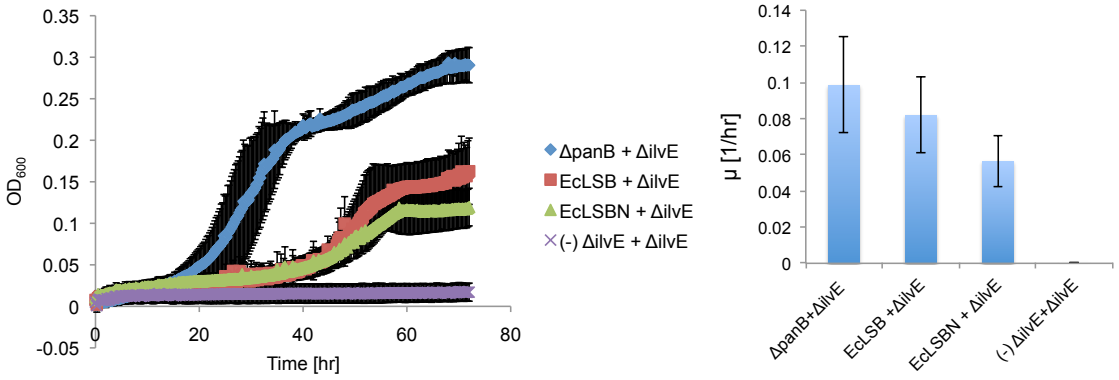

Figure 4.10 Microplate growth results with the secretor and sensor strains. Growth profile over time (left) and growth rates of the co-cultures (right). ΔpanB is the Keio collection pantothenate auxotroph. Error bars represent the standard deviation from the mean of four biological replicates. No leucine was added to the medium.

Although the growth was slower as more mutations were incorporated, rendering the *ilvN* gene feedback-resistant did increase the ratio of the sensor strain to the secretor strain, as evidenced via differential plate counting at the end of the cultivation (Table 4.2). With the Keio-based pantothenate auxotroph, ΔpanB the sensor:secretor ratio was 0.647, but with the EcLSBN strain it increased to 3.28, indicating that there may be an increased level of valine secretion occurring with the *ilvN* mutations incorporated.

Table 4.2 Differential plate count results. Co-cultures were diluted and plated from two wells at the end of the above microplate experiment (at 72 hours) on either N (M9+biotin) + sodium pantothenate, or M9 + L-valine + L-isoleucine plates. The ratio of the secretor: sensor is the L-valine:pantothenate auxotroph.

Co-culture	Ratio sensor:secretor
ΔpanB + ΔilvE	0.647
EcLSBN + ΔilvE	3.28

The potential increase in growth rate from increased valine secretion may be over-shadowed by a growth defect in the EcLSB and EcLSBN strains. A possible solution to the problem is to remove the *mutS*⁻ genotype and/or λRed cassette and see if that restores the growth rate. If not, then instead of knocking out the PanB function by inserting a premature stop codon, we could try to delete the entire gene using homologous recombination or by using P1 transduction of the Keio *panB::kan* cassette into the EcHW24 base strain. The problem with these two methods is that deleting an entire gene is less efficient that making a point mutation (*84*), and that with the P1 transduction a FRT scar sequence is left in place of the *panB* locus. Both methods are also generally irreversible.

The problem may also be due in part to transcriptional attenuation of the *ilvN* locus by L-valine. Although the allosteric inhibition should have been removed, excess L-valine can still inhibit the *ilvN* operon if present in high concentrations (*95*). To relieve this additional inhibition, we could swap out the chromosomal *ilvN* promoter with an inducible promoter such as the IPTG-inducible promoter P_{lac}, or amplify the feedback-resistant *ilvN* from the chromosome and place it behind an inducible promoter on a plasmid. This second method may be preferable to demonstrate a proof-of-concept pair, as this would also increase the copy number of the genes and may be easier to accomplish.

4.5 Future Work

Our secretor and sensor strains need to be further optimized in order to fully demonstrate that the microbial consortium can indeed be utilized detect increased levels of L-valine secretion. There may be a growth defect in the EcLSB and EcLSBN strains,

which could be solved by removing the *mutS*⁻ genotype and/or λRed cassette. Additionally, instead of making the PanB⁻ phenotype by inserting a premature stop codon, we could delete the entire gene using homologous recombination or by using P1 transduction of the Keio *panB::kan* cassette into the EcHW24 base strain. The lack of observable growth benefits may also be due in part to transcriptional attenuation of the *ilvN* locus by L-valine. To relieve this additional inhibition, we could amplify the feedback-resistant *ilvN* from the chromosome and place it behind an inducible promoter on a plasmid. This would be also be beneficial for proof-of-concept demonstration as it would increase the copy number of the *ilvN* gene.

Additional tube and/or flask experiments should be performed to more accurately confirm the growth and composition characteristics and L-valine secretion profiles. The isobutanol plasmids can also be incorporated via transformation to determine if the increased L-valine secretion does lead to increased isobutanol production with the proof-of-concept strains. The increased L-valine secretion should also be detected either by HPLC or by using a bioassay, where a L-valine auxotroph can be grown on the supernatants from secretor strain cultures and then the metabolite concentration determined from a calibration curve. Increased isobutanol production can then also be measured by HPLC once the pSA55 and pSA69 plasmids are incorporated into the system. The change in composition can be monitored via plate counting combined with fluorescence measurements.

Eventually we would like to incorporate the secretion detection pair into a larger process for production strain development and high-throughput screening using a microfluidic sorting device (as depicted in Figure 4.5). This is discussed further in the Future Directions, Section 5.2.3.

Chapter 5 Concluding Remarks and Future Directions

5.1 Concluding Remarks

5.1.1 Design and construction of a programmable, synthetic *E. coli* consortium via tunable symbiosis

In this work we have demonstrated the possibility the creation of a tunable, microbial consortium that can be "programmed" to provide desired outputs. Our symbiotic circuit enables continuous tuning of the growth rate and composition of a synthetic, cross-feeding consortium. We developed a basic model to capture the dynamics of this consortium, and demonstrated that the growth rate and composition could be controlled via manipulating the export rate or synthesis of essential metabolites. We implemented our general design through the exchange of tryptophan and tyrosine by two *E. coli* auxotrophs. By regulating the expression of genes related to the export of tyrosine or production of tryptophan via inducible promoters, we were able to tune the metabolite exchanges and achieve a wide range of growth rates and strain ratios. We discovered that the burden of gene expression often outweighed the growth rate benefits conferred by the increased cross-feeding, so we adapted our model to capture the effect of inducing the export or synthesis proteins on the growth rate and/or strain "affinity" for the essential metabolite.

In addition, by inverting the relationship of growth/ratio vs. inducer concentrations to create two-dimensional design space plots, we were able to "program" the co-culture in order to achieve desired outcomes. This programmable proof-of-concept circuit or its variants can be applied to more complex systems where precise tuning of the consortium would facilitate the optimization of specific objectives, such as increasing the overall efficiency of microbial production of biofuels or pharmaceuticals.

5.1.2 Engineering a two-member *E. coli* consortium for conversion of five- and six-carbon sugars to isobutanol

We have designed a two-member *E. coli* consortium that is capable of converting hexose monosaccharides and pentose mono- and oligosaccharides into isobutanol. We have shown that the co-culture of a five- and six-carbon specialist (NC5/NC6) produces higher titers of isobutanol than a diauxic strain (NC6) under the same conditions and also demonstrated that this co-culture grows well on AFEX-pretreated corn stover (CS) hydrolysate and produces almost up to ~3 g/L isobutanol (at ~65% of the theoretical yield) without supplementation (Figure 3.15). This work addresses some of the remaining challenges that remain in the conversion of lignocellulosic feedstocks to next-generation biofuels, such as complete utilization of five carbon sugars and achieving high titers on actual biomass substrates. Although we did not achieve as high of isobutanol titers as other studies, our yields are comparable or even higher in some cases. As discussed above we could possibly increase the titer by having more feeding cycles throughout the cultivation.

It should also be noted that our main goal in this work was to design a system that can produce isobutanol on lignocellulosic biomass, not necessarily to produce the highest titers on defined laboratory media. Since our ultimate goal is to combine this NC5-NC6 pair with a fungus to complete the consolidated bioprocessing (CBP) design (see Future Directions, Section 5.2.2), we were not as concerned with feeding cycles or additional supplementation and instead desired to mimic the eventual culture conditions when grown with a cellulolytic specialist. This is a different approach than in some previous studies, which focus first on biofuel production on defined media rather than on designing a robust process for use on lignocellulosic substrates. We feel that our two member consortium that has been proven to grow well on corn stover hydrolysate may prove to be more robust and adaptable than other production strains that may produce more isobutanol when grown on *defined* media.

5.1.3 Use of microbial consortia in high-throughput strain development for over-production of L-valine and isobutanol

In this work we designed a microbial detection system which will be utilized in sensing L-valine secretion from highly-secreting production strains. Secretor and sensor "proof-of-concept" strains were created and grown in co-culture on a microplate reader. While the pantothenate auxotroph and L-valine auxotroph were able to grow well in co-culture, additional mutations meant to increase L-valine production may overshadow growth benefits conferred on this sensor strain. Although there was not an observed growth rate benefit from incorporating the *ilvN* feedback-resistant mutations, the ratio of the ΔilvE to EcLSBN strain increased to favor the sensor strain, ΔilvE, indicating possible increased L-valine secretion by strain EcLSBN. This preliminary result will be confirmed in future studies.

5.2 Future directions

5.2.1 Remove metabolic burden of the tunable circuit and application of the circuit in isobutanol production

One issue with our tunable circuit is the fact that there was an obvious growth rate decrease due to the expression of the cross-feeding genes, which we termed the "metabolic burden". A potential solution to this problem, discussed above, is to tune the genes on the chromosome rather than on a plasmid. Since YddG and TrpED are native *E. coli* proteins we could either change the promoter sequence of the chromosomal genes or move the entire cassette, including the tunable promoter, from the plasmid to the chromosome in another non-essential location, creating an extra copy of each gene. For TrpED it might be easier to do the latter, since we would also have to introduce the feedback-resistant mutation. These changes could be accomplished using the λRed recombination system (which would also need to be introduced into the cells) or via P1 viral transduction. While this would likely decrease the burden of expression, it would also likely lessen the effect of the genes overall due to the changes in copy number, leading to a decrease in cross-feeding. In that case, we would need to optimize the inducer concentrations again in order to see the same effect. A possible benefit might be that the co-culture is more stable since there would be only one or two copies of the

cross-feeding genes. This would then decrease the time for the cultures to reach equilibrium, making the consortium easier to "program" and fit more in line with the original theoretical model.

Second, an obvious future direction for the tunable circuit is to apply the circuit to production of a desired output, such as isobutanol. We have done extensive work to begin moving this system into the isobutanol producer JCL260 (*61*), however since we use yeast extract (YE) in our media (a common practice for bench-scale biofuel production) and since the hydrolysate contains amino acids (*58*), this rendered the circuit ineffective for our specific purposes. However, we could still use the circuit in this strain or the NV3 strains in minimal media without YE, since this would be more industrially relevant and cheaper. We have continued to use YE so far since in microplate studies we observed that it supported the cells' ability to grow in the presence of isobutanol (data not shown) and also led to increased isobutanol titers. If we were to get rid of this component we would likely see much lower titers unless we could utilize a more isobutanol-tolerant strain that has been optimized for growth without YE. As for growth on lignocellulosic biomass, we could try the circuit on a different feedstock that does not contain amino acids, or redesign the circuit to be based on cross-feeding nutrients that are not typically produced by plants.

There is evidence that a tunable circuit would be useful in our co-utilization consortium; in differential plating tests the co-culture ratio at the end of the cultivation period sometimes favored the NC5 and sometimes favored the NC6, depending on the experiment and medium (Figure 3.14). As the co-utilization relationship is not mutualistic, one partner is free to outgrow the other and therefore is not a very stable interaction. Engineering a control system into the NC5/NC6 pair would ensure that both partners are present in the culture in the optimal ratio.

5.2.2 Optimization of the isobutanol production system and incorporation into the multispecies consortium

The two-member isobutanol consortium has room for further optimization with regard to several aspects of its design. As mentioned earlier, we observed much variability in isobutanol production, especially with the NC6 and NC5+NC6 cultures,

which may result from plasmid loss during the cultivation. Moving the plasmid-borne genes onto the chromosome may solve this issue but would also likely need further optimization as the chromosomal expression level will be much lower than the expression level from multi-copy plasmids. To increase our titers, we could scale up our process to a much larger reactor and could also incorporate a process for isobutanol removal, such as the gas stripping process (*67*) or distillation. As mentioned previously, as the toxicity limit of isobutanol is ~7-8 g/L an isobutanol removal system will need to be put in place in order to reach industrially relevant titers, which will also become more important as titers increase with the larger reactors. In our process the sugar was not completely consumed, so it is not clear that feeding cycles would increase titers with our current setup. More details on possible genetic improvements are given in the Discussion section of Chapter 3, above.

As mentioned earlier, the ultimate end goal for the two-member *E. coli* consortium is to combine it with a cellulolytic fungus that can break down unhydrolyzed, pre-treated corn stover directly into fermentable sugars, skipping the costly enzymatic hydrolysis (Figure 5.1). Significant work has been done to optimize conditions for the growth of one bacterial C6 member and a fungus, *Trichoderma reesei*, which can hydrolyze cellulose and hemicellulose into mono- and oligosaccharides (*99*). *T. reesei* is an aerobic, mesophilic fungus that is often used in heterologous protein production as well as for commercial production of cellulases and hemicellulases due to its naturally cellulolytic nature (*100, 101*). The genome of *T. reesei* has also been sequenced (*100*), and tools for manipulating this fungus have been fairly well studied (*101, 102*) due to its utility in lignocellulosic biomass degradation. Since cellulose production by *T. reesei* is much more efficient under aerobic conditions than under anaerobic (*103*), we will likely continue this process under aerobic conditions unless we decide to switch to an anaerobic cellulose producer.

The next step will be to combine the NC5/NC6 pair with either the pSA55/69 plasmids or the pAK6/pSA69 plasmids with *T. reesei* to complete the conversion of corn stover into isobutanol in one reactor. Obviously, there will need to be significant optimization of co-culture conditions, however the work by another member of our

laboratory, Jeremy Minty, on the C6 and fungal co-culture will give us much background experience to hopefully expedite the optimization process (*99*).

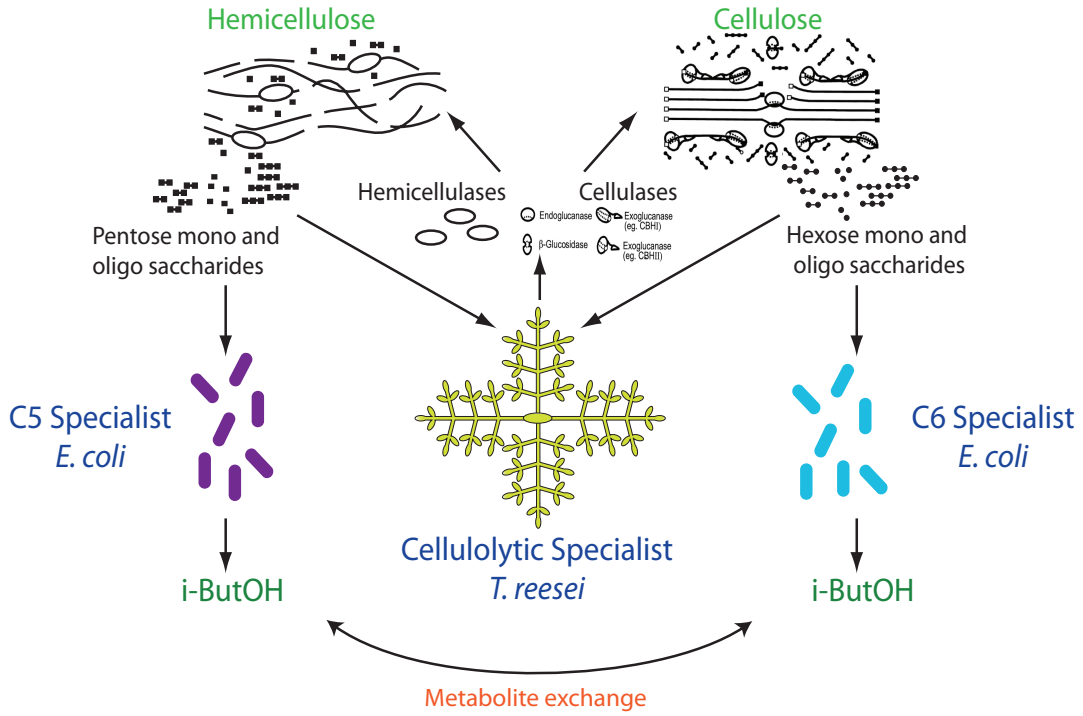

Figure 5.1 Multispecies consortium for isobutanol production. A *T. reesei* cellulolytic specialist breaks down the lignocellulosic biomass into pentose and glucose mono- and oligo-saccharides for the two bacterial specialists to ferment into isobutanol.

5.2.3 Method for production strain development using a consortium-based HTS

Finally, we would like to incorporate the secretor/sensor detection consortium into a larger system: a high-throughput method for overall production strain development and screening. A diagram of the entire process is shown in the previous chapter (Figure 4.5). We will first create a mutant library employing such techniques as the recently-developed genome manipulation technique Multiplex Automated Genome Engineering, or MAGE (*84*), to simultaneously and rapidly introduce various mutations throughout the secretor chromosome. This method, or similar methods, will allow us to simultaneously introduce numerous mutations (up to 30-40) over several rounds, thereby providing a unique examination of the combinatorial effects of some of the mutations that would not be otherwise observed. MAGE uses the same method of recombination as used to construct the secretor proof-of-concept strain EcLSBN, λRed-mediated ssDNA

recombination, so we can use the same base strain, EcHW24, with the PanB function removed. Instead of one oligo, however, a pool of oligos is mixed with the cells, and then multiple rounds of recombination are performed with the oligo pool, as well as enrichment steps, if desired (*84*). While this can be done by hand, recently the Church lab has been working on automating the system. This will then be much faster than incorporating the mutations one by one, leading to a high-throughput method for over-producer construction and library generation. The resultant library of mutants will then, theoretically, secrete various levels of L-valine. The benefit of using a method such as MAGE, as opposed to evolution or completely rational design, is that various combinations of mutations can be studied, as opposed to only a final combination that results from evolution, or a chosen combination from rational design. We will use both rational design studies (*64*) and evolution experiments (*63*) to inform our oligo design for L-valine over-production.

Next, the mutant library of secretors will be cultivated with the sensor strains in droplets on a microfluidic device. The device will allow us to isolate one pair per droplet, and, after cultivation, to sort the droplets by their level of growth or composition (i.e. fluorescence). The droplet generation and cultivation will take place on a microfluidic device developed for such purposes by Jihyang Park (*104*), and will then be harvested and sorted on another device that was under development previously by Jihyang and currently by Mathieu Rossion. Labview software will be used to sort the droplets based on the level of YFP expression from the sensor strain.

Once the droplets are harvested and sorted, the strains can then be tested off-chip in flask experiments to confirm that those that have faster-growing pairs do indeed contain secretor strains that make more L-valine, and hopefully, isobutanol, once they are transformed with the relevant KDC- and ADH-containing plasmids. The secretors can then also be sequenced to determine which mutations they have incorporated. As mentioned in previous sections, we may want to switch to other plasmids for isobutanol production that have enzymes with higher activity, such as pSA65 (contains *adhA*, *66*) instead of pSA55 (*61*). Additionally, since the pSA69 plasmid contains several genes from the valine synthesis pathway or homologues of these genes (such as *alsS*) we should

consider this when reincorporating the plasmids for isobutanol production. It is likely that several of these native genes will be mutated as a result of the MAGE process, so instead of using plasmid pSA69, the mutant genes (i.e. *ilvIHCD*) could be re-amplified from the *E. coli* chromosome if any are successfully mutated and then placed behind an inducible promoter. A similar effect of over-expressing genes and removing native regulation could also be accomplished by mutating the promoter region ahead of the genes using a degenerate oligo pool, as demonstrated previously (*84*).

Appendix A

Mutations in NV3 base strain

Appendix Table 1 Point mutations in strain NV3, from (*63*).

Enzyme	Pathway/annotation	Mutation
Metabolism		
ProC	proline biosynthesis	A98T
Dxs	isoprenoid biosynthesis	G235S
AcnA	TCA cycle	S522G
DapE	lysine biosynthesis	M107I
XylB	xylose degradation	G370S
GpmM	glycolysis	G72S
Tdh	threonine dehydrogenase	R108C
FsaB	glycolysis	G24E
MetH	methionine biosynthesis	T216I
LdhA	D-lactate dehydrogenase	R118C
PfkB	glycolysis	P243L
AnsB	asparagine/aspartate biosynthesis	T157I
Regulation		
RpoS	RNA polymerase σ^S-factor	Q304STOP
RelA	ppGpp biosynthesis	P532S
OsmY	stress response factor	G164D
DNA/RNA manipulation		
GltX	glutamyl-tRNA synthetase	A313V
PolA	DNA polymerase I	L18F
RplA	50S ribosomal subunit	E190K
RplL	50S ribosomal subunit	A42V
RpoB	RNA polymerase β subunit	A1043V
RpoC	RNA polymerase β′ subunit	R311H, T1024I
DbpA	RNA helicase	P28L
RecB	recombinase	P212L
TufB	elongation factor Tu	T29I
PheT	phenylalanine-tRNA synthetase	D423N
Transport		
FucP	fucose transport	A233T
XylH	xylose transport	P212S
GltS	glutamate Transport	S28F
BtuB	outer membrane porin	A162G
EamA	cystine transport	A95T
AcrD	RND transporter component	N939K
AcrB	RND transporter component	G740D, G625S
Fpr	fructose transport	R133H

References

1. H. Daims, M. W. Taylor, M. Wagner, Wastewater treatment: a model system for microbial ecology. *Trends Biotechnol* **24**, 483 (Nov, 2006).
2. P. J. Turnbaugh *et al.*, The human microbiome project. *Nature* **449**, 804 (Oct 18, 2007).
3. T. R. Zuroff, W. R. Curtis, Developing symbiotic consortia for lignocellulosic biofuel production. *Appl Microbiol Biotechnol* **93**, 1423 (Feb, 2012).
4. Y. Feng *et al.*, Degradation of raw corn stover powder (RCSP) by an enriched microbial consortium and its community structure. *Bioresource Technology* **102**, 742 (2011).
5. E. N. Lamsen, S. Atsumi, Recent progress in synthetic biology for microbial production of C3–C10 alcohols. *Frontiers in Microbiology* **3**, (2012).
6. M. A. Eiteman, S. A. Lee, E. Altman, A co-fermentation strategy to consume sugar mixtures effectively. *Journal of Biological Engineering* **2**, 3 (2008).
7. K. Brenner, D. K. Karig, R. Weiss, F. H. Arnold, Engineered bidirectional communication mediates a consensus in a microbial biofilm consortium. *Proceedings of the National Academy of Sciences* **104**, 17300 (2007).
8. S. L. Tsai, G. Goyal, W. Chen, Surface display of a functional minicellulosome by intracellular complementation using a synthetic yeast consortium and its application to cellulose hydrolysis and ethanol production. *Applied and Environmental Microbiology* **76**, 7514 (Nov, 2010).
9. F. K. Balagadde *et al.*, A synthetic Escherichia coli predator-prey ecosystem. *Molecular Systems Biology* **4**, 187 (2008).
10. S. Regot *et al.*, Distributed biological computation with multicellular engineered networks. *Nature* **469**, 207 (2010).
11. M. Tigges, T. T. Marquez-Lago, J. Stelling, M. Fussenegger, A tunable synthetic mammalian oscillator. *Nature* **457**, 309 (Jan 15, 2009).
12. S. H. Hong *et al.*, Synthetic quorum-sensing circuit to control consortial biofilm formation and dispersal in a microfluidic device. *Nat Commun* **3**, 613 (2012).
13. F. K. Balagadde, L. You, C. L. Hansen, F. H. Arnold, S. R. Quake, Long-term monitoring of bacteria undergoing programmed population control in a microchemostat. *Science* **309**, 137 (Jul 1, 2005).
14. A. Prindle *et al.*, A sensing array of radically coupled genetic 'biopixels'. *Nature* **481**, 39 (Jan 5, 2012).
15. W. S. Choi, D. Ha, S. Park, T. Kim, Synthetic multicellular cell-to-cell communication in inkjet printed bacterial cell systems. *Biomaterials* **32**, 2500 (Apr, 2011).
16. L. Lynd, W. Zyl, J. McBride, M. Laser, Consolidated bioprocessing of cellulosic biomass: an update. *Current Opinion in Biotechnology* **16**, 577 (2005).
17. L. R. Lynd, P. J. Weimer, W. H. van Zyl, I. S. Pretorius, Microbial Cellulose Utilization: Fundamentals and Biotechnology. *Microbiology and Molecular Biology Reviews* **66**, 506 (2002).
18. G. Bokinsky *et al.*, Synthesis of three advanced biofuels from ionic liquid-pretreated switchgrass using engineered Escherichia coli. *Proc Natl Acad Sci U S A* **108**, 19949 (Dec 13, 2011).

19. A. Kerner, J. Park, A. Williams, X. N. Lin, A Programmable <italic>Escherichia coli</italic> Consortium via Tunable Symbiosis. *PLoS ONE* **7**, e34032 (2012).
20. S. Basu, Y. Gerchman, C. H. Collins, F. H. Arnold, R. Weiss, A synthetic multicellular system for programmed pattern formation. *Nature* **434**, 1130 (Apr 28, 2005).
21. W. Shou, S. Ram, J. M. Vilar, Synthetic cooperation in engineered yeast populations. *P Natl Acad Sci USA* **104**, 1877 (Feb 6, 2007).
22. W. Weber, M. Daoud-El Baba, M. Fussenegger, Synthetic ecosystems based on airborne inter- and intrakingdom communication. *P Natl Acad Sci USA* **104**, 10435 (Jun 19, 2007).
23. K. Brenner, D. K. Karig, R. Weiss, F. H. Arnold, Engineered bidirectional communication mediates a consensus in a microbial biofilm consortium. *Proceedings of the National Academy of Sciences of the United States of America* **104**, 17300 (2007).
24. K. Brenner, F. H. Arnold, Self-Organization, Layered Structure, and Aggregation Enhance Persistence of a Synthetic Biofilm Consortium. *PLoS One* **6**, (Feb, 2011).
25. V. Doroshenko *et al.*, YddG from Escherichia coli promotes export of aromatic amino acids. *FEMS Microbiol Lett* **275**, 312 (Oct, 2007).
26. J. Pittard, H. Camakaris, J. Yang, The TyrR regulon. *Mol Microbiol* **55**, 16 (Jan, 2005).
27. S. Aiba, H. Tsunekawa, T. Imanaka, New approach to tryptophan production by Escherichia coli: genetic manipulation of composite plasmids in vitro. *Appl Environ Microbiol* **43**, 289 (Feb, 1982).
28. S. Azuma, H. Tsunekawa, M. Okabe, R. Okamoto, S. Aiba, Hyper-production of l-trytophan via fermentation with crystallization. *Applied Microbiology and Biotechnology* **39**, 471 (1993).
29. J. Bongaerts, M. Kramer, U. Muller, L. Raeven, M. Wubbolts, Metabolic engineering for microbial production of aromatic amino acids and derived compounds. *Metab Eng* **3**, 289 (Oct, 2001).
30. G. Xie, N. O. Keyhani, C. A. Bonner, R. A. Jensen, Ancient Origin of the Tryptophan Operon and the Dynamics of Evolutionary Change. *Microbiology and Molecular Biology Reviews* **67**, 303 (2003).
31. M. Santillan, M. C. Mackey, Dynamic regulation of the tryptophan operon: a modeling study and comparison with experimental data. *P Natl Acad Sci USA* **98**, 1364 (Feb 13, 2001).
32. G. Spraggon *et al.*, The structures of anthranilate synthase of Serratia marcescens crystallized in the presence of (i) its substrates, chorismate and glutamine, and a product, glutamate, and (ii) its end-product inhibitor, L-tryptophan. *P Natl Acad Sci USA* **98**, 6021 (May 22, 2001).
33. T. C. Dodge, J. M. Gerstner, Optimization of the glucose feed rate profile for the production of tryptophan from recombinantE coli. *Journal of Chemical Technology & Biotechnology* **77**, 1238 (2002).
34. E. C. Chan, Cloning a mutated Trp operon for the biosynthesis of an antibiotic agent. *Biotechnology Letters* **16**, 1021 (1994).

35. M. G. Caligiuri, R. Bauerle, Identification of amino acid residues involved in feedback regulation of the anthranilate synthase complex from Salmonella typhimurium. Evidence for an amino-terminal regulatory site. *The Journal of biological chemistry* **266**, 8328 (May 5, 1991).
36. C. Yanofsky, RNA-based regulation of genes of tryptophan synthesis and degradation, in bacteria. *Rna* **13**, 1141 (Aug, 2007).
37. H. Horowitz, T. Platt, Identification of trp-p2, an internal promoter in the tryptophan operon of Escherichia coli. *J Mol Biol* **156**, 257 (Apr 5, 1982).
38. "Trp operon." (Wikipedia, The Free Encyclopedia.), vol. 2012. Access date: 11-26-12. <<http://upload.wikimedia.org/wikipedia/commons/thumb/9/95/Trpoperon.svg/753px-Trpoperon.svg.png>>
39. K. Terpe, Overview of bacterial expression systems for heterologous protein production: from molecular and biochemical fundamentals to commercial systems. *Applied Microbiology and Biotechnology* **72**, 211 (Sep, 2006).
40. S. K. Lee *et al.*, Directed evolution of AraC for improved compatibility of arabinose- and lactose-inducible promoters. *Applied and Environmental Microbiology* **73**, 5711 (Sep, 2007).
41. S. K. Lee, J. D. Keasling, A propionate-inducible expression system for enteric bacteria. *Appl Environ Microbiol* **71**, 6856 (Nov, 2005).
42. K. A. Datsenko, B. L. Wanner, One-step inactivation of chromosomal genes in Escherichia coli K-12 using PCR products. *P Natl Acad Sci USA* **97**, 6640 (Jun 6, 2000).
43. T. Baba *et al.*, Construction of Escherichia coli K-12 in-frame, single-gene knockout mutants: the Keio collection. *Molecular Systems Biology* **2**, 2006 0008 (2006).
44. M. B. Elowitz, A. J. Levine, E. D. Siggia, P. S. Swain, Stochastic gene expression in a single cell. *Science* **297**, 1183 (Aug, 2002).
45. T. Nagai *et al.*, A variant of yellow fluorescent protein with fast and efficient maturation for cell-biological applications. *Nat Biotech* **20**, 87 (2002).
46. W. Harcombe, Novel cooperation experimentally evolved between species. *Evolution* **64**, 2166 (Jul, 2010).
47. K. L. Hillesland, D. A. Stahl, Rapid evolution of stability and productivity at the origin of a microbial mutualism. *Proc Natl Acad Sci U S A* **107**, 2124 (Feb 2, 2010).
48. N. Fu, P. Peiris, J. Markham, J. Bavor, A novel co-culture process with Zymomonas mobilis and Pichia stipitis for efficient ethanol production on glucose/xylose mixtures. *Enzyme and Microbial Technology* **45**, 210 (Sep, 2009).
49. M. A. Eiteman, S. A. Lee, R. Altman, E. Altman, A Substrate-Selective Co-Fermentation Strategy With Escherichia coli Produces Lactate by Simultaneously Consuming Xylose and Glucose. *Biotechnology and Bioengineering* **102**, 822 (Feb, 2009).
50. M. B. Sticklen, Plant genetic engineering for biofuel production: towards affordable cellulosic ethanol. *Nature Reviews Genetics* **9**, 433 (2008).
51. E. M. Rubin, Genomics of cellulosic biofuels. *Nature* **454**, 841 (Aug 14, 2008).

52. R. D. Perlack *et al.*, "Biomass as feedstock for a bioenergy and bioproducts industry: the technical feasibility of a billion-ton annual supply" (DTIC Document, 2005).
53. R. Maheshwari, Cellulosic ethanol as transportation fuel: hype no longer. *Current science* **96**, 455 (2009).
54. M. Hess *et al.*, Metagenomic discovery of biomass-degrading genes and genomes from cow rumen. *Science* **331**, 463 (Jan 28, 2011).
55. L. da Costa Sousa, S. P. S. Chundawat, V. Balan, B. E. Dale, 'Cradle-to-grave' assessment of existing lignocellulose pretreatment technologies. *Current Opinion in Biotechnology* **20**, 339 (2009).
56. E. Sendich *et al.*, Recent process improvements for the ammonia fiber expansion (AFEX) process and resulting reductions in minimum ethanol selling price. *Bioresource Technology* **99**, 8429 (2008).
57. M. W. Lau, C. Gunawan, B. E. Dale, The impacts of pretreatment on the fermentability of pretreated lignocellulosic biomass: a comparative evaluation between ammonia fiber expansion and dilute acid pretreatment. *Biotechnology for Biofuels* **2**, 30 (2009).
58. M. W. Lau, B. E. Dale, Cellulosic ethanol production from AFEX-treated corn stover using Saccharomyces cerevisiae 424A(LNH-ST). *Proceedings of the National Academy of Sciences* **106**, 1368 (2009).
59. R. E. H. Sims, W. Mabee, J. N. Saddler, M. Taylor, An overview of second generation biofuel technologies. *Bioresource Technology* **101**, 1570 (2010).
60. P. P. Peralta-Yahya, F. Zhang, S. B. del Cardayre, J. D. Keasling, Microbial engineering for the production of advanced biofuels. *Nature* **488**, 320 (2012).
61. S. Atsumi, T. Hanai, J. C. Liao, Non-fermentative pathways for synthesis of branched-chain higher alcohols as biofuels. *Nature* **451**, 86 (2008).
62. S. Atsumi *et al.*, Metabolic engineering of Escherichia coli for 1-butanol production. *Metabolic Engineering* **10**, 305 (2008).
63. K. M. Smith, J. C. Liao, An evolutionary strategy for isobutanol production strain development in Escherichia coli. *Metabolic Engineering* **13**, 674 (2011).
64. J. H. Park, K. H. Lee, T. Y. Kim, S. Y. Lee, Metabolic engineering of Escherichia coli for the production of L-valine based on transcriptome analysis and in silico gene knockout simulation. *P Natl Acad Sci USA* **104**, 7797 (May 8, 2007).
65. E. S. Sentheshanmuganathan S, The mechanism of the formation of tyrosol by Saccharomyces cerevisiae. *J. Biochem* **69**, 210 (1958).
66. S. Atsumi *et al.*, Engineering the isobutanol biosynthetic pathway in Escherichia coli by comparison of three aldehyde reductase/alcohol dehydrogenase genes. *Applied microbiology and biotechnology* **85**, 651 (Jan, 2010).
67. A. Baez, K.-M. Cho, J. C. Liao, High-flux isobutanol production using engineered Escherichia coli: a bioreactor study with in situ product removal. *Applied Microbiology and Biotechnology* **90**, 1681 (2011).
68. S. Atsumi *et al.*, Evolution, genomic analysis, and reconstruction of isobutanol tolerance in Escherichia coli. *Molecular Systems Biology* **6**, (2010).
69. A. Geng, Y. He, C. Qian, X. Yan, Z. Zhou, Effect of key factors on hydrogen production from cellulose in a co-culture of Clostridium thermocellum and Clostridium thermopalmarium. *Bioresource Technology* **101**, 4029 (Jun, 2010).

70. S. J. Ha *et al.*, Engineered Saccharomyces cerevisiae capable of simultaneous cellobiose and xylose fermentation. *Proc Natl Acad Sci U S A* **108**, 504 (Jan 11, 2011).
71. P. Vinuselvi, S. K. Lee, Engineered Escherichia coli capable of co-utilization of cellobiose and xylose. *Enzyme and Microbial Technology* **50**, 1 (2012).
72. M. A. Eiteman, S. A. Lee, R. Altman, E. Altman, A substrate-selective co-fermentation strategy withEscherichia coliproduces lactate by simultaneously consuming xylose and glucose. *Biotechnology and Bioengineering* **102**, 822 (2009).
73. T. Xia, M. A. Eiteman, E. Altman, Simultaneous utilization of glucose, xylose and arabinose in the presence of acetate by a consortium of Escherichia coli strains. *Microbial Cell Factories* **11**, 77 (2012).
74. Y. Qian, L. P. Yomano, J. F. Preston, H. C. Aldrich, L. O. Ingram, Cloning, Characterization, and Functional Expression of the Klebsiella oxytoca Xylodextrin Utilization Operon (xynTB) in Escherichia coli. *Applied and Environmental Microbiology* **69**, 5957 (2003).
75. P. W. Postma, J. W. Lengeler, PHOSPHOENOLPYRUVATE - CARBOHYDRATE PHOSPHOTRANSFERASE SYSTEM OF BACTERIA. *Microbiol. Rev.* **49**, 232 (1985).
76. D. Meyer, C. Schneider-Fresenius, R. Horlacher, R. Peist, W. Boos, Molecular characterization of glucokinase from Escherichia coli K-12. *J Bacteriol* **179**, 1298 (Feb, 1997).
77. P. Vinuselvi, S. K. Lee, Engineering Escherichia coli for efficient cellobiose utilization. *Applied Microbiology and Biotechnology* **92**, 125 (2011).
78. C. T. Trinh, P. Unrean, F. Srienc, Minimal Escherichia coli cell for the most efficient production of ethanol from hexoses and pentoses. *Applied and Environmental Microbiology* **74**, 3634 (Jun, 2008).
79. D. G. Gibson *et al.*, Enzymatic assembly of DNA molecules up to several hundred kilobases. *Nat Methods* **6**, 343 (May, 2009).
80. S. Bastian *et al.*, Engineered ketol-acid reductoisomerase and alcohol dehydrogenase enable anaerobic 2-methylpropan-1-ol production at theoretical yield in Escherichia coli. *Metabolic Engineering* **13**, 345 (May, 2011).
81. L. W. Doner, High-performance thin-layer chromatography of starch, cellulose, xylan, and chitin hydrolyzates. *Methods in Enzymology* **160**, 176 (1988).
82. J. A. Dietrich, A. E. McKee, J. D. Keasling, High-throughput metabolic engineering: advances in small-molecule screening and selection. *Annu Rev Biochem* **79**, 563 (2010).
83. S. A. Lynch, R. T. Gill, Synthetic biology: New strategies for directing design. *Metabolic Engineering* **14**, 205 (2012).
84. H. H. Wang *et al.*, Programming cells by multiplex genome engineering and accelerated evolution. *Nature* **460**, 894 (Aug 13, 2009).
85. H. H. Wang *et al.*, Genome-scale promoter engineering by coselection MAGE. *Nat Methods* **9**, 591 (Jun, 2012).
86. N. Costantino, D. L. Court, Enhanced levels of lambda red-mediated recombinants in mismatch repair mutants. *P Natl Acad Sci USA* **100**, 15748 (Dec 23, 2003).

87. C. N. Santos, G. Stephanopoulos, Melanin-based high-throughput screen for L-tyrosine production in Escherichia coli. *Applied and Environmental Microbiology* **74**, 1190 (Feb, 2008).
88. N. Mustafi, A. Grunberger, D. Kohlheyer, M. Bott, J. Frunzke, The development and application of a single-cell biosensor for the detection of L-methionine and branched-chain amino acids. *Metabolic Engineering* **14**, 449 (Jul, 2012).
89. S. Binder *et al.*, A high-throughput approach to identify genomic variants of bacterial metabolite producers at the single-cell level. *Genome Biology* **13**, R40 (2012).
90. B. F. Pfleger, D. J. Pitera, J. D. Newman, V. J. Martin, J. D. Keasling, Microbial sensors for small molecules: development of a mevalonate biosensor. *Metabolic Engineering* **9**, 30 (Jan, 2007).
91. N. Q. Balaban, J. Merrin, R. Chait, L. Kowalik, S. Leibler, Bacterial persistence as a phenotypic switch. *Science* **305**, 1622 (Sep 10, 2004).
92. F. M. You *et al.*, BatchPrimer3: a high throughput web application for PCR and sequencing primer design. *BMC Bioinformatics* **9**, 253 (2008).
93. E. H. Wintermute, P. A. Silver, Emergent cooperation in microbial metabolism. *Molecular Systems Biology* **6**, 407 (Sep 7, 2010).
94. J. M. Calvo, R. G. Matthews, THE LEUCINE-RESPONSIVE REGULATORY PROTEIN, A GLOBAL REGULATOR OF METABOLISM IN ESCHERICHIA-COLI. *Microbiol. Rev.* **58**, 466 (Sep, 1994).
95. J. H. Park, S. Y. Lee, Fermentative production of branched chain amino acids: a focus on metabolic engineering. *Applied Microbiology and Biotechnology* **85**, 491 (Jan, 2010).
96. V. Elisakova *et al.*, Feedback-resistant acetohydroxy acid synthase increases valine production in Corynebacterium glutamicum. *Applied and Environmental Microbiology* **71**, 207 (Jan, 2005).
97. J. H. Park, Y. S. Jang, J. W. Lee, S. Y. Lee, Escherichia coli W as a new platform strain for the enhanced production of L-valine by systems metabolic engineering. *Biotechnology and Bioengineering* **108**, 1140 (May, 2011).
98. J. H. Park, T. Y. Kim, K. H. Lee, S. Y. Lee, Fed-batch culture of Escherichia coli for L-valine production based on in silico flux response analysis. *Biotechnology and Bioengineering* **108**, 934 (Apr, 2011).
99. M. E. S. Jeremy J. Minty, Chang Hoon Bae, JungHo Ahn, Cliff E. Foster, James C. Liao, and Xiaoxia Nina Lin. , Design and characterization of synthetic fungal-bacterial consortia for direct production of isobutanol from cellulosic biomass. *Submitted to PNAS*, (2012).
100. D. Martinez *et al.*, Genome sequencing and analysis of the biomass-degrading fungus Trichoderma reesei (syn. Hypocrea jecorina). *Nat Biotech* **26**, 553 (2008).
101. M. Penttila, Heterologous protein production in Trichoderma. *Trichoderma and gliocladium* **2**, 365 (1998).
102. V. Meyer, Genetic engineering of filamentous fungi--progress, obstacles and future trends. *Biotechnol Adv* **26**, 177 (Mar-Apr, 2008).
103. I. Persson, F. Tjerneld, B. r. Hahn-H√ § gerdal, Fungal cellulolytic enzyme production: A review. *Process Biochemistry* **26**, 65 (1991).

104. J. Park, A. Kerner, M. A. Burns, X. N. Lin, Microdroplet-Enabled Highly Parallel Co-Cultivation of Microbial Communities. *PLoS ONE* **6**, e17019 (2011).